PROPERTIES OF ROTATING ULTRACOLD BOSONIC QUANTUM GASES

BY

SOHEIL BAHARIAN KHOSHKHOU

DISSERTATION

Submitted in partial fulfillment of the requirements
for the degree of Doctor of Philosophy in Physics
in the Graduate College of the
University of Illinois at Urbana-Champaign, 2013

Urbana, Illinois

Doctoral Committee:

Professor David Ceperley, Chair
Professor Gordon Baym, Director of Research
Professor Brian DeMarco
Professor John Stack

Abstract

In this dissertation, we study rotational properties of ultracold bosonic quantum gases in two trapped configurations, a quasi-two-dimensional gas in a harmonic trap and a quasi-one-dimensional gas in a toroidal trap.

First, we investigate the effects of correlations on the properties of the ground state of the rotating harmonically-trapped Bose gas by adding Bogoliubov fluctuations to the mean-field ground state of an N-particle single-vortex system. We demonstrate that the fluctuation-induced correlations lower the energy compared to that of the mean-field ground state, that the vortex core is pushed slightly away from the center of the trap, and that an unstable mode with negative energy (for rotations slower than a critical frequency) emerges in the energy spectrum, thus, pointing to a better state for slow rotation. We construct mean-field ground states of 0-, 1-, and 2-vortex states as a function of rotation rate and determine the critical frequencies for transitions between these states, as well as the critical frequency for appearance of a metastable state with an off-center vortex and its image vortex in the evanescent tail of the cloud.

Then, we show how the configuration-space form of the above-mentioned Bogoliubov ground-state wave function of a bosonic condensate with a single vortex in a harmonic trap can be described in terms of bosonic Jastrow correlations. We then generalize this result to study the effects of such correlations on a mean-field vortex lattice state and show that the included correlations lower the energy below that of the mean-field state. Although the reduction is relatively small, it is a precursor of the more general expected effect of correlations in describing the melting of the vortex lattice at a high angular momentum per particle.

Finally, we study the stability and dynamics of an ultracold bosonic gas trapped in a toroidal geometry and driven by rotation in the absence of dissipation. We first delineate, via the Bogoliubov mode expansion, the regions of stability and the nature of instabilities of the system for both repulsive and attractive interaction strengths. To study the response of the system to variations in the rotation rate, we introduce a disorder potential, breaking the rotational symmetry. We demonstrate the breakdown of adiabaticity as the rotation rate is slowly varied and find forced tunneling between the eigenstates of the system. The nonadiabaticity is signaled by the appearance of a swallow-tail loop in the lowest-energy level, a general sign of hysteresis.

Then, we show that this system is in one-to-one correspondence with a trapped gas in a double-well potential and thus exhibits macroscopic quantum self-trapping. Finally, we show that self-trapping is a direct manifestation of the behavior of the lowest-energy level.

To my mother and father.

Acknowledgments

First, I would like to thank my research advisor, Professor Gordon Baym, for his guidance, support, encouragement, and patience during my time as a student in his group. He unreservedly shared his knowledge with me, and I learned a great deal of physics from him; his approach to problems and his intuition in solving them were inspirational to me, and I am truly grateful that I had the opportunity to work with him. I am also thankful that he kept reminding me that I am indeed making progress, even though that concept seemed so unreachable – of course, he was right. I also want to thank him wholeheartedly for his understanding when I decided to switch fields from physics and pursue another path in science; knowing that I had his full support made the transition much less stressful.

I thank Professor Brian DeMarco for letting me be a part of his group during my second year in graduate school and for showing me the beauties and challenges of experimental physics. I am indebted to him for all his help in the years after and for his critical comments about my research. I also would like to thank him for his kind help during the last months of graduate school, when it was time for me to prepare for graduation. I am grateful to Professor Philip Phillips for giving me the opportunity to be his teaching assistant for a year, which benefited me immensely on many different levels, for his most wonderful course on condensed matter physics, and for his support during my time in Urbana. I am indebted to Professors Lance Cooper and John Stack for their support and advice whenever I talked to them. I am thankful to Professor Andrew Ferguson for a fascinating colloquium on computational biology which set the stage for my career after graduation. I would also like to thank Professors David Ceperley, Brian DeMarco, and John Stack for being on my final defense committee.

I am grateful to Professors Keivan Esfarjani and Vahid Karimipour for all they taught me and for their support during my undergraduate years at Sharif University of Technology and afterwards. I would also like to express my gratitude towards my teachers in high school, middle school, and elementary school.

I thank the members of Central Illinois Aikikai, past and present, who practiced with me and taught me the art of peace. My humble thanks go to Knut Bauer Sensei for everything he has done for the dojo, for his sincere passion in passing on his knowledge, for his tranquility and composure, and for all the exquisite

throws and pins. I consider myself extremely lucky to have found this dojo when I came to Urbana, and I will never forget my time there.

I have been exceedingly fortunate to have met and known some wonderful people in Urbana. I am most grateful to Akbar Jaefari, Mohammad Edalati, Esfandiar Alizadeh, Reza Vafabakhsh, and Mohammad Sahrapour for the unforgettable memories, the time we spent together, all the cheerful and serious discussions about anything and everything, their never-ending support, and all they've done for me. I would like to especially thank my friends and classmates, Alexandros Gezerlis for the adventures and discussions, Vasilica Crecea and Vikram Jadhao for their wonderful company and good spirits, Themis Athanassiadou and Abhishek Mukherjee for their hospitality and generosity, and Ghazi Zouaoui for the Jedi mind tricks. For the pleasant time in 341 Loomis and the discussions about science, life, religion, and many random topics, I thank Tomoki Ozawa and Philip Powell (whom I thank again for sharing with me his TEX knowledge).

Although we were not geographically close during my time in Urbana, I consider myself blessed to have the honor of knowing the following marvelous human beings. I would like to specifically thank my cousin, Sahand Mohsen, for his thoughtfulness and 33 years of friendship, Reza Pedrami for every single time he called me in the last ten years (even though I kept forgetting to call him back), and Roozbeh Behroozmand for his company and advice whenever I needed them the most. I thank my dear friends Rostam Dinyari, Khosrow Allaf-Akbari, Nima Saeidi, Morad Masjedi, Hamid Ohadi, and Idin Karuei for all their encouragements and good will and for the memories.

I am forever indebted to Amélie Bernard for her blissful friendship, for her boundless compassion, and for what she brought into my life. I thank her for 'being'.

Finally, I would like to thank my family, even though words surely fail me in expressing my gratitude towards them. I am indebted to my brother, Arya, for teaching me how to be a brother and for filling the void of my absence from the family for our parents – I am truly sorry that I was not there for you. I thank my sister, Golsheed, for being an inspiration to me, for lightening up my life when it seemed too gloomy, and for all her kindness – I wish you all the best, and I know you will have all the best. My most sincere gratitude goes to my mother, Roya, and my father, Khalil, for their unconditional support and love – your immense sacrifices made it possible for me to be where I am now, and I humbly thank you for all the ones I know about and all the ones I don't know about.

I acknowledge funding support from the National Science Foundation through grants No. PHY07-01611 and No. PHY09-69790 and from the Department of Physics at the University of Illinois at Urbana-Champaign through assistantships.

Table of Contents

List of Figures . . . . . **ix**

List of Abbreviations . . . . . **xi**

Chapter 1 Introduction **1**
1.1 General outline 1
1.2 Bose-Einstein condensates under rotation 3
1.3 Vortex lattice 5
1.4 Correlations and the fate of the vortex lattice 12
1.5 Toroidally trapped condensates 17

Chapter 2 Quantum fluctuations and stability of a single-vortex condensate **21**
2.1 Introduction 21
2.2 Basic model 23
2.3 Bogoliubov Hamiltonian in the lowest Landau level 25
2.4 The Bogoliubov Ground State 28
2.4.1 Properties of the Bogoliubov Ground State 30
2.5 The Stable Condensate 32
2.5.1 The Energy Valley and the Metastable Point 38

Chapter 3 Correlations in lowest-Landau-level vortex states **43**
3.1 Introduction 43
3.2 Basic Model 45
3.3 Correlations in the single-vortex Bogoliubov ground state 46
3.4 Extension to mean-field vortex lattices 48
3.5 Conclusion 50

Chapter 4 Bose-Einstein condensates in toroidal traps **52**
4.1 Introduction 52
4.2 Stability of the ground state 55
4.3 Depletion of the condensate 62
4.4 Two-mode approximation 62
4.5 Symmetry breaking in mean-field theory 64
4.5.1 Swallow-tail loops 65
4.5.2 Self-trapping 67
4.6 Summary 73

Chapter 5 Discussion **74**
5.1 Other correlated states 74
5.2 Effects of non-zero temperature 80

Appendix A Two-dimensional harmonic oscillator in polar coordinates **87**

Appendix B Bogoliubov approximation in the Landau level manifold 90

Appendix C The canonical transformations 97

Appendix D Symmetric polynomials and Jastrow factors 102

Appendix E Expansion terms in the single-vortex Bogoliubov ground state 107

Appendix F Coarse-grained quantities for the vortex lattice state 109
F.1 Mean-field state 109
F.2 Trial correlated state 111

References 119

List of Figures

1.1 Schematic diagram of a vortex and the contour $\mathcal{C}$ around it. 4

1.2 Vortex formation in a rotating BEC of 10^5 atoms at 80 nK, achieved by the ENS group in 2000. The rotation frequency $\Omega/2\pi$ varies from 145 Hz for (c) to 168 Hz for (g). Vortex core size before the free-fall expansion is ~ 0.4 μm in a condensate of size ~ 2.6 μm. Image from Phys. Rev. Lett. **84**, 806-809 (2000). Copyright (2000) by The American Physical Society. . 6

1.3 A triangular vortex lattice with 130 vortices in a BEC of 5×10^7 Na atoms, achieved by the MIT group in 2001. Intervortex separation is ~ 5 μm with the transverse cloud radius of ~ 50 μm before the expansion. From Science **292**, 476-479 (2001). Reprinted with permission from AAAS. 7

1.4 Single-particle energy levels in the laboratory frame $\epsilon_{(n_\perp,m,0)}$ in units of $\hbar\omega_\perp$ as functions of m (black is for $n_\perp = 0$, red is for $n_\perp = 1$, blue is for $n_\perp = 2$, and green is for $n_\perp = 3$). 8

1.5 Single-particle energy levels in the rotating frame $\epsilon_{(n_\perp,m,0)} - m\hbar\Omega$ in units of $\hbar\omega_\perp$ as functions of m for $\Omega/\omega_\perp = 0.925$ (black is for $n_\perp = 0$, red is for $n_\perp = 1$, blue is for $n_\perp = 2$, and green is for $n_\perp = 3$). 9

1.6 Density of a condensate with $L/(\hbar N) = 91$, calculated numerically by minimizing the GP energy, showing a highly-ordered triangular lattice of vortices. Note that the vortex core size is comparable to the intervortex spacing. Image from Phys. Rev. A **70**, 033604 (2004). Copyright (2004) by The American Physical Society. 11

1.7 Condensate density for $0 \leq L/(\hbar N) \leq 1$, calculated numerically by minimizing the GP energy, showing the appearance of a vortex at the edge of the cloud and its subsequent transition to the center. Reprinted by permission from Macmillan Publishers Ltd: Nature **397**, 327-329, copyright (1999). 13

1.8 The collapse of excitation energies for two-dimensional bosons on a torus as the filling factor is increased, obtained numerically. The dark, filled symbols represent states with momenta commensurate with a triangular lattice whose excitation energies decrease substantially for $\nu > 6$ (the empty symbols represent other non-commensurate states). Image from Phys. Rev. Lett. **87**, 120405 (2001). Copyright (2001) by The American Physical Society. 15

1.9 A Tkachenko oscillation of the vortex lattice, observed in an experiment at JILA. Black lines denote sine fits to the distortions. Image from Phys. Rev. Lett. **91**, 100402 (2003). Copyright (2003) by The American Physical Society. 16

1.10 Cartoon picture of the energy landscape of a superfluid in a toroidal container. Metastable states correspond to local minima which are separated by energy barriers. 18

1.11 Density modulations observed experimentally in a gas of ^{87}Rb atoms by the interference of rotating toroidal condensates with winding numbers $n_\phi = 3, 5, 10$ (left to right) and a non-rotating toroidal condensate. Image from Phys. Rev. A **86**, 013629 (2012). Copyright (2012) by The American Physical Society. 19

1.12 Energy landscape of the two-level model as a function of the number of particles in state $|1\rangle$. Note the energy barrier between the single-vortex and ground states for $gN/V > \hbar^2/2mR^2$ (solid line, in black); for $gN/V = \hbar^2/2mR^2$ (dashed line, in red), the slope vanishes at $N_1 = N$, while for $gN/V < \hbar^2/2mR^2$ (dot-dashed line, in blue) no barrier exists, indicating instability of the single-vortex state. 19

2.1 Schematic phase diagram of the condensate. 22
2.2 Density (in units of $1/\pi d_\perp^2$) of the Bogoliubov (solid line) and mean-field (dashed line) ground states for $N = 10$, showing a vortex at the center. The black dots denote the positions at which the two densities are equal. 32
2.3 Contour plot of E' for $N = 10^3$, $NV_0 = 0.1\,\hbar\omega_\perp$, and $\Omega = \omega_\perp - \frac{3}{8\hbar}NV_0$. Darker shades indicate lower energies. The straight dashed line represents the direction given by $\tanh\theta_m = \sqrt{8}/3$ whereas the curved solid line is the solution of Eq. (2.80), discussed below. 35
2.4 Energy landscapes for $\Omega = \omega_\perp - (2.1824/8\hbar)NV_0$ (top), $\omega_\perp - (2.1094/8\hbar)NV_0$ (middle), and $\omega_\perp - (1/4\hbar)NV_0$ (bottom), for $N = 10^3$ and $NV_0 = 0.1\,\hbar\omega_\perp$. The dots represent the critical points with `SP` and `MIN` indicating the saddle-points and minima respectively. 39
2.5 The position of the two off-center vortices for $N = 10^3$, $NV_0 = 0.1\,\hbar\omega_\perp$, and $\Omega_m \le \Omega \le \Omega_c$. Note the different vertical scales for z_m^+ and z_m^-. 42

4.1 A toroidally trapped Bose-Einstein condensate of ^{87}Rb atoms, formed by imparting angular momentum to the atoms from a Laguerre-Gauss mode of the trapping laser. The white mark is 30 μm in length. Image from Phys. Rev. A **86**, 013629 (2012). Copyright (2012) by The American Physical Society. 52
4.2 Energy landscape of the two-level model as a function of the number of particles in state $|1\rangle$. Note the energy barrier between the single-vortex and ground states for $gN/V > \hbar^2/2mR^2$ (solid line, in black); for $gN/V = \hbar^2/2mR^2$ (dashed line, in red), the slope vanishes at $N_1 = N$, while for $gN/V < \hbar^2/2mR^2$ (dot-dashed line, in blue) no barrier exists, indicating instability of the single-vortex state. 54
4.3 Single-particle energy levels in the rotating frame, measured in units of $\hbar\Omega_0$, as functions of Ω. 56
4.4 Stability phase diagram in the rotation rate vs interaction strength plane, for the $\nu = -1$ normal mode of a condensate with one unit of angular momentum per particle. Energetic instabilities are caused by excitations with negative energy, whereas those with complex energies lead to dynamical instabilities. 60
4.5 The energy per particle, in units of $\hbar\Omega_0$, of the states $|N, 0\rangle$ (labeled 0) and $|0, N\rangle$ (labeled 1) and that of the barrier state $|b\rangle$ (dashed line) as functions of the rotation frequency, for $\eta N = 1/4$. An energy loop (labeled by L_b, L_0, and L_1) emerges due to the existence of a maximum in the energy landscape. 63
4.6 Adiabatic energy levels, measured in units of $\hbar\Omega_0$, as functions of $\bar\Omega$ for $\eta N = \nu$ (top), $\eta N = 2\nu$ (middle), and $\eta N = 3\nu$ (bottom), with $\nu = 1/5$. In all plots, the lowest-energy branch is indicated by I and the top energy level by II. The arrows A and B in the right column indicate the discontinuous change in the population of $|0\rangle$ and the forced tunneling of particles to $|1\rangle$ as $\bar\Omega$ is changed past the folding point. 68
4.7 Occupation probabilities of $|0\rangle$ as functions of $\bar\Omega$ for $\eta N = \nu$ (top), $\eta N = 2\nu$ (middle), and $\eta N = 3\nu$ (bottom), with $\nu = 1/5$. In all plots, the population branch corresponding to the lowest-energy level is indicated by I, and the one corresponding to the higher-energy level by II. The arrows A and B in the bottom plot indicate the discontinuous change in the population of $|0\rangle$ and the forced tunneling of particles to $|1\rangle$ as $\bar\Omega$ is changed past the folding point. . . . 69
4.8 Population difference z (solid line, in red) and phase difference ϕ/π (dashed line, in blue) as functions of τ for $\Delta E = 1/2$ and (a) $\Lambda = 1$ below the critical value, (b) 7.75, (c) 8.2365 just below the critical value, and (d) 8.2374 the critical value. The initial conditions are $z(\tau = 0) = 0.6$ and $\phi(\tau = 0) = 0$. Note how the oscillatory behavior of $z(\tau)$ changes from purely harmonic to anharmonic as Λ increases; finally, $z(\tau)$ and $\phi(\tau)$ both become time-independent as Λ reaches the critical value. 72

5.1 Occupations of LLLs (normalized to unity) for different triangular lattices with intervortex separation $a_\mathrm{v} = d_\perp\sqrt{2\pi/\sqrt{3}}$ achieved for $\Omega = \omega_\perp$. 75
5.2 The ratio of the interaction energy of the Fock state to that of the coherent (mean-field) state as a function of the filling factor for $V_0/\hbar\omega_\perp \simeq 9 \times 10^{-4}$. Different colors represent different number of vortices with $N_\mathrm{v} = 31$ (black), 37 (red), 43 (purple), 55 (blue), and 61 (orange). . . 78

List of Abbreviations

BEC	Bose-Einstein Condensate.
LLL	Lowest Landau Level.
HLL	Higher Landau Level.
GP	Gross-Pitaevskii.
ODE	Ordinary Differential Equation.
CoM	Center-of-Mass.
FQHE	Fractional Quantum Hall Effect.
RBM	Rotating Boson Molecule.
RVC	Rotating Vortex Cluster.
ZNG	Zaremba-Nikuni-Griffin.

Chapter 1

Introduction

1.1 General outline

In this dissertation, we discuss rotational properties of ultracold bosonic gases in two configurations, a quasi-two-dimensional gas in a harmonic trap and a quasi-one-dimensional gas in a toroidal trap.

First, we investigate the stability (or lack there of) of a single-vortex Bose-Einstein condensate due to quantum fluctuations in the system. Using the Bogoliubov formalism, we build a very simple model (in which the first three lowest-energy states of the Coriolis force are coupled) and find the corresponding excitations and a lower-energy ground state which, by construction, includes correlations between particles. These correlations are induced by Bogoliubov quantum fluctuations of the particles. This simple treatment shows the favorable effects of correlations in lowering the energy of the system, which is the precursor to the melting of a vortex lattice in the limit of very high angular momentum per particle. We also show that the quantum fluctuations of particles indeed translate to an effective quantum fluctuation of the vortex which was stationary at the center of the trap in the mean-field formalism. Due to these fluctuations, the vortex is now pushed off-center by $\mathcal{O}(1/\sqrt{N})$ (in units of the characteristic length scale of the transverse harmonic trap). With the insight gained from the Bogoliubov quantum treatment, we return back to the classical mean-field model and find the transition rotation frequency for the appearance of the second vortex in the system and also investigate the dynamics of this two-vortex system as a function of the rotation frequency. These results, presented in Chapter 2, are based on the paper S. Baharian and G. Baym, Phys. Rev. A **82**, 063606 (2010).

Next, we study the interparticle correlations induced by the quantum fluctuations in the single-vortex Bogoliubov ground state and find their real-space representation by recasting the constituents in terms of monomial symmetric polynomials (discussed below). We present two new algebraic identities which recast these monomials in terms of another symmetric polynomial with successive numbers of Jastrow factors $(z_i - z_j)^2$; using these identities, we arrive at the position representation of the Bogoliubov ground state, showing the presence of Jastrow correlations (which appear in the Laughlin and the Read-Rezayi states, discussed below) at very low angular momenta. Armed with this result, we propose a trial correlated state

which builds correlations on top of the mean-field GP vortex state by removing two particles from the condensate and pairing them through a Jastrow factor. We find that this new wave function has a lower energy compared to the original mean-field state (with relative reduction in energy of $\mathcal{O}(1/N)$) and results in fluctuations of vortices (just like the single-vortex case). This result, which is another confirmation of the favorable effect of correlations, is the first step towards finding the exact ground state in the vortex lattice regime (which is still an open problem). These results, presented in Chapter 3, are based on the paper S. Baharian and G. Baym, Phys. Rev. A **87**, 033619 (2013).

Finally, the last system we address is a bosonic gas in a toroidal trap, a quasi-one-dimensional system. Using the Bogoliubov formalism, we find the normal modes (low-energy quasiparticle excitations) of such a system and identify regions in the phase space (a function of the interparticle interaction strength and the external rotation frequency) where the system becomes unstable to fluctuations (either energetically or dynamically). With a simple two-level mean-field model, we study the phenomenon of symmetry-breaking and its consequences by introducing a disorder potential as a model for the imperfections of the container walls. We find stationary states of the system in the presence of this disorder by solving a non-linear eigenvalue problem and identify swallow-tail loops in the energy spectrum, indicating the hysteretic behavior of the system and the non-adiabatic dynamics in certain regions of the phase space. Finally, we recast this problem in terms of the dynamics of a condensate trapped in a double-well potential with Josephson tunneling which, in turn, enables us to study the macroscopic phenomenon of self-trapping in a toroidally trapped condensate. These results, presented in Chapter 4, are based on the paper S. Baharian and G. Baym, Phys. Rev. A **87**, 013619 (2013).

In the remainder this chapter, we introduce the general framework and the basic formalism of trapped bosonic gases under rotation and discuss the results obtained so far in the literature and the open questions. Chapters 2, 3, and 4 constitute the main body of this dissertation and discuss and explain the basic ideas and the approximations employed by us to understand the underlying physics of their respective systems in terms of simple models. In Chapter 5, we introduce and discuss some possible extensions to the material presented in the main body of this dissertation, both for the vortex lattice systems and for toroidally trapped ones. In order to not take away the focus from the physics, all the important calculations and mathematical derivations are presented in the appendices. In Appendix A, the two-dimensional quantum harmonic oscillator problem is solved in the polar coordinates, revealing the Landau levels as the eigenstates. The Bogoliubov formalism applied to the Landau level manifold (both the higher and the lower levels) of the rotating atoms is derived in Appendix B. The necessary steps to diagonalize the Bogoliubov Hamiltonian are described in detail in Appendix C. The two new general algebraic identities between N-variable monomial symmetric polynomials

and Jastrow polynomials are derived in Appendix D, and their use in the single-vortex Bogoliubov ground state is explained in Appendix E. Finally, we calculate in detail, in Appendix F, some useful coarse-grained quantities for the trial correlated vortex-lattice state introduced in this dissertation.

1.2 Bose-Einstein condensates under rotation

Consider an ideal, i.e., non-interacting, uniform three-dimensional gas of atoms of mass m, temperature T, and mean number density n. The mean interparticle spacing l is set by the density, $l \sim n^{-1/3}$, whereas the non-zero temperature leads to the thermal wavelength via the de Broglie relation, $\hbar^2/m\lambda_T^2 \sim k_{\rm B}T$. When the temperature is low enough such that $\lambda_T \gtrsim l$, quantum mechanical effects become relevant. For bosons, these effects cause the onset of the quantum phenomenon of Bose-Einstein condensation [1] at a critical temperature $T_{\rm c}$ which, in general, depends on the properties of the gas as well as its container. The first realization of a Bose-Einstein condensate (BEC) was the observed superfluid transition of liquid ^{4}He (density $n \sim 10^{22}$ cm^{-3}) at $T_c \simeq 2$ K [2]. In 1995, the first atomic Bose-Einstein condensates were observed independently by the groups at JILA and MIT in dilute alkali gases (densities $n \sim 10^{12}$ and 10^{14} cm^{-3}) with transition temperatures $T_c \sim 2$ μK [3, 4].

The quantum nature of a BEC gives rise to many interesting properties, one of which is the response of such a system to external rotation. As noted by Onsager [5] and Feynman [6], a superfluid's response to rotation is different from that of a normal fluid. A normal fluid will eventually rotate along with its container with the same angular velocity $\boldsymbol{\Omega}$ due to the microscopic roughness of the container walls and, hence, will have a rigid-body rotation flow, $\mathbf{v} = \boldsymbol{\Omega} \times \mathbf{r}$, with uniform vorticity, $\boldsymbol{\nabla} \times \mathbf{v} = 2\,\boldsymbol{\Omega}$. A superfluid, described by an order parameter

$$\psi(\mathbf{r}) = \sqrt{n(\mathbf{r})}\, e^{{\rm i}\phi(\mathbf{r})} \tag{1.1}$$

with n and ϕ the density and phase, has the fluid velocity $\mathbf{v}_s(\mathbf{r}) = (\hbar/m)\boldsymbol{\nabla}\phi(\mathbf{r})$ which results in a vanishing vorticity, $\boldsymbol{\nabla} \times \mathbf{v}_s \sim \boldsymbol{\nabla} \times \boldsymbol{\nabla}\phi = 0$, in the absence of any singularity in the simply-connected region of the container; hence, a superflow is irrotational. However, there could exist a line-like singularity (a vortex) in the fluid, as first seen experimentally in 1974 by rotating He II [7]. The existence of a line-like singularity in the fluid (or, equivalently, trapping the fluid in a toroidal geometry) implies that the phase of the order parameter changes by a multiple of 2π around the singularity due to the single-valuedness of ψ. Therefore, the circulation, defined as

$$\Gamma = \oint_{\mathcal{C}} \mathbf{v} \cdot d\mathbf{s} \tag{1.2}$$

with $\mathcal{C}$ a contour around the vortex (located at $\mathbf{r}_0$ and pointing along $\hat{\mathbf{n}}_0$) and $d\mathbf{s}$ the element of length along

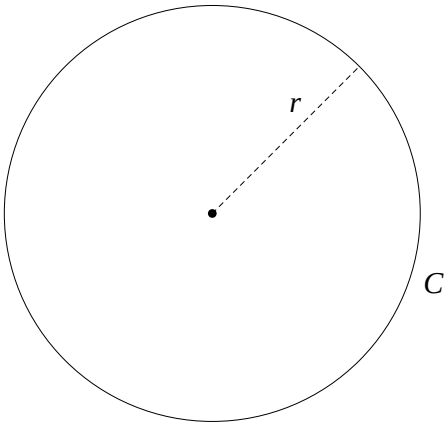

Figure 1.1: Schematic diagram of a vortex and the contour $\mathcal{C}$ around it.

$\mathcal{C}$, will be quantized for the superfluid since

$$\Gamma = \frac{\hbar}{m} \oint_{\mathcal{C}} \boldsymbol{\nabla}\phi \cdot d\mathbf{s} = \frac{\hbar}{m} \Delta\phi\big|_{\mathcal{C}} = \frac{2\pi\hbar}{m}\, n_\phi \tag{1.3}$$

where $\Delta\phi\big|_{\mathcal{C}}$ is the total phase change around the contour and n_ϕ is an integer; the quantization is in units of $2\pi\hbar/m$. Using Stoke's theorem, we immediately see that the vorticity is nonzero only at the vortex, i.e., $\boldsymbol{\nabla} \times \mathbf{v}_s = \Gamma\, \hat{\mathbf{n}}_0\, \delta(\mathbf{r} - \mathbf{r}_0)$. A vortex in an ultracold quantum gas was first created at JILA in 1999 by manipulating the relative phase between the two components (the hyperfine states $|F = 1, m_F = -1\rangle$ and $|F = 2, m_F = 1\rangle$) of a BEC of ^{87}Rb atoms [8].

Using Eq. (1.3) and a symmetric contour (as shown in Fig. 1.1) around the vortex (assumed to be at the origin for simplicity) or, equivalently, for a fluid in a toroidal container (with radius r), we find that $\Gamma = 2\pi r\, \mathbf{v}_s$; in other words, the fluid velocity profile for a vortex at origin is

$$\mathbf{v}_s(\mathbf{r}) = n_\phi\, \frac{\hbar}{mr}\, \hat{\boldsymbol{\theta}} \tag{1.4}$$

which diverges for $r \to 0$. Therefore, in order for the kinetic energy to remain finite, the superfluid density has to vanish at the core, going from the average density far from the vortex to zero over a length scale ξ, the healing length.

The equation of motion for the order parameter can be derived by linearizing the Heisenberg equation of motion for the field operator $\Psi(\mathbf{r}, t)$ around the classical field (the macroscopic condensate) $\psi(\mathbf{r}, t)$. This leads to the time-dependent Gross-Pitaevskii (GP) equation [1, 9]

$$\mathrm{i}\hbar \frac{\partial}{\partial t}\psi(\mathbf{r}, t) = \left[-\frac{\hbar^2}{2m}\boldsymbol{\nabla}^2 + V(\mathbf{r}) + g\,|\psi(\mathbf{r}, t)|^2 \right] \psi(\mathbf{r}, t) \tag{1.5}$$

where $V(\mathbf{r})$ is an external (trapping) potential and $g = 4\pi\hbar^2 a/m$ is the two-body interaction coupling constant [10] with a the s-wave scattering length. The steady-state solution $\psi(\mathbf{r},t) = \psi(\mathbf{r})e^{-\mathrm{i}\mu t}$, then, gives the time-independent GP equation

$$\left[-\frac{\hbar^2}{2m}\boldsymbol{\nabla}^2 + V(\mathbf{r}) + g\left|\psi(\mathbf{r})\right|^2\right]\psi(\mathbf{r}) = \mu\,\psi(\mathbf{r}) \tag{1.6}$$

where μ, the chemical potential, ensures the proper normalization of the order parameter, namely

$$\int d^3\mathbf{r}\left|\psi(\mathbf{r})\right|^2 = N. \tag{1.7}$$

One can also obtain Eq. (1.6) by variations of the GP energy functional

$$E[\psi] = \int d^3\mathbf{r}\left[\frac{\hbar^2}{2m}\left|\boldsymbol{\nabla}\psi(\mathbf{r})\right|^2 + V(\mathbf{r})\left|\psi(\mathbf{r})\right|^2 + \frac{1}{2}g\left|\psi(\mathbf{r})\right|^4\right] \tag{1.8}$$

with respect to ψ^* subject to the constraint (1.7). For a uniform condensate (with density $n = N/V$), we find from Eq. (1.6) that $\mu = gn$. The healing length (the length scale over which a density perturbation returns back to the average value) is given by the balance between the kinetic term and the interaction term, i.e., $\frac{\hbar^2}{2m\xi^2} = gn$, and we have

$$\xi = \sqrt{\frac{\hbar^2}{2m\mu}} = \frac{1}{\sqrt{8\pi an}}. \tag{1.9}$$

This length scale is (usually) a good approximation to the vortex core size for slow rotations and, in atomic BECs, is $\xi \sim 0.5$ μm.

1.3 Vortex lattice

As mentioned previously, setting superfluid helium in rotation results in the appearance of vortices [7] arranged in a dilute ordered structure (with the healing length ~ 1 Å, much smaller than the intervortex spacing ~ 1 mm), aligned along the axis of rotation (assumed to be the z axis) and rotating with the container. Similarly, arrays of vortices can be produced in rotating BECs as well. The first experimental realization of an array of vortices was achieved in 2000 at École Normale Supérieure [11] where a cigar-shaped BEC of ^{87}Rb atoms in a magnetic trap was stirred with a rotating laser beam, generating an anisotropy in the trap, to produce up to four vortices, as shown in Fig. 1.2. The same group also achieved configurations with up to eleven vortices in a regular array [12]. In 2001, the MIT group reported the observation of a highly-ordered triangular vortex lattice with up to 130 vortices [13]. These vortices nucleate due to the

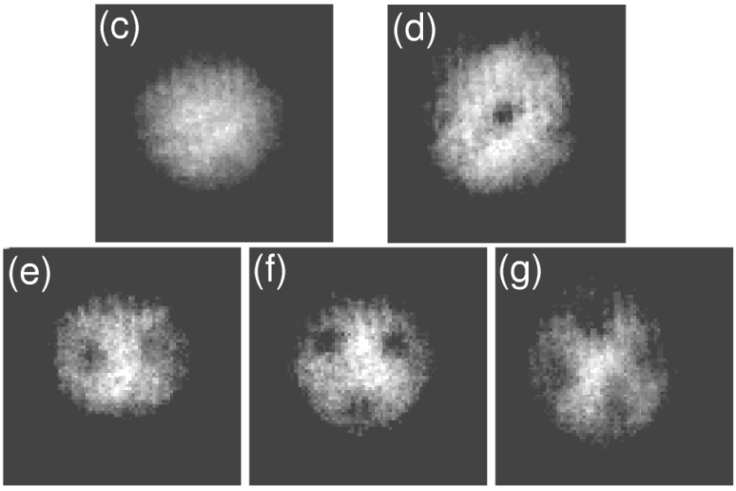

Figure 1.2: Vortex formation in a rotating BEC of 10^5 atoms at 80 nK, achieved by the ENS group in 2000. The rotation frequency $\Omega/2\pi$ varies from 145 Hz for (c) to 168 Hz for (g). Vortex core size before the free-fall expansion is ~ 0.4 μm in a condensate of size ~ 2.6 μm. Image from Phys. Rev. Lett. **84**, 806-809 (2000). Copyright (2000) by The American Physical Society.

Landau instability of the surface mode of the condensate, excited through a rotating deformation [14]. These experiments induce an intervortex spacing $\sim 2-5$ μm which is larger than the core size ~ 0.5 μm. In this limit (where vortex core are non-overlapping), the main factor determining the vortex arrangement is the kinetic energy [15], implying that the vortices interact pairwise logarithmic. As shown in Fig. 1.3, the lowest-energy configuration of such a system is a triangular lattice [16]. It is easy to show that an array of evenly distributed $N_{\rm v}$ vortices induces an average fluid velocity with rigid-body flow pattern [17] with $|\boldsymbol{\nabla} \times \langle \mathbf{v}_s \rangle| = 2(\pi\hbar/m)n_{\rm v}$ where $n_{\rm v} = N_{\rm v}/A$ is the uniform vortex density over an area A. Comparing this result with the vorticity of a rigid-body flow with rotation rate Ω immediately leads to the average vortex density

$$n_{\rm v} = \frac{m\Omega}{\pi\hbar} \tag{1.10}$$

first calculated by Feynman.

In order to impart angular momentum to the system and set it into rotation, it has to interact with and feel the presence of a rotating container; this implies the existence of a time-dependent potential doing work on the system. For such a system under rotation, thus, the laboratory frame is not an appropriate frame of reference for equilibrium statistical mechanics calculations [18], and we need to transform to a frame rotating with the container so as to make the external potential time-independent. Such a transformation can be formally written as

$$\mathcal{H}' = \mathcal{H} - \boldsymbol{\Omega} \cdot \mathcal{L} \tag{1.11}$$

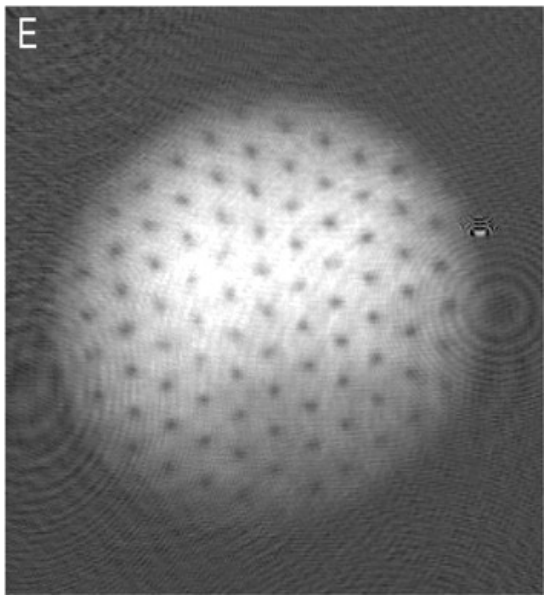

Figure 1.3: A triangular vortex lattice with 130 vortices in a BEC of 5×10^7 Na atoms, achieved by the MIT group in 2001. Intervortex separation is ~ 5 μm with the transverse cloud radius of ~ 50 μm before the expansion. From Science **292**, 476-479 (2001). Reprinted with permission from AAAS.

where $\mathcal{H}$ and $\mathcal{H}'$ are, respectively, the Hamiltonians in the laboratory and rotating frames and $\mathcal{L}$ is the total angular momentum. For particles of mass m in a harmonic trap of transverse and axial frequencies $\omega_\perp$ and ω_z, the single-particle Hamiltonian in the rotating frame, for $\mathbf{\Omega} = \Omega\hat{\mathbf{z}}$, can be recast as

$$\begin{aligned} \mathcal{H}^0 - \mathbf{\Omega}\cdot\mathcal{l} &= \left\{ \frac{\mathbf{p}^2}{2m} + \frac{1}{2}m\big[\omega_\perp^2(x^2+y^2) + \omega_z^2 z^2\big] \right\} - \mathbf{\Omega}\cdot(\mathbf{r}\times\mathbf{p}) \\ &= \left[\frac{(\mathbf{p}_\perp - m\mathbf{\Omega}\times\mathbf{r}_\perp)^2}{2m} + \frac{1}{2}m\big(\omega_\perp^2 - \Omega^2\big)\mathbf{r}_\perp^2 \right] + \left[\frac{p_z^2}{2m} + \frac{1}{2}m\omega_z^2 z^2 \right] \end{aligned} \tag{1.12}$$

where $\mathbf{r}_\perp = (x, y)$ and $\mathbf{p}_\perp = (p_x, p_y)$ are the transverse position and momentum and $\mathcal{l} = \mathbf{r}\times\mathbf{p}$ is the angular momentum operator. The first term is similar to the kinetic energy of a charge-q particle moving in a magnetic field $\mathbf{B} = 2m\mathbf{\Omega}/q$. It is this direct analogy that connects the physics of ultracold trapped bosons under rotation to the physics of the quantum Hall effect [19]. Moreover, we find that the transverse harmonic trap strength is now reduced due to the centrifugal force which implies the condition $\Omega \leq \omega_\perp$ for the stability of the trapped particles. Due to this weakening of the trap confinement, the cloud of atoms now expands further away from the center and becomes pancake-shaped. Therefore, for very rapid rotations, the system enters a very low-density regime with weak interactions. An experiment at JILA in 2004 achieved rotation speeds of $\Omega/\omega_\perp \simeq 0.993$ [20].

As we show in Appendix A, the single-particle Hamiltonian (in the laboratory frame) has the energy

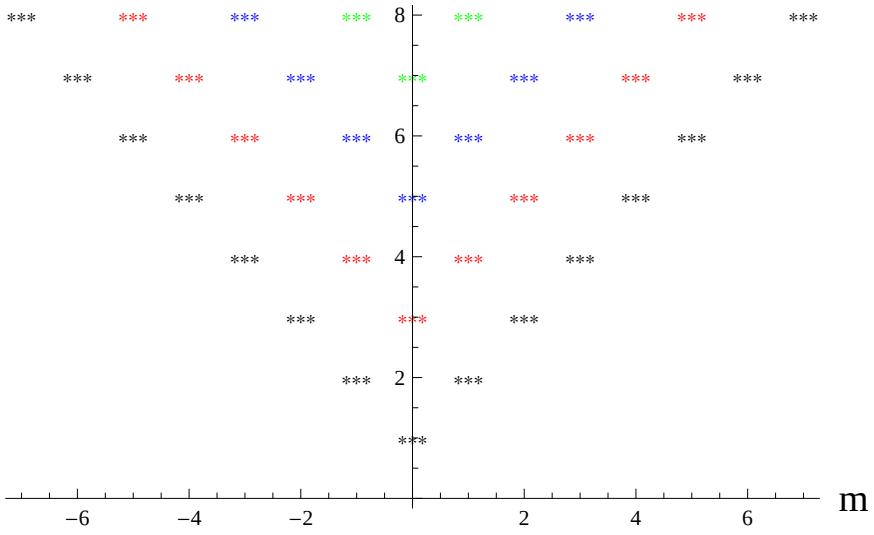

Figure 1.4: Single-particle energy levels in the laboratory frame $\epsilon_{(n_\perp,m,0)}$ in units of $\hbar\omega_\perp$ as functions of m (black is for $n_\perp = 0$, red is for $n_\perp = 1$, blue is for $n_\perp = 2$, and green is for $n_\perp = 3$).

spectrum (see Eq. (A.17))

$$\epsilon_{(n_\perp,m,n_z)} = \hbar\omega_\perp(2n_\perp + |m| + 1) + \hbar\omega_z\big(n_z + \tfrac{1}{2}\big) \tag{1.13}$$

with $n_\perp, n_z \geq 0$ are the transverse and axial quantum numbers and $m \in \{0, \pm1, \pm2, \dots\}$ is the quantum number associated with angular momentum around the z axis. In the limit of weak interactions (at high rotation rates), the chemical potential, $\sim gn$, becomes much smaller than the energy gap between adjacent axial levels

$$gn \ll \hbar\omega_z\,. \tag{1.14}$$

It is thus safe to assume that at extremely low temperatures ($T \simeq 0$ K), the system is restricted to the lowest-energy single-particle states with $n_z = 0$ (which have a Gaussian density profile in the axial direction), depicted in Fig. 1.4. In other words, the system (which resides in the axial ground state) is now quasi-two-dimensional. The corresponding transverse eigenstates (see Eq. (A.21))

$$\phi_{n_\perp,m}(r_\perp,\varphi) = \frac{1}{d_\perp}\sqrt{\frac{n_\perp!}{\pi\,(n_\perp+|m|)!}}\,e^{-\frac{1}{2}(r_\perp/d_\perp)^2}\,(r_\perp/d_\perp)^{|m|}\,L_{n_\perp}^{(|m|)}\big((r_\perp/d_\perp)^2\big)\,e^{\mathrm{i}m\varphi} \tag{1.15}$$

are called the Landau levels (in analogy with the eigenstates of a charged particle in magnetic field) where $d_\perp = \sqrt{\hbar/m\omega_\perp}$ is the characteristic trap length in the transverse direction. Similarly, the chemical potential

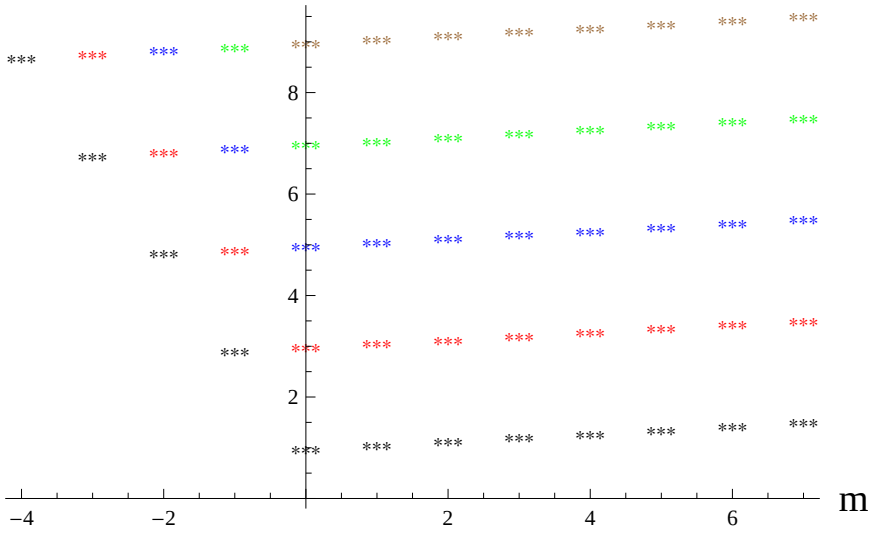

Figure 1.5: Single-particle energy levels in the rotating frame $\epsilon_{(n_\perp,m,0)} - m\hbar\Omega$ in units of $\hbar\omega_\perp$ as functions of m for $\Omega/\omega_\perp = 0.925$ (black is for $n_\perp = 0$, red is for $n_\perp = 1$, blue is for $n_\perp = 2$, and green is for $n_\perp = 3$).

is also much smaller than the energy gap between adjacent transverse levels

$$gn \ll 2\hbar\omega_\perp \tag{1.16}$$

as achieved in the experiment of Ref. [20] where $\mu/(2\hbar\omega_\perp) \simeq 0.6$. Hence, we can also assume that the system resides in the lowest-energy manifold of Landau levels ($n_\perp = 0$) among which only states with $m \geq 0$ should be occupied in order to minimize the total energy [21]. This picture will be especially clear if we look at the system from the rotating frame; shown in Fig. 1.5 are the energy levels in the rotating frame, and we see that the lowest-lying levels are those with $n_\perp = 0$ and $m \geq 0$. This is the so-called two-dimensional lowest Landau level (LLL) regime [15]. The LLL eigenstates (with angular momentum $\hbar m$) are

$$\phi_{m\geq 0}(r_\perp, \varphi) = \frac{1}{d_\perp \sqrt{\pi m!}}\, e^{-\frac{1}{2}(r_\perp/d_\perp)^2} \left(\frac{r_\perp}{d_\perp}\right)^m e^{\mathrm{i}m\varphi}. \tag{1.17}$$

The energy separation between adjacent LLL states is $\hbar(\omega_\perp - \Omega)$. In comparison, the energy gap separating the LLL manifold from the next higher Landau level (HLL) manifold is $\sim 2\hbar\omega_\perp$. Using the mean square radius $\langle r_\perp^2 \rangle_m = (m+1)d_\perp^2$, we find that

$$\frac{1}{\hbar}\langle \ell \rangle_m = \left\langle \frac{r_\perp^2}{d_\perp^2} \right\rangle_m - 1. \tag{1.18}$$

For an LLL system of N particles with total angular momentum L, we find from Eq. (1.13), ignoring the

zero-point energy of axial confinement, that the total single-particle energy is

$$E^0 = \sum_{i=1}^{N} \epsilon_{(0,m,0)_i} = N\hbar\omega_\perp + \omega_\perp L. \tag{1.19}$$

Thus, all LLL systems with the same total angular momentum are highly degenerate based solely on their total *non-interacting* single-particle energies. Interactions remove this degeneracy and determine the final arrangement of particles among the LLLs. For a wide range of angular momenta (discussed later), the total energy of the system is well approximated by the mean-field GP energy (1.8). Given that the system is frozen in the axial direction in the state $|n_z = 0\rangle$, we rescale the interaction coupling strength to (see, e.g., Ref. [22])

$$g_{2\mathrm{D}} = g \int dz \, |\langle z| \, n_z = 0\rangle|^4 = \frac{g}{\sqrt{2\pi}\, d_z} \tag{1.20}$$

where $d_z = \sqrt{\hbar/m\omega_z}$ is the axial trap length scale. From now on, we work only with the transverse energy and find (in the laboratory frame)

$$E = \int d^2\mathbf{r}_\perp \left[\frac{\hbar^2}{2m} \left|\boldsymbol{\nabla}_\perp \psi(\mathbf{r}_\perp)\right|^2 + \frac{1}{2} m\omega_\perp^2 r_\perp^2 \left|\psi(\mathbf{r}_\perp)\right|^2 + \frac{1}{2} g_{2\mathrm{D}} \left|\psi(\mathbf{r}_\perp)\right|^4 \right] \tag{1.21}$$

whose minimization leads to the ground state.

Given that the system effectively lives in the LLL manifold, we use a linear combination of the states (1.17) to denote the GP condensate wave function [23]

$$\psi(\mathbf{r}_\perp) = \sum_{m\geq 0} c_m \, \phi_m(\mathbf{r}_\perp) \tag{1.22}$$

with $\sum_{m\geq 0} |c_m|^2 = N$; variations with respect to c_m can then be used to minimize the GP energy. This requires the chemical potential to be larger than the energy spacing between LLL states [24], namely $gn \gg \hbar(\omega_\perp - \Omega)$, so that higher-angular momentum LLL states can be excited through the effect of interactions. Using Eq. (1.18) leads to

$$L = \hbar \int d^2\mathbf{r}_\perp \left(\frac{r_\perp^2}{d_\perp^2} - 1 \right) \left|\psi(\mathbf{r}_\perp)\right|^2 \tag{1.23}$$

which is valid for *any* wave function in the LLL manifold. Then, using Eqs. (1.21), (1.19), and (1.23), we can recast the GP energy in the rotating frame as [24]

$$E' = E - \Omega L = N\hbar\Omega + \int d^2\mathbf{r}_\perp \left[\hbar(\omega_\perp - \Omega) \frac{r_\perp^2}{d_\perp^2} \left|\psi(\mathbf{r}_\perp)\right|^2 + \frac{1}{2} g_{2\mathrm{D}} \left|\psi(\mathbf{r}_\perp)\right|^4 \right]. \tag{1.24}$$

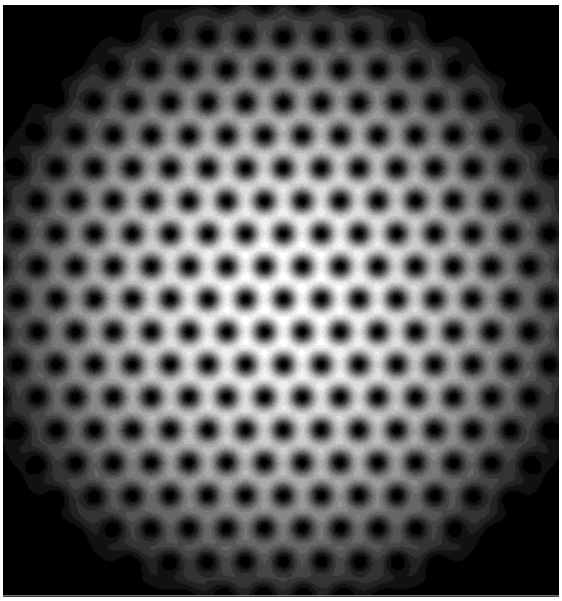

Figure 1.6: Density of a condensate with $L/(\hbar N) = 91$, calculated numerically by minimizing the GP energy, showing a highly-ordered triangular lattice of vortices. Note that the vortex core size is comparable to the intervortex spacing. Image from Phys. Rev. A **70**, 033604 (2004). Copyright (2004) by The American Physical Society.

Variations of the energy in the lab frame, (1.21), subject to the constraint of constant L is equivalent to variations of the energy in the rotating frame, (1.24), for constant Ω.

Introducing the (unitless) complex variable $z = (x + \mathrm{i}y)/d_\perp$ (note that this new variable is different from the coordinate along the axis of rotation), we can recast LLL eigenstates as

$$\phi_m(z) = \frac{1}{d_\perp \sqrt{\pi m!}}\, z^m\, e^{-|z|^2/2}. \tag{1.25}$$

Therefore, the GP wave function (1.22) is essentially a complex polynomial times the LLL exponential factor $e^{-|z|^2/2}$. Using the fundamental theorem of algebra, we rewrite the GP wave function as a product over its roots,

$$\psi(z) \sim e^{-|z|^2/2} \prod_j (z - \xi_j). \tag{1.26}$$

This wave function vanishes, as it should, at each ξ_j and acquires a phase of 2π when z moves around each ξ_j; therefore, the set of points $\{\xi_j\}$ denotes the complex positions of vortices. For very rapid rotations (cf. the experiment of Ref. [20] where $\Omega/\omega_\perp \simeq 0.993$), leading to very dilute quasi-two-dimensional clouds, vortex core size become comparable to the intervortex spacing (see also theoretical predictions of Ref. [25]). Unlike slow and moderate rotations (for which core size is small and kinetic energy is the deciding factor), vortex arrangement will now be determined entirely by the interaction term, much like that in a type-II

superconductor [26, 27]. Note that the properties of the system are now completely determined by the positions of vortices. Therefore, variations of the GP energy, (1.21) or (1.24), can be done through varying the positions of vortices [28, 29]. Figure 1.6 shows the condensate density and vortices (which exhibit large cores) for a BEC with angular momentum per particle of 91 (in units of $\hbar$) obtained by numerical variations of vortex positions [29] to minimize the GP energy (1.21).

We can determine the coarse-grained density profile (averaged over a distance larger than intervortex spacing) by substituting the density $n(\mathbf{r}_\perp) = |\psi(\mathbf{r}_\perp)|^2$ with its coarse-grained average $\overline{n(\mathbf{r}_\perp)}$ in Eq. (1.24). In doing so, we should also renormalize the interaction coupling strength [25] by a factor of $b = 1.158$ to take into account the substitution of $\overline{[n(\mathbf{r}_\perp)]^2}$ with $\big[\overline{n(\mathbf{r}_\perp)}\big]^2$. Then, minimizing the GP energy in the rotating frame, (1.24), leads to [24, 30, 22]

$$\overline{n(\mathbf{r}_\perp)} = \frac{2N}{\pi R^2}\left(1 - \frac{r_\perp^2}{R^2}\right) \tag{1.27}$$

$$\mu = \sqrt{\frac{2Nb\, g_{2\mathrm{D}}\hbar(\omega_\perp - \Omega)}{\pi d_\perp^2}} \tag{1.28}$$

where μ is the chemical potential at the center of the trap and

$$R = \left[\frac{2Nb\, g_{2\mathrm{D}} d_\perp^2}{\pi\hbar(\omega_\perp - \Omega)}\right]^{1/4} \tag{1.29}$$

is the Thomas-Fermi transverse radius of the cloud. It is shown analytically in Refs. [24, 30] and numerically in Ref. [29] that this minimization leads to very small deviations, $\mathcal{O}(1/N_\mathrm{v})$, of vortices from a perfect triangular lattice (mostly near the edge of the cloud) which help lower the energy compared to that of a perfect lattice. In this limit, the number of vortices is $N_\mathrm{v} \simeq 3L/(\hbar N)$.

1.4 Correlations and the fate of the vortex lattice

It is obvious from the construction of the GP theory that the mean-field condensate wave function does not include any correlations between particles [31, 32]. As an example, consider a BEC in the LLL with very small angular momentum per particle $0 \le L/N \le \hbar$. Mean-field theory (GP equation) predicts that as the angular momentum per particle of the condensate is increased from 0 to 1 (in units of $\hbar$), a vortex appears in the system, moving from the edge of the cloud (for very small angular momenta) towards the center where it becomes stable for unit angular momentum per particle [28, 33]; a numerical simulation of such a transition is shown in Fig. 1.7. The mean-field many-body wave function is $\psi(z_1, \ldots, z_N) = \prod_{i=1}^{N} \psi(z_i)$ where the GP

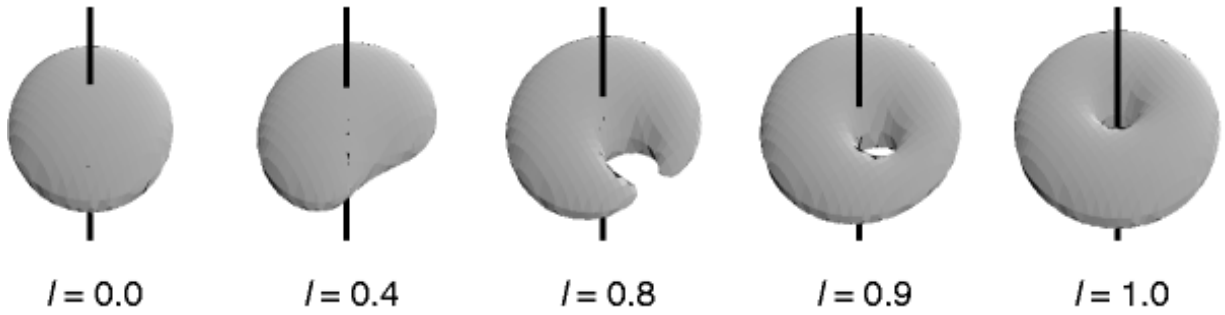

Figure 1.7: Condensate density for $0 \leq L/(\hbar N) \leq 1$, calculated numerically by minimizing the GP energy, showing the appearance of a vortex at the edge of the cloud and its subsequent transition to the center. Reprinted by permission from Macmillan Publishers Ltd: Nature **397**, 327-329, copyright (1999).

condensate wave function $\psi(z)$ takes the form

$$\psi(z) \sim (z - \xi)\, e^{-|z|^2/2} \tag{1.30}$$

with $\xi \to 0$ as $L/N \to \hbar$; this state is a superposition of the two lowest-energy LLL states $|m = 0\rangle$ and $|m = 1\rangle$. The *exact* ground states for these values of angular momentum are also known:

- The ground states for $L = 0$ is $\psi_{L=0}(z_1, \ldots, z_N) \sim 1$. In other words, all particles are in the LLL state $|m = 0\rangle$.

- The ground states for $L = \hbar$ is $\psi_{L=\hbar}(z_1, \ldots, z_N) \sim z_c$ where $z_c = \sum_{i=1}^{N} z_i/N$ is the center-of-mass (CoM) coordinate. This state is a CoM excitation of the $L = 0$ many-body state and has the same interaction energy since the interparticle interactions depend only on the relative distance between particles and not on the CoM coordinate (for a formal proof, see Ref. [34]).

- First postulated (and tested numerically) in 1999 by Bertsch and Papenbrock [35] and proved analytically in 2000 by Smith and Wilkin [36] and independently in 2001 by Papenbrock and Bertsch [37, 38], the ground state for $2\hbar \leq L \leq N\hbar$ is

$$\psi_L(z_1, \ldots, z_N) \sim \sum_{i_1 < i_2 < \cdots < i_{L/\hbar}} (z_{i_1} - z_c)(z_{i_2} - z_c) \cdots (z_{i_{L/\hbar}} - z_c). \tag{1.31}$$

  The $L = N\hbar$ limit, therefore, is $\psi_{L=N\hbar}(z_1, \ldots, z_N) \sim \prod_{i=1}^{N}(z_i - z_c)$ which could be interpreted as a "vortex" located at the CoM (note, however, that this is not a fully condensed state). In this state, the CoM coordinate fluctuates according to [15] $\langle |z_c|^2 \rangle \sim N^{-1}$. In the thermodynamic limit ($N \to \infty$), the CoM fluctuations are suppressed, and we arrive at the GP state (1.30) with $\xi = 0$.

For larger values of angular momentum, $L/(\hbar N) > 2$, the exact ground states of a system of rotating interacting bosons are not known.

Let us now focus on the other end of the spectrum, the extremely fast rotations with very large angular momenta per particle. In 1998, Wilkin *et al.* showed that the *exact* ground state (with zero interaction energy) for the very large angular momentum of $L = \hbar N(N-1)$ is the strongly correlated bosonic Laughlin state [21]

$$\psi_{\rm La.}(z_1, \ldots, z_N) \sim \prod_{i<j} (z_i - z_j)^2 \tag{1.32}$$

which has a vanishing condensate fraction. Early numerical studies of rapidly rotating bosons in two dimensions found evidence of strong correlations by generalizing Jain's composite fermion theory [39] of the fractional quantum Hall effect (FQHE) to the case of bosons [40] and also by considering condensates of new entities, composite bosons, which pair particles and vortices [41]. The ground states encountered are all incompressible liquids [15, 19] (with large gaps between the ground states and the lowest-lying excited states) with vanishing condensate fractions. Examples of such observed states are the Moore-Read (Pfaffian) state [42] and its generalization, the Read-Rezayi states [43] which are the zero-interaction-energy eigenstates of $(k+1)$-body contact interactions, $\sum_{i_1<i_2<\cdots<i_{k+1}} \delta(z_{i_1} - z_{i_2})\delta(z_{i_2} - z_{i_3}) \cdots \delta(z_{i_k} - z_{i_{k+1}})$. These states are constructed as

$$\psi^{(k)}_{\rm RR}(z_1, \ldots, z_N) \sim \mathcal{S}\left[\prod_{i_1<j_1 \in G_1} (z_{i_1} - z_{j_1})^2 \prod_{i_2<j_2 \in G_2} (z_{i_2} - z_{j_2})^2 \cdots \prod_{i_k<j_k \in G_k} (z_{i_k} - z_{j_k})^2 \right] \tag{1.33}$$

where $\mathcal{S}$ denotes the necessary symmetrization over all possible partitions of N particles in k groups $G_1, G_2, \ldots, G_k$ each with N/k particles. For $k = 1$, we recover the Laughlin state, whereas $k = 2$ yields the Moore-Read state. In general, the $k^{\rm th}$ Read-Rezayi state has angular momentum $L = \hbar N(N/k - 1)$. One important feature of all these strongly correlated states is their rotational symmetry, whereas the GP ground states – vortex lattices – have broken rotational symmetry.

This analogy between the physics of two-dimensional rapidly rotating bosons with that of electrons in the FQHE has an interesting consequence. The phases of electrons in the FQHE are categorized by the electron filling factor [44] $\nu_{\rm e} = (2\pi\hbar/eB)n_{\rm e}$ where $n_{\rm e}$ is the electron density and B is the magnetic field strength. We can define a similar quantity for the bosons, namely $\nu = (2\pi\hbar/2m\Omega)n$. Using Eq. (1.10), we find the bosonic filling factor

$$\nu = \frac{n}{n_{\rm v}} \tag{1.34}$$

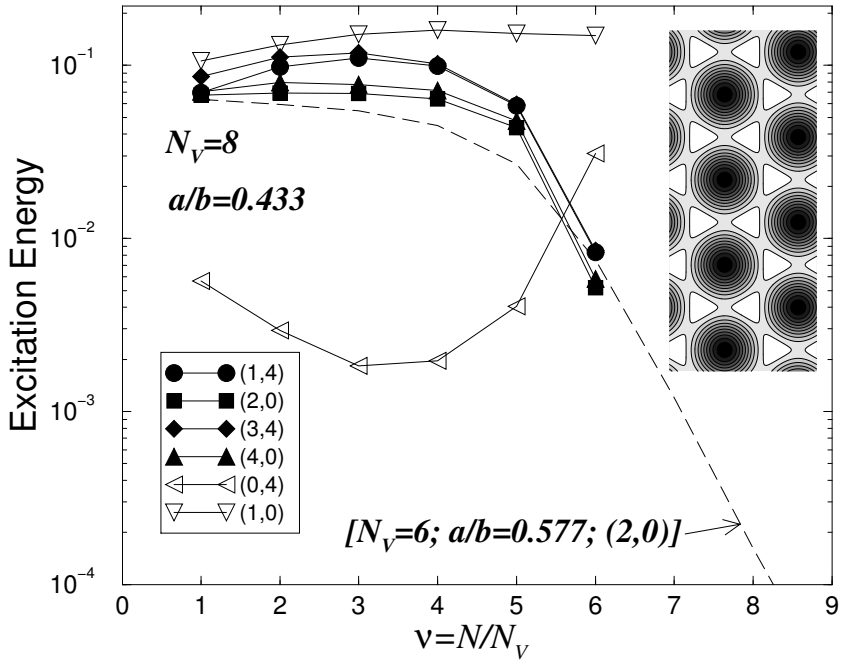

Figure 1.8: The collapse of excitation energies for two-dimensional bosons on a torus as the filling factor is increased, obtained numerically. The dark, filled symbols represent states with momenta commensurate with a triangular lattice whose excitation energies decrease substantially for $\nu > 6$ (the empty symbols represent other non-commensurate states). Image from Phys. Rev. Lett. **87**, 120405 (2001). Copyright (2001) by The American Physical Society.

which is, in general, a local quantity in a non-uniform trapped rotating condensate and reduces to

$$\nu = N/N_{\rm v} \tag{1.35}$$

in the uniform limit. In 2001, Cooper, Wilkin, and Gunn numerically investigated the phase of a rapidly rotating bosonic gas in terms of its filling factor [45]. They found, for $N_{\rm v} = 8$ vortices and up to $N = 48$ particles on a torus with an aspect ratio which is geometrically consistent with a triangular lattice, that incompressible strongly correlated states are ground states for low filling factors, whereas the triangular vortex lattice becomes the ground state for large filling factors, past the critical value $\nu_{\rm c} \sim 6$. The evidence for this transition is collapse of the energy gap between the ground state and a specific set of low-lying excited states that can support the broken symmetry of a triangular lattice [45, 15] such that these states become quasi-degenerate, as shown in Fig. 1.8. The combination of these states, then, leads to a new state with spontaneously broken symmetry [46, 47], namely the vortex lattice (see also Ref. [48] for similar broken-symmetry states).

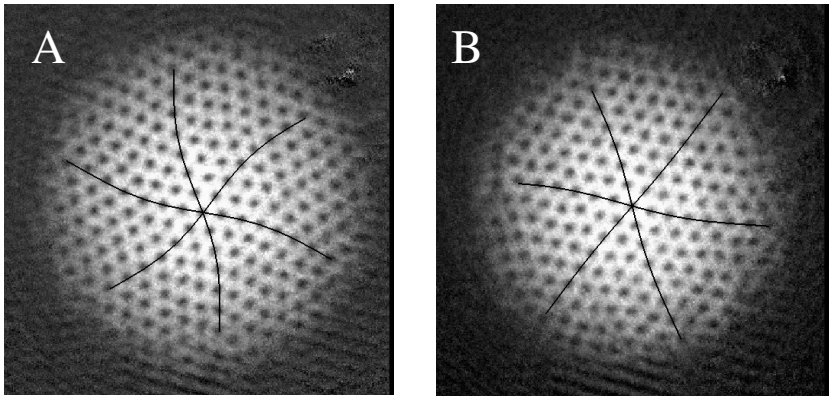

Figure 1.9: A Tkachenko oscillation of the vortex lattice, observed in an experiment at JILA. Black lines denote sine fits to the distortions. Image from Phys. Rev. Lett. **91**, 100402 (2003). Copyright (2003) by The American Physical Society.

In order to understand the evolution of the system from the vortex lattice phase to the strongly correlated phase, we need to look at the fluctuations of vortices. As the rotation rate increases, higher-angular momentum single-particle states which were empty before can now be occupied; this increase in the size of the configuration space could result in possible quasi-degeneracies between states with different single-particle occupations and, consequently, in the onset of quantum fluctuations [32]. Using Eq. (1.22), we see that these quasi-degeneracies mean different values for $\{c_m\}$ or different vortex positions $\{\xi_j\}$. Therefore, vortices, which were previously completely localized, now have the freedom to wiggle around their equilibrium positions. These quantum fluctuations, which become more pronounced with increasing angular momentum and lower particle density, ultimately lead to the melting of the vortex lattice. Collective motions of vortices in a lattice, the Tkachenko oscillations [49, 50, 51], were first observed in an atomic BEC at JILA in 2003 [52] (see Fig. 1.9). The first analytical calculations of the melting transition (loss of phase coherence in the condensate) based on collective fluctuations of vortices were done by Sinova *et al.* [53] in 2002 and by Baym [54] in 2004, respectively revealing a transition at $\nu_c \sim 8$ and at $\nu_c \sim 17$. It should be noted that both calculations used the Lindemann criterion, stating that melting occurs when the zero-point motion of vortices reaches a certain fraction (~ 0.15) of intervortex separation [55]. It is not entirely clear that this criterion is applicable to the case discussed here given its origins in the melting theory of solids, since the motion of vortices in a condensate is inherently different from that of atoms in a solid. With this in mind, Ghosh and Baskaran used the cooperative ring exchange model (first proposed for the FQHE by Kivelson *et al.* [56]) to formulate an effective theory of vortices [57] and found a melting transition at $\nu_c \sim 2$; however, their method is using a pairwise logarithmic interaction between vortices which is not consistent with the LLL regime [58].

This apparent disagreement between analytical results shows the need for a consistent theory of the melting of the vortex lattice. In order to investigate the fate of the vortex lattice as the rotation rate is increased (and as more vortices enter the condensate), it is extremely important to know the underlying correlations in the system. Unfortunately, this many-body problem, like most other many-body problems, is not exactly solvable, and the exact ground states of the system for different filling factors are not known (except for the bosonic Laughlin wave function (1.32) which has $\nu = 1/2$). To gain a better insight into the role of interparticle correlations in the lattice-melting phase transition, one can study the role of correlations starting from simple systems, e.g., a single-vortex condensate. We undertake this task in Chapter 2 by including Bogoliubov quantum fluctuations on top of the mean-field ground state of a single-vortex system in the LLL. With a very simple model in which the first three lowest-energy states of the Coriolis force are coupled, we find that such coupling leads to lowering of the energy of the ground state and to small fluctuations of the vortex around the initial position, a precursor to the melting phase transition in a lattice. Then, in Chapter 3, we investigate the interparticle correlations induced by these quantum fluctuations and find their real-space representation in terms of Jastrow factors. We use these type of correlations to propose a trial correlated state for the vortex lattice phase of a rotating BEC which has a lower energy compared to the mean-field state and, hence, is closer to the true ground state.

1.5 Toroidally trapped condensates

As discussed previously, nucleation of a quantized vortex is one of the distinct properties of superfluidity. A quantized vortex could form in a simply-connected region, as shown in Refs. [8, 11, 13], or, equivalently, the superfluid could be set in rotation in a toroidal container (a multiply-connected geometry), as first reported in 1957 for He-II in Ref. [59]. The current-carrying states of a superfluid have phases which change by integer multiples of 2π by going around (while staying within) the container (see Eq. (1.3)). These states are metastable in the sense that there exist energy barriers between them preventing the system from moving from one state to another (cf. Refs. [60, 16]), as shown in Fig. 1.10. Since ultra-cold quantum gases can be tuned and controlled to a very high degree, they have attracted a lot of interest lately, both for studies related to fundamental properties of superfluidity and also for their practical applications, e.g., in interferometry [61, 62] and atomtronics [63]. Some examples of recent experiments on BECs in toroidal traps, observing supercurrents and metastable states, are given in Refs. [64, 65, 66, 67, 68].

According to the classic argument for superfluidity [18, 69], proposed by Landau [70], the metastability of a current-carrying state is due to the absence of low-energy excitations which, depending on their energy and momentum, could remove momentum from the system and, thus, lead to the decay of the current,

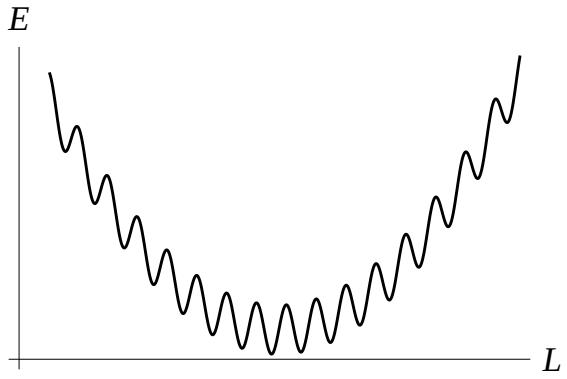

Figure 1.10: Cartoon picture of the energy landscape of a superfluid in a toroidal container. Metastable states correspond to local minima which are separated by energy barriers.

just as they do in a normal fluid in motion relative to the walls of its container. The absence of these excitations in a superfluid (which is described by a macroscopic order parameter) indicates the fact that the defects of the container are masked through a collective reshaping of the order parameter, and, therefore, the container effectively appears smooth to the fluid. However, low-energy excitations start to appear in the system as surface modes [71] above a critical velocity, which is equal to the speed of sound in a uniform weakly interacting bosonic gas [72] but is smaller in a non-uniform setting, e.g., a very long cigar-shaped condensate [73]. In a toroidal geometry, the existence of the centrifugal force of the rotation and the difference between the inner and outer radii of the container tend to slightly complicate this picture [74], with surface mode excitations (vortices or antivortices) forming either on the inner or the outer edges respectively depending on the initial conditions. The need for the presence of excitations to change the state of the system is another indication of the existence of energy barriers throughout the energy landscape. Since the topology of states with different circulations are distinct, as shown in Fig. 1.11, a transition from one topology to another requires the entrance of a phase slip (which has a vanishing density) into the system; these phase slips are precisely the vortices or antivortices mentioned previously and result in a change in the local density. They, hence, have an energy cost which is exactly the energy barrier (maximum) between the metastable current-carrying states (local minima of the energy).

The basic physics of the metastability of a state can be most simply understood by considering just two single-particle levels of the annulus, the non-rotating state, $|0\rangle$, and the state with azimuthal angular momentum $\hbar$ per particle, $|1\rangle$. The Hamiltonian of this system has the familiar Nozières form [75]

$$\mathcal{H}_2 = \frac{\hbar^2}{2mR^2}N_1 + \frac{g}{2V}(N_0^2 + N_1^2 + 4N_0N_1) \tag{1.36}$$

where $V = 2\pi^2 r_0^2 R$ is the volume of the annulus and N_0 and N_1 are the number of particles in $|0\rangle$ and $|1\rangle$

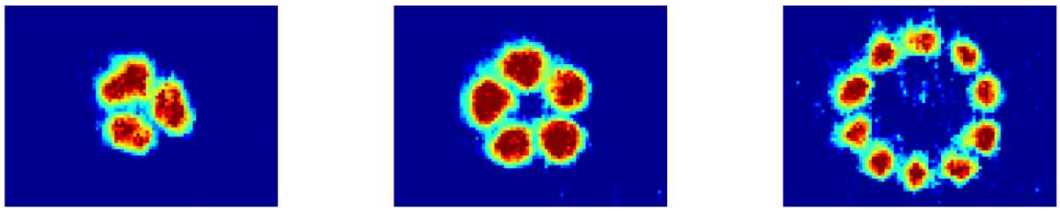

Figure 1.11: Density modulations observed experimentally in a gas of ^{87}Rb atoms by the interference of rotating toroidal condensates with winding numbers $n_\phi = 3, 5, 10$ (left to right) and a non-rotating toroidal condensate. Image from Phys. Rev. A **86**, 013629 (2012). Copyright (2012) by The American Physical Society.

respectively with $N = N_0 + N_1$ the total number of particles. The state with $N_1 = N$ is a single-vortex state and that with $N_0 = N$ is the ground state. Figure 1.12, which shows the energy per particle as a function of N_1 for different values of the interparticle interaction strength, illustrates the energy barrier that appears between the single-vortex state and the non-rotating ground state when $gN/V > \hbar^2/2mR^2$. With weakening interaction strength, the barrier height decreases, and for $gN/V \leq \hbar^2/2mR^2$, it disappears, leading to instability of the single-vortex state.

The existence of multiple minima separated by maxima in the energy landscape leads to hysteresis [76], where there is a lag between an external perturbation to the system (e.g., an applied magnetic field) and the response of the system to that perturbation (e.g., the magnetization). The reason for a hysteretic behavior is that the system could become trapped in a local minimum of energy even though the ground state for

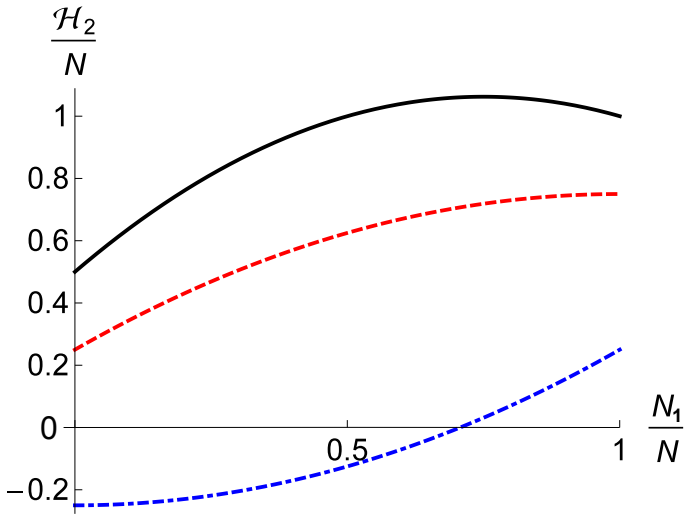

Figure 1.12: Energy landscape of the two-level model as a function of the number of particles in state $|1\rangle$. Note the energy barrier between the single-vortex and ground states for $gN/V > \hbar^2/2mR^2$ (solid line, in black); for $gN/V = \hbar^2/2mR^2$ (dashed line, in red), the slope vanishes at $N_1 = N$, while for $gN/V < \hbar^2/2mR^2$ (dot-dashed line, in blue) no barrier exists, indicating instability of the single-vortex state.

that particular value of external perturbation is the global minimum which has a lower energy. Changing the strength of the external perturbation results in a change in the height of the energy barrier which vanishes at a critical value for the strength of the external perturbation; at this point, the local minimum merges with the maximum (and both annihilate), and the system can finally transition to the lower-energy state. Therefore, the response lags behind the external perturbation, indicating the presence of hysteresis. (This change in the number of extrema is called a catastrophe [77] or a saddle-node bifurcation [78] in the mathematics literature.) For a superfluid in a toroidal container, we can see the presence of hysteresis through the following experiment. If we start to rotate the container (initially at rest in the laboratory frame) very slowly and gradually increase the rotation rate, the superfluid will remain at rest until the rotation becomes fast enough such that the critical velocity between the fluid and the container walls is reached and excitations start to appear. At this point, the fluid starts to rotate and can support a persistent current. Likewise, in order to slow down the rotation of the superfluid, it is not enough to slow down the rotation frequency of the container by a small amount; we need large enough changes such that the relative velocity between the fluid (which is still rotating fast) and the container (which is now rotating slow) exceeds the critical velocity. Then, the superfluid begins to slow down due to formation of new excitations. We can say that the response of the superfluid to an external rotation exhibits hysteresis.

As discussed in Ref. [76], the energy extrema of a hysteretic system, if plotted as functions of the external control parameter, form a very distinct structure, a *swallow-tail loop* [79] (see, e.g., Fig. 4.5, to be discussed later). A consequence of this loop is the lack of adiabaticity in the system due to a forced Landau-Zener tunneling between the quantum states as the external control parameter is varied [80]; in other words, once the system reaches the point in the parameter space at which the swallow-tail loop terminates, it cannot adiabatically follow the control parameter anymore, no matter how slow the latter is changing. Swallow-tail loops, and their consequences, have been a subject of great interest in recent years, pioneered by the experimental observation of superfluidity and dissipation in a BEC trapped in an optical lattice [81] which ensued many theoretical studies afterwards [79, 82, 83, 84, 85].

In Chapter 4, we study a quasi-one-dimensional BEC trapped a toroidal geometry. We find the normal modes of the condensate and identify energetic and dynamical instabilities of the system towards fluctuations. Using a two-level mean-field model, we study the phenomenon of a symmetry-breaking by introducing a disorder potential as a model for the imperfections of the container walls. This disorder leads to the appearance of swallow-tail loops in the energy spectrum, indicating the hysteretic behavior of the system and the non-adiabatic dynamics in certain regions of the phase space whose implications we discuss in detail.

Chapter 2

Quantum fluctuations and stability of a single-vortex condensate

2.1 Introduction

A rotating ultracold harmonically-trapped Bose gas is predicted to pass through many exotic phases with increasing rotation rate (for a recent review, see Ref. [15]). The mean-field description, which omits all correlations, predicts the zero-temperature ground state for a large number of particles to be a vortex lattice [28, 33, 23, 24, 29, 30], and is in good agreement with current experiments [13, 52, 20]. However, exact diagonalization of the many-body Hamiltonian [45] suggests the breakdown at very high rotation rates of the mean-field picture and a melting transition to strongly-correlated ground states, bosonic analogues of quantum Hall states [40, 41, 86, 87, 88, 19]. The onset of correlations and quantum fluctuations can be expected to play a significant role in this transition to a strongly-correlated quantum liquid. However, a consistent theory of the zero-temperature melting of the vortex lattice does not exist so far [53, 54, 57, 89] (for a theory of thermal melting of the lattice, see Ref. [90]). A crucial first step in constructing such a theory is to understand better how correlations affect the system.

With increasing rotation rate, the cloud expands in the transverse direction, and the particle density decreases. In each unit cell of the lattice, the vortex core occupies a larger fraction of the area of the cell [25], and the average displacement of the vortex from its equilibrium position increases [54] due to the zero-point motion of the Tkachenko mode [49, 50, 51]. Hence, the uncertainty in the position of vortices, which plays a leading role in the melting, increases at faster rotation rates [15]. This uncertainty is completely absent in the mean-field picture, in which the vortex positions are fixed and do not fluctuate.

The nature of the correlations between particles changes as the rotation rate increases. For angular momentum per particle less than or equal to unity (in units of $\hbar$), correlations in the exact ground state wave function [36] are described by polynomials in the relative distance of the particles from the center-of-mass, i.e.,

$$\psi \sim \sum_{i_1<i_2<\cdots<i_L} (z_{i_1} - z_c)(z_{i_2} - z_c)\cdots(z_{i_L} - z_c) \tag{2.1}$$

where $z \sim (x + iy)$ are the positions of the particles and z_c the center-of-mass in the complex plane. On

the other hand, when the angular momentum per particle is of order the number of particles, correlations appear in the distances of particles from each other, as in the bosonic Laughlin wave function [21]

$$\psi \sim \prod_{i<j}(z_i - z_j)^2. \tag{2.2}$$

The aim of the first part of this Chaper is to build relevant correlations on top of the mean-field many-body ground state and to investigate their effects on the energetics and physical properties of the ground state. Based on the inferred modifications of the ground state, the second part of this Chapter investigates, at the mean-field level, different ground states of the (0-, 1-, and 2-vortex) Bose gas and their respective transitions as the external rotation rate increases.

Small-amplitude Bogoliubov fluctuations around the mean-field ground state induce correlations by allowing small numbers of excitations to appear in nearby single-particle states. In a condensate with large number of vortices, the number of excited modes (single-particle harmonic oscillator eigenstates) involved is of order the number of vortices. Therefore, carrying out the general diagonalization is a mathematically challenging task for a many-vortex condensate. However, one can gain insight by working with a few-vortex system; for example, including the first three harmonic oscillator states is sufficient to describe systems with up to two vortices, as we show below. The simplest such system is a condensate with one singly-quantized vortex at the center of the trap, rotating at the critical frequency Ω_c, at which the vortex becomes thermodynamically stable [28, 91], and, hence, having unit angular momentum per particle.

We find, indeed, that the correlations induced by Bogoliubov fluctuations lead to a better ground state in the thermodynamic limit, lower in energy than the mean-field one. We also see that the fluctuations drive the vortex core away from the center of the trap by a fluctuating distance of $\mathcal{O}(1/\sqrt{N})$ (in units of the characteristic length of the trap). Moreover, for rotations slower than the critical frequency Ω_c, we find excitations with negative eigenenergy in the spectrum [91] which remove one unit of angular momentum from the gas, indicating an instability towards a lower-energy non-rotating state for rotation rate $\Omega < \Omega_c$ and emphasizing the fact that the single-vortex mean-field ground state is not the best starting state.

Based on these results, we construct a more energetically favorable mean-field condensate which, as a

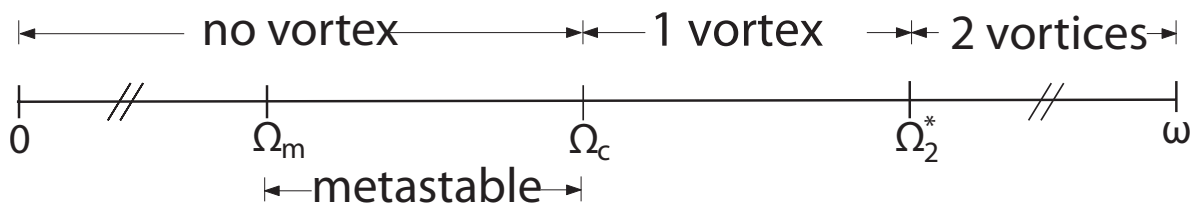

Figure 2.1: Schematic phase diagram of the condensate.

function of Ω, is either non-rotating, a single-vortex state, or a two-vortex state. The phase diagram in Fig. 2.1 summarizes our results. At a certain frequency Ω_m (below Ω_c), there exists a metastable state (a local minimum of the energy) with two off-center vortices in the cloud which are asymmetric about the origin; for a vortex close to the center of the trap, there exists an image vortex much further away where the particle density is negligible, in agreement with Ref. [92]. We calculate the critical frequencies, Ω_c and Ω_2^* respectively, at which the first and second vortices enter the cloud. The former agrees with the numerical result of Ref. [28], while the latter is somewhat larger owing to our incorporating only a restricted number of single-particle eigenstates in the mean-field ground state.

In the next section, we outline the basic description of the rotating Bose gas in terms of Landau levels in the Coriolis force. In Sec. 2.3, we determine the small-amplitude fluctuations about the mean-field condensate and their effect on the properties of the ground state, and then in Sec. 2.5, we present the stable mean-field wave function that encapsulates the various phases of the rotating gas and their respective critical rotation frequencies.

2.2 Basic model

We consider a cloud of N bosons of mass m in a harmonic trap with frequencies $\omega_\perp$ in the x–y plane and ω_z in the z direction (with $\omega_z \gg \omega_\perp$ to tightly confine the gas in the axial direction), rotating around the z axis with angular velocity Ω. The characteristic oscillator lengths are $d_\perp = \sqrt{\hbar/m\omega_\perp}$ in the transverse direction and $d_z = \sqrt{\hbar/m\omega_z}$ in the axial direction. We assume weak two-body repulsive interactions of strength $g = 4\pi\hbar^2 a/m$ where a is the s-wave scattering length. In the limit of fast rotation, $\Omega \lesssim \omega_\perp$, the gas becomes quasi-two-dimensional, and at zero temperature, it resides approximately in the ground state of the harmonic trap in the z direction. The many-body Hamiltonian in the rotating frame is

$$\mathcal{H}' = \sum_{i=1}^{N} (\hbar_i^0 - \Omega \ell_i) + \sum_{i<j} g_{2\mathrm{D}}\, \delta(\mathbf{r}_i - \mathbf{r}_j) \tag{2.3}$$

with the non-interacting single-particle Hamiltonian and angular momentum

$$\hbar^0 = \frac{\mathbf{p}^2}{2m} + \frac{1}{2} m\omega_\perp^2 \mathbf{r}^2 \tag{2.4}$$

$$\ell = \hat{\mathbf{z}} \cdot (\mathbf{r} \times \mathbf{p}) \tag{2.5}$$

where $\mathbf{r}$ and $\mathbf{p}$ are the particle positions and momenta in the x–y plane, and

$$g_{2\mathrm{D}} = \frac{g}{\sqrt{2\pi}d_z} \tag{2.6}$$

is the effective interaction strength in two dimensions.

The eigenstates of the single-particle Hamiltonian, $\hbar^0$, are the Landau levels $|nm\rangle$ (derived in detail in Appendix A), where the Landau level index n is the radial quantum number, and $m \in \mathbb{Z}$ is the angular momentum along the rotation axis, with eigenvalues

$$\epsilon'_{nm} = \hbar\big[(2n + |m| + 1)\omega_\perp - m\Omega\big]. \tag{2.7}$$

The characteristic energy scale of the two-body interaction is

$$V_0 = \frac{g_{2\mathrm{D}}}{2\pi d_\perp^2}. \tag{2.8}$$

The energy difference between two successive higher Landau levels ($n \neq 0$) is $\mathcal{O}(\hbar[\omega_\perp + \Omega])$ which, for $\Omega \to \omega_\perp$, is much larger than that $\mathcal{O}(\hbar[\omega_\perp - \Omega])$ between two states in a given Landau level. We assume the interactions to be sufficiently weak that $V_0 \ll 2\hbar\omega_\perp$; thus, we ignore the small higher Landau level components in the wave function and safely assume that the system resides in the manifold of the $n = 0$ lowest Landau level (LLL) states. With this assumption, the only relevant quantum number is the angular momentum index m; from now on, we drop the Landau level index n from the eigenfunctions, operators, and occupation numbers for simplicity, unless otherwise noted.

The LLL eigenfunctions and eigenenergies are

$$\phi_m(z) \equiv \langle \mathbf{r} \,|0m\rangle = \frac{1}{d_\perp\sqrt{\pi m!}}\, z^m e^{-|z|^2/2} \tag{2.9a}$$

$$\epsilon'_m \equiv \epsilon'_{0m} = \hbar\big[\omega_\perp + (\omega_\perp - \Omega)m\big] \tag{2.9b}$$

where $z = (x + \mathrm{i}y)/d_\perp$ is the position in the complex plane; we use $\mathbf{r}$ and z interchangeably. In terms of the corresponding creation and annihilation operators $a_m^\dagger$ and a_m, the second-quantized Hamiltonian in the rotating frame in the LLL manifold is (see also Eq. (B.6) for a general form which includes HLLs as well)

$$\mathcal{H}' = \sum_m \epsilon'_m a_m^\dagger a_m + \frac{1}{2}\sum_{\{m_i\}} \mathrm{V}^{m_4 m_3}_{m_2 m_1}\, a_{m_4}^\dagger a_{m_3}^\dagger a_{m_2} a_{m_1} \tag{2.10}$$

where the interaction matrix element in the LLL is

$$\begin{aligned} \mathrm{V}_{m_2 m_1}^{m_4 m_3} &= \int d^2\mathbf{r}\, d^2\mathbf{r}'\, \phi_{m_4}^*(\mathbf{r})\, \phi_{m_3}^*(\mathbf{r}')\, g_{2\mathrm{D}}\, \delta(\mathbf{r}-\mathbf{r}')\, \phi_{m_2}(\mathbf{r}')\, \phi_{m_1}(\mathbf{r}) \\ &= V_0\, \frac{(m_1+m_2)!}{2^{m_1+m_2}\sqrt{m_4!m_3!m_2!m_1!}}\, \delta_{m_3+m_4,m_1+m_2}. \end{aligned} \tag{2.11}$$

2.3 Bogoliubov Hamiltonian in the lowest Landau level

We now turn to determining the effects of small-amplitude Bogoliubov fluctuations about the mean-field condensate on the properties of the system. We start with a condensate with a vortex at the center which rotates with angular frequency Ω_c, to be determined. We derive an effective LLL Hamiltonian along with its excitation spectrum (which includes an unstable normal mode) and show that its ground state has lower energy than the initial mean-field state in which *all* particles are condensed into the state $|01\rangle$. The initial condensate is

$$\psi(\mathbf{r}) = \sqrt{N_1}\, \phi_1(\mathbf{r}) \tag{2.12}$$

with N_1 particles in $|01\rangle$, describing a vortex at the center with winding number 1. For $N_1 \lesssim N$, we make the usual replacement of the operators $a_1^\dagger$ and a_1, corresponding to $|01\rangle$, by $\sqrt{N_1}$ in the limit of large N. Although the total number of particles is fixed, interactions cause the number of particles in the condensate to fluctuate; the number of condensed particles can, thus, be written in terms of the total and the non-condensed particle numbers as

$$N_1 = N - {\sum_m}' a_m^\dagger a_m \tag{2.13}$$

where the prime indicates that $|01\rangle$ is excluded from the sum.

In the thermodynamic limit ($N \to \infty$ with NV_0 constant), interaction terms that represent scattering of only one condensate particle or no condensate particles are respectively $\mathcal{O}(1/\sqrt{N})$ and $\mathcal{O}(1/N)$ smaller than those that involve two particles from the condensate and, thus, can be ignored. Following the standard procedure, e.g., that denoted in Appendix B, to write the Hamiltonian up to quadratic order in the excitation operators and using Eq. (2.13) to conserve the total number of particles, we derive the LLL Hamiltonian in the rotating frame,

$$\begin{aligned} \mathcal{H}' =& \big[N\hbar(2\omega_\perp - \Omega) + \tfrac{1}{4}N^2V_0\big] + \big[\tfrac{1}{2}NV_0 - \hbar(\omega_\perp - \Omega)\big] a_0^\dagger a_0 \\ &+ \big[\tfrac{1}{4}NV_0 + \hbar(\omega_\perp - \Omega)\big] a_2^\dagger a_2 + \tfrac{1}{\sqrt{8}}NV_0\big(a_0^\dagger a_2^\dagger + a_0 a_2\big). \end{aligned} \tag{2.14}$$

In Appendix B, a more general Bogoliubov Hamiltonian involving HLL states is derived, namely Eq. (B.21). The above equation is just the truncated version of the final result of Appendix B to the smaller LLL manifold. The constant first term in square brackets above is the energy of the mean-field state with all N particles condensed into $|01\rangle$ and no fluctuations present. The only two states in the LLL connected by the interactions in the presence of a condensate in $|01\rangle$ are $|00\rangle$ and $|02\rangle$, i.e., for a LLL system, the maximum angular momentum transferred in any scattering process is ± 1, whereas allowing higher Landau levels brings in and connects $|10\rangle$ and $|12\rangle$, $|20\rangle$ and $|22\rangle$, etc. Larger transfers of angular momentum take the system out of the LLL as well, e.g., $|03\rangle$ is connected to $|1,-1\rangle$ by a transfer of ± 2 units, $|2,-2\rangle$ to $|04\rangle$ by a transfer of ± 3 units, etc.

Conservation of angular momentum is reflected in the fact that any scattering process involves simultaneous transfers of $+m$ and $-m$ units of angular momentum (relative to the condensate). The same method presented here was previously used by Linn and Fetter [91] to include higher Landau levels perturbatively in the Bogoliubov excitation spectrum of this system. Also, Dodd *et al.* [93] have used a similar argument to describe angular momentum conservation in this system in the presence of an external perturbation. Later, Rokhsar reinterpreted their argument to show [94] the existence of a negative energy excitation (the anomalous mode) with vortex core properties similar to those we find in Sec. 2.4.1.

The canonical transformations to the bosonic quasiparticle operators

$$\begin{aligned} \alpha_{+1} &= u\, a_2 + v\, a_0^\dagger \\ \alpha_{-1} &= u\, a_0 + v\, a_2^\dagger \end{aligned} \tag{2.15}$$

(with u and v real and positive) diagonalize the Hamiltonian, provided that $u^2 = 2$ and $v^2 = 1$. The new operators describe quasiparticles with ± 1 units of angular momentum relative to the condensate. Thus, the LLL Hamiltonian in the rotating frame becomes

$$\mathcal{H}' = \left[N\hbar(2\omega_\perp - \Omega) + \tfrac{1}{4}N^2 V_0 - \tfrac{1}{4}NV_0\right] + \hbar\,(\Omega - \Omega_c)\,\alpha_{-1}^\dagger \alpha_{-1} + \hbar\,(\omega_\perp - \Omega)\,\alpha_{+1}^\dagger \alpha_{+1} \tag{2.16}$$

where

$$\Omega_c = \omega_\perp - \frac{1}{4\hbar} NV_0. \tag{2.17}$$

This equation shows that the Bogoliubov ground state (with no excited quasiparticles) has lower energy compared to the mean-field one by $-NV_0/4$. Also, the normal mode denoted by -1 has negative eigenenergy in the region $\Omega < \Omega_c$, indicating an instability in the system against being condensed into $|01\rangle$; this is the anomalous mode (see Ref. [95] and references therein). Its existence shows that $\psi(\mathbf{r})$ is not the correct

condensate for $\Omega < \Omega_c$ and, therefore, the Hamiltonian in Eq. (2.16) is not the correct one for this regime. As the rotation rate increases beyond Ω_c, further LLL states beyond $\{|00\rangle, |01\rangle, |02\rangle\}$ come into play in the ground state, especially once two or more vortices enter the cloud (see Sec. 2.5). Then, one must include Bogoliubov fluctuations around this new ground state in order to find the Bogoliubov Hamiltonian and its normal modes. For simplicity, we limit the discussion here to $\Omega = \Omega_c$ which corresponds to our starting point, a system fully-condensed in $|01\rangle$.

In the manifold of the first three lowest Landau levels, the field operator for removing a particle at position $\mathbf{r}$ is

$$\Psi(\mathbf{r}) = \phi_0(\mathbf{r})\, a_0 + \phi_1(\mathbf{r})\, a_1 + \phi_2(\mathbf{r})\, a_2. \tag{2.18}$$

Inverting Eq. (2.15) gives

$$\begin{aligned} a_0 &= u\,\alpha_{-1} - v\,\alpha_{+1}^\dagger \\ a_2 &= u\,\alpha_{+1} - v\,\alpha_{-1}^\dagger \end{aligned} \tag{2.19}$$

and, thus, the expansion of $\Psi(\mathbf{r})$ in terms of the quasiparticles is

$$\Psi(\mathbf{r}) = \psi(\mathbf{r}) + \Big[u\,\phi_2(\mathbf{r})\,\alpha_{+1} - v\,\phi_0(\mathbf{r})\,\alpha_{+1}^\dagger\Big] + \Big[u\,\phi_0(\mathbf{r})\,\alpha_{-1} - v\,\phi_2(\mathbf{r})\,\alpha_{-1}^\dagger\Big]. \tag{2.20}$$

This is just the mode expansion $\Psi(\mathbf{r}) = \psi(\mathbf{r}) + \sum_j \left[u_j(\mathbf{r})\alpha_j - v_j^*(\mathbf{r})\alpha_j^\dagger\right]$ in terms of the quasiparticles (see, e.g., Ref. [96]). Hence, the amplitudes for the -1 eigenmode are

$$\begin{aligned} u_{-1}(\mathbf{r}) &= u\,\phi_0(\mathbf{r}) \\ v_{-1}(\mathbf{r}) &= v\,\phi_2^*(\mathbf{r}). \end{aligned} \tag{2.21}$$

This mode, although having a negative eigenenergy for $\Omega < \Omega_c$, has a positive norm, since

$$\int d^2\mathbf{r}\big[\,|u_{-1}(\mathbf{r})|^2 - |v_{-1}(\mathbf{r})|^2\,\big] = u^2 - v^2 = 1, \tag{2.22}$$

and is thus physical. Since $\langle \mathbf{r}\,|02\rangle^* = \langle \mathbf{r}\,|2,-2\rangle$, we arrive at the same amplitudes as derived up to zeroth order in V_0 in Sec. III of Ref. [91]. We note, however, that the only two states that are mixed, in fact, are $|00\rangle$ and $|02\rangle$ which are in the LLL, and not $|2,-2\rangle$ which is a higher Landau level; up to the level of the approximation used in this article, the fluctuations reside solely in the LLL.

2.4 The Bogoliubov Ground State

We now find the stable ground state of the Hamiltonian (2.16) for $\Omega = \Omega_c$. The order parameter is

$$\psi(\mathbf{r}) = \langle \Psi(\mathbf{r}) \rangle \tag{2.23}$$

or, in terms of annihilation operators, $\langle a_1 \rangle = \sqrt{N_1}$ for the macroscopic condensate with N_1 particles in $|01\rangle$. The condensed state $|N_1\rangle$ is a coherent state that satisfies the eigenvalue equation

$$a_1 |N_1\rangle = \sqrt{N_1}\, |N_1\rangle \tag{2.24}$$

with the normalized solution

$$|N_1\rangle = e^{-N_1/2} \exp\left[\sqrt{N_1}\, a_1^\dagger\right] |\text{vac}\rangle \tag{2.25}$$

where $|\text{vac}\rangle$ is the vacuum. This state does not conserve particle number.

The Bogoliubov ground state is defined by the condition that no quasiparticles be present, i.e.,

$$\alpha_{\pm 1} |\text{G}\rangle = 0. \tag{2.26}$$

We can expand $|\text{G}\rangle$ in terms of the unperturbed (non-interacting) states $|n_{-1} n_{+1}\rangle$ in which there are n_{-1} particles with -1 units of angular momentum relative to the condensate (in $|00\rangle$) and n_{+1} particles with $+1$ units of angular momentum relative to the condensate (in $|02\rangle$) in addition to all the condensed particles, N_1, in $|01\rangle$. We, thus, write [10]

$$|\text{G}\rangle = \sum_{n_{-1} n_{+1}} C_{n_{-1} n_{+1}} |n_{-1} n_{+1}\rangle \tag{2.27}$$

with the coefficients $C_{n_{-1} n_{+1}}$ to be determined. Due to the way the Hamiltonian in Eq. (2.14) is derived, only states with relative ± 1 units of angular momentum are present in the expansion. Plugging Eq. (2.27) in Eq. (2.26) and using Eq. (2.15) leads to the following equation for the coefficients

$$\sum_{nm} C_{nm} \left(u\sqrt{n}\, |n-1, m\rangle + v\sqrt{m+1}\, |n, m+1\rangle \right) = 0. \tag{2.28}$$

Changing the indices of summation for both terms leads to

$$\sum_{nm} \left(u\sqrt{n+1}\, C_{n+1,m} + v\sqrt{m}\, C_{n,m-1} \right) |nm\rangle = 0. \tag{2.29}$$

Since this equation has to be satisfied for all $|nm\rangle$, we need

$$u\sqrt{n+1}\,C_{n+1,m} + v\sqrt{m}\,C_{n,m-1} = 0. \tag{2.30}$$

Assume, for the moment, that $m = 0$. This means $\sqrt{n+1}\,C_{n+1,0} = 0$, or, in other words, $C_{n+1,0} = 0$ if $n + 1 \neq 0 = m$. Hence, for $m = 0$, we have $C_{nm} = 0$ for $n \neq m$, and it can be proved by induction [10] that it is also true for any m. Therefore, only the diagonal elements are non-zero, and after substituting $n \to m - 1$, we end up with the recursive equation $u\sqrt{m}\,C_{mm} + v\sqrt{m}\,C_{m-1,m-1} = 0$ with the solution

$$C_{mm} = \left(-\frac{v}{u}\right)^m C_{00}. \tag{2.31}$$

Thus, the Bogoliubov ground state expansion can be written, using the values of u and v determined previously, as

$$|\mathrm{G}\rangle = C_{00}\sum_m \left(-\tfrac{1}{\sqrt{2}}\right)^m |mm\rangle = C_{00}\sum_m \left(-\tfrac{1}{\sqrt{2}}\right)^m \left[\frac{\left(a_2^\dagger\right)^m}{\sqrt{m!}}\frac{\left(a_0^\dagger\right)^m}{\sqrt{m!}}\right]|N_1\rangle = C_{00}\,\exp\left[-\frac{1}{\sqrt{2}}\,a_2^\dagger a_0^\dagger\right]|N_1\rangle\,. \tag{2.32}$$

Note that in the expansion above, the term corresponding to $m = 0$ is just the state $C_{00}\,|N_1\rangle$ with no particles excited into $|00\rangle$ or $|02\rangle$. All other terms represent states that include some particles out of the condensate and, hence, are orthogonal to the condensed state. Thus, we have $\langle N_1|\,\mathrm{G}\rangle = C_{00}$. In order to determine the numerical value of C_{00} to normalize the Bogoliubov ground state, we write

$$\langle \mathrm{G}|\,\mathrm{G}\rangle = C_{00}^2\sum_{mm'}\left(-\tfrac{1}{\sqrt{2}}\right)^{m+m'}\overbrace{\langle m'm'|\,mm\rangle}^{\delta_{mm'}} = C_{00}^2\sum_{m=0}^{\infty}\left(\frac{1}{2}\right)^m = 2C_{00}^2. \tag{2.33}$$

Therefore, the normalization constant is $C_{00} = 1/\sqrt{2}$, and the normalized Bogoliubov ground state becomes

$$|\mathrm{G}\rangle = \frac{1}{\sqrt{2}}\,\exp\left[-\frac{1}{\sqrt{2}}\,a_2^\dagger a_0^\dagger\right]|N_1\rangle \tag{2.34}$$

which has an expectation value of the angular momentum operator $\mathcal{L} = \sum_m \hbar m\, a_m^\dagger a_m$ given by

$$\langle \mathrm{G}|\,\mathcal{L}\,|\mathrm{G}\rangle = N\hbar. \tag{2.35}$$

2.4.1 Properties of the Bogoliubov Ground State

Here, we investigate the energetics of the new ground state and show that fluctuations drive the vortex away from the center of the trap and modify its velocity profile.

We first compare the lab-frame energy of $|\mathrm{G}\rangle$ with that of the mean-field and exact ground states. The exact non-normalized many-body ground state for $2 \leq L \leq N$ is [36]

$$\psi_{\mathrm{x}}^{L}(z_1 \dots z_N) = \sum_{i_1<i_2<\cdots<i_L} (z_{i_1} - z_c)(z_{i_2} - z_c)\cdots(z_{i_L} - z_c) \tag{2.36}$$

where $z_c = \sum_{i=1}^{N} z_i/N$ is the center-of-mass coordinate; we suppress the factor $\exp[-\sum_{k=1}^{N} |z_k|^2/2]$ common to all N-particle LLL states from now on for brevity. This state has energy [36]

$$E_{\mathrm{x}}^{L} = (N+L)\hbar\omega_{\perp} + V_0 N(N-1-L/2)/2 \tag{2.37}$$

in the lab frame. The mean-field ground state for $L = N$ with a vortex at origin,

$$\psi_{\mathrm{mf}}(z_1 \dots z_N) = \prod_{i=1}^{N} \phi_1(z_i), \tag{2.38}$$

has energy

$$E_{\mathrm{mf}} = 2N\hbar\omega_{\perp} + V_0 N^2/4 \tag{2.39}$$

in the lab frame. Therefore, at $L = N$ (and, hence, at $\Omega = \Omega_c$), the Bogoliubov ground state lies exactly half-way in energy between the mean-field ground state and the exact one.

A diagnostic of the structure of the vortex is the circulation around a closed contour $\mathcal{C}$ encircling the center of the trap,

$$\Gamma = \oint_{\mathcal{C}} \mathbf{v}(\mathbf{r}) \cdot d\mathbf{r}, \tag{2.40}$$

quantized in units of $2\pi\hbar/m$ for a quantum vortex. The velocity is

$$\mathbf{v}(\mathbf{r}) = \frac{\langle \mathbf{j}(\mathbf{r}) \rangle}{\langle \rho(\mathbf{r}) \rangle} \tag{2.41}$$

where $\langle \mathbf{j}(\mathbf{r}) \rangle = (\hbar/m)\mathrm{Im}\left\langle \Psi^{\dagger}(\mathbf{r}) \boldsymbol{\nabla} \Psi(\mathbf{r}) \right\rangle$ is the expectation value of the current operator and $\langle \rho(\mathbf{r}) \rangle = \left\langle \Psi^{\dagger}(\mathbf{r})\Psi(\mathbf{r}) \right\rangle$ is that of the density operator. In the mean-field state, (2.38), we have

$$\mathbf{v}_{\mathrm{mf}}(\mathbf{r}) = \frac{\hbar}{m}\frac{\hat{\boldsymbol{\theta}}}{r} \tag{2.42}$$

which describes an irrotational superflow (except at the origin where the vortex is located) with circulation

$$\Gamma_{\rm mf} = \frac{2\pi\hbar}{m}. \tag{2.43}$$

However, the Bogoliubov ground state, (2.34), gives

$$\langle \mathbf{j}(z)\rangle = \frac{\hbar}{m}\left[N\left(1-\frac{2}{N}+\frac{3}{N^2}\right)+|z|^2\right]|z|\ \frac{e^{-|z|^2}}{\pi d_\perp^2}\,\hat{\boldsymbol{\theta}}, \tag{2.44}$$

$$\langle \rho(z)\rangle = \left[1+N\left(1-\frac{2}{N}+\frac{3}{N^2}\right)|z|^2+\frac{|z|^4}{2}\right]\frac{e^{-|z|^2}}{\pi d_\perp^2}. \tag{2.45}$$

Thus, in the limit of large N, the velocity field is

$$\mathbf{v}_{\rm G}(\mathbf{r}) = \frac{\hbar}{m}\,\frac{r\hat{\boldsymbol{\theta}}}{r^2+\Delta(r)} \tag{2.46}$$

where $\Delta(r) = (1-\frac{1}{2}r^4)/(N+r^2)$ is the correction due to quantum fluctuations. The circulation in $|{\rm G}\rangle$ is then

$$\Gamma_{\rm G}(\mathbf{r}) = \Gamma_{\rm mf}\times\frac{r^4+Nr^2}{\frac{1}{2}r^4+Nr^2+1}. \tag{2.47}$$

For large but finite N, we now find three regimes:

- As $r\to 0$, we have $\Gamma_{\rm G}/\Gamma_{\rm mf}\to 0$.
- For the large range $1/\sqrt{N}\lesssim r\lesssim\sqrt{N}$, we have $\Gamma_{\rm G}/\Gamma_{\rm mf}\sim 1$ (increasing from 1/2 to 4/3).
- As $r\to\infty$, we have $\Gamma_{\rm G}/\Gamma_{\rm mf}\to 2$.

The vortex (at the center of the trap in the mean-field model) is now pushed off-center by quantum fluctuations, hence the vanishing circulation as the contour shrinks towards the origin. The off-center vortex fluctuates very close about the origin as shown by the circulation approaching its mean-field value as the contour radius expands past $\mathcal{O}(1/\sqrt{N})$. On the other hand, as the contour expands even further towards infinity, the circulation grows to twice its mean-field value, indicating the presence of an image vortex (with the same sense of rotation) much further from the origin. These results agree with those of Sec. 2.5. In the thermodynamic limit ($N\to\infty$), however, $\Gamma_{\rm G}$ equals the quantum of circulation everywhere except at the origin (where it is zero) and at infinity (where it is twice the quantum of circulation); therefore, increasing number of particles suppresses quantum fluctuations of the vortex and leads to the vortex being driven less further from the center of the trap and the image vortex being driven more outward to infinity.

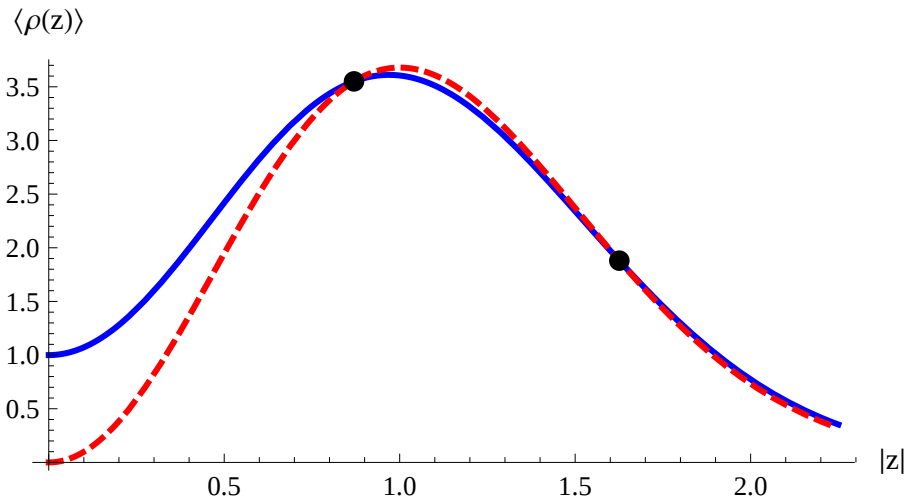

Figure 2.2: Density (in units of $1/\pi d_\perp^2$) of the Bogoliubov (solid line) and mean-field (dashed line) ground states for $N = 10$, showing a vortex at the center. The black dots denote the positions at which the two densities are equal.

Quantum fluctuations change the particle density of the ground state compared to its mean-field value

$$\rho_{\rm mf} = \frac{N}{\pi d_\perp^2}\,|z|^2\,e^{-|z|^2}. \tag{2.48}$$

The average density is now non-zero at the center of the trap, and we find

$$\langle\rho(0)\rangle = \frac{1}{\pi d_\perp^2} \tag{2.49}$$

(see Fig. 2.2). One can understand this finite density in terms of the vortex fluctuating about the origin, as discussed above. Snapshots of the cloud in the laboratory would reveal a vortex at random positions (varying from shot to shot due to Bogoliubov fluctuations); averaging over these density snapshots would lead to Eq. (2.45) for the average particle density of $|{\rm G}\rangle$. One can also understand the finite density at the origin in terms of the single-particle quantum states, in particular, the non-zero occupation of $|00\rangle$ whose wave function does not vanish at the origin.

2.5 The Stable Condensate

The anomalous mode, denoted by -1 in Eq. (2.16), suggests that a condensate with a singly-quantized vortex at the center of the trap is not stable against fluctuations for $\Omega < \Omega_c$. However, Eqs. (2.20) and (2.21) indicate that a mean-field condensate wave function of the form

$$\psi(z) = \sqrt{N_1}\,\phi_1(z) + u\,\phi_0(z) - v\,\phi_2(z) \tag{2.50}$$

can have lower energy and be stable, depending on the values of u and v (which can be taken to be real). We search for a better ground state by tuning the two extra degrees of freedom, u and v, as follows.

Normalizing $\psi(z)$ leads to $N = N_1 + u^2 + v^2$; hence, u and v are bounded by

$$u^2 + v^2 \leq N. \tag{2.51}$$

The energy in the rotating frame, then, becomes

$$\begin{aligned} E' =& \Big[N\hbar(2\omega_\perp - \Omega) + \frac{1}{4}N^2V_0\Big] + \Big\{\Big[\hbar(\Omega - \omega_\perp) + \frac{NV_0}{2}\Big]u^2 + \Big[\hbar(\omega_\perp - \Omega) + \frac{NV_0}{4}\Big]v^2 - \frac{NV_0}{\sqrt{2}}uv\Big\} \\ &+ V_0\Big(-\frac{1}{4}u^4 - \frac{5}{16}v^4 - \frac{3}{4}u^2v^2 + \frac{1}{\sqrt{2}}u^3v + \frac{1}{\sqrt{2}}uv^3\Big). \end{aligned} \tag{2.52}$$

The constant term is the energy of a condensate with N particles in $|01\rangle$. Note that E' is invariant under the simultaneous transformation $u \to -u$ and $v \to -v$. We choose $0 \leq v \leq u$ as this sector of the u–v plane is energetically favorable.

We denote

$$\tilde{E}' = E' - \big[N\hbar(2\omega_\perp - \Omega) + N^2V_0/4\big] \tag{2.53}$$

as the energy contribution from the mixing of $|00\rangle$ and $|02\rangle$ with the condensate. Then, introducing the parametrization $u = \zeta\cosh(\theta/2)$ and $v = \zeta\sinh(\theta/2)$, we find

$$\begin{aligned} \tilde{E}' =& \zeta^2\Big\{\Big[\hbar(\Omega - \omega_\perp) + \frac{NV_0}{8}\Big] + \frac{NV_0}{8}\big(3\cosh\theta - \sqrt{8}\sinh\theta\big)\Big\} \\ &+ \zeta^4\Big\{\frac{V_0}{128}\big[-15 + 4\cosh\theta - 21\cosh(2\theta) + 16\sqrt{2}\sinh(2\theta)\big]\Big\}. \end{aligned} \tag{2.54}$$

Ignoring the quartic part for now, i.e., assuming $u, v \ll \sqrt{N_1}$ or $N_1 \lesssim N$, we minimize the quadratic part with respect to θ and find

$$\tanh\theta_m = \frac{\sqrt{8}}{3} \tag{2.55}$$

which is depicted by the straight dashed line in the u–v plane in Fig. 2.3. With this value of θ, we have

$$\tilde{E}' = \hbar(\Omega - \Omega_c)\zeta^2 + \frac{3V_0}{16}\,\zeta^4. \tag{2.56}$$

The quadratic term shows that up to second order in the mixing due to interactions, the system is unstable for $\Omega < \Omega_c$, similar to the quantum treatment.

For $\Omega > \Omega_c$, Eq. (2.56) is a monotonically increasing function of ζ with a minimum at $\zeta = 0$ or

$$u_m^> = v_m^> = 0, \tag{2.57}$$

describing a system fully condensed into $|01\rangle$ with one vortex at the center of the trap. (The superscripts "<" or ">" denote rotations slower or faster than Ω_c.) The energy in the rotating frame becomes

$$E_m'^> = \left(N\hbar\omega_\perp + \frac{1}{2}N^2V_0\right) + N\hbar(\Omega_c - \Omega) \tag{2.58}$$

where the first term is just the energy were all N particles condensed into $|00\rangle$. For $\Omega \leq \Omega_c$, though, minimizing Eq. (2.56) gives

$$\begin{aligned} u_m^< &= \sqrt{\frac{16\hbar(\Omega_c - \Omega)}{3V_0}} \\ v_m^< &= \sqrt{\frac{8\hbar(\Omega_c - \Omega)}{3V_0}} \end{aligned} \tag{2.59}$$

so that $u_m^< = \sqrt{2}\, v_m^<$, and the rotating-frame energy becomes

$$E_m'^< = \left(N\hbar\omega_\perp + \frac{1}{2}N^2V_0\right) + N\hbar(\Omega_c - \Omega) - \frac{4\hbar^2(\Omega_c - \Omega)^2}{3V_0}. \tag{2.60}$$

The boundedness of u and v implies $0 \leq \zeta_m^2 \cosh\theta_m \leq N$. Hence, the region of validity of Eqs. (2.59) and (2.60) is $\Omega_m \leq \Omega \leq \Omega_c$ where

$$\Omega_m = \omega - \frac{3}{8\hbar}NV_0. \tag{2.61}$$

Then, for $\Omega < \Omega_m$, the point $(u_m^<, v_m^<)$ lies outside the circle defined by $u^2 + v^2 = N$ and does not represent a physical solution.

In order to check for the existence of lower-energy states on the edge of the circle, where $u^2 + v^2 = N$, we have to compare $E_m'^{\lessgtr}$ with the corresponding energy $E_e'^{\lessgtr}$ for points on the edge. Since $N_1 = 0$ on the edge, we find

$$E_e' = \left(N\hbar\omega_\perp + \frac{1}{2}N^2V_0\right) + 2\hbar(\Omega_c - \Omega)v^2 + \frac{3V_0}{16}\, v^4. \tag{2.62}$$

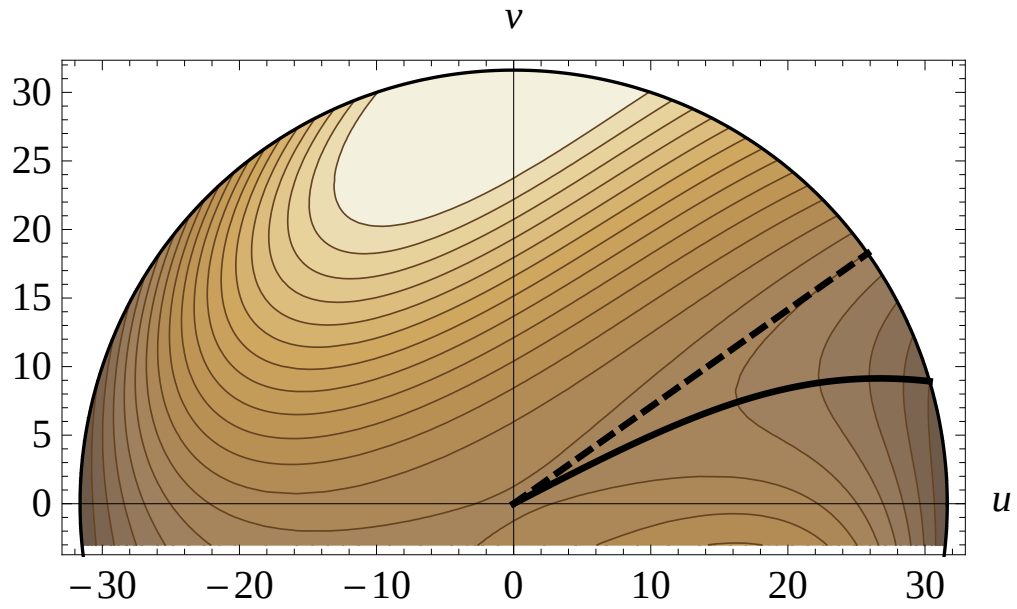

Figure 2.3: Contour plot of E' for $N = 10^3$, $NV_0 = 0.1\,\hbar\omega_\perp$, and $\Omega = \omega_\perp - \frac{3}{8\hbar}NV_0$. Darker shades indicate lower energies. The straight dashed line represents the direction given by $\tanh\theta_m = \sqrt{8}/3$ whereas the curved solid line is the solution of Eq. (2.80), discussed below.

For $\Omega \leq \Omega_c$, this energy increases monotonically with v, with the minimum at

$$\begin{aligned} u_e^< &= \sqrt{N} \\ v_e^< &= 0 \end{aligned} \tag{2.63}$$

representing a system fully condensed into $|00\rangle$ (with no vortex) with the rotating-frame energy

$$E_e'^< = N\hbar\omega_\perp + \frac{1}{2}N^2V_0. \tag{2.64}$$

For $\Omega > \Omega_c$, however, the minimum is at

$$\begin{aligned} u_e^> &= \sqrt{N - \frac{16\hbar(\Omega-\Omega_c)}{3V_0}} \\ v_e^> &= \sqrt{\frac{16\hbar(\Omega-\Omega_c)}{3V_0}}, \end{aligned} \tag{2.65}$$

and the energy in the rotating frame is

$$E_e'^> = \left(N\hbar\omega_\perp + \frac{1}{2}N^2V_0\right) - \frac{16\hbar^2(\Omega-\Omega_c)^2}{3V_0}. \tag{2.66}$$

Therefore, for $\Omega_m \leq \Omega \leq \Omega_c$, the difference between the two energies is

$$E_m'^{<} - E_e'^{<} = \frac{4\hbar^2}{3V_0}(\Omega_c - \Omega)(\Omega - \Omega_1^*) \tag{2.67}$$

where $\Omega_1^* = \omega_\perp - \frac{1}{\hbar}NV_0$. Since $\Omega_1^* < \Omega_m$, we find that the point $(u = \sqrt{N}, v = 0)$ corresponds to the *global* minimum of the energy for the entire region $0 \leq \Omega \leq \Omega_c$, indicating that the system has fully condensed into $|00\rangle$ with no vortex, whereas a *local* minimum of the energy appears at $(u = u_m^<, v = v_m^<)$ for $\Omega_m \leq \Omega \leq \Omega_c$. This latter point corresponds to a metastable state which describes two vortices (asymmetric with respect to the origin) in the condensate; hence, the metastability frequency Ω_m is the rotation frequency at which a metastable state appears in the energy spectrum. On the other hand, for $\Omega > \Omega_c$, the difference between the two energies is

$$E_m'^{>} - E_e'^{>} = \frac{16\hbar^2}{3V_0}(\Omega - \Omega_c)(\Omega - \Omega_2^*) \tag{2.68}$$

where

$$\Omega_2^* = \omega_\perp - \frac{1}{16\hbar}NV_0. \tag{2.69}$$

Thus, if $\Omega_c < \Omega \leq \Omega_2^*$, the point $(u = 0, v = 0)$, i.e., the center of the circle, corresponds to the *global* minimum of the energy, indicating that the system has fully condensed into $|01\rangle$ with one vortex at the center. For $\Omega > \Omega_2^*$, however, the *global* minimum of the energy is at $(u = u_e^>, v = v_e^>)$ on the edge of the circle, and the ground state is a coherent superposition of $|00\rangle$ and $|02\rangle$ with two vortices in a symmetric configuration with respect to the origin.

Hence, Ω_c is the critical frequency for creating a centered vortex, and Ω_2^* is the critical frequency at which two vortices nucleate in the condensate. Note that Ω_c agrees with the external rotation frequency derived in Refs. [91, 28]; however, Ω_2^* is bigger than the two-vortex nucleation frequency, $\omega_\perp - \frac{0.078}{\hbar}NV_0$, calculated numerically in Ref. [28] due to the very limited Hilbert space used here with only $\{|00\rangle, |01\rangle, |02\rangle\}$ as opposed to a rather large one used in Ref. [28].

The metastable state, for which $u_m^< = \sqrt{2}\, v_m^<$, has two vortices at the zeroes of $\psi(z)$, i.e.,

$$z_m^{\pm}(\Omega) = \frac{\sqrt{N - 3(v_m^<)^2} \pm \sqrt{N + (v_m^<)^2}}{\sqrt{2}\, v_m^<} \tag{2.70}$$

where Ω enters through $v_m^<$ on the right side. Using Eq. (2.59), we find $v_m^< = \sqrt{N/3}$ at $\Omega = \Omega_m$. Hence,

$$z_m^{\pm}(\Omega_m) = \pm\sqrt{2}. \tag{2.71}$$

However, as Ω increases towards Ω_c, we find for small $v_m^<$ that

$$z_m^\pm \to \pm\sqrt{2}(v_m^</\sqrt{N})^{\mp 1} \tag{2.72}$$

or, in other words, $z_m^+ \to +\infty$ whereas $z_m^- \to 0$. As Ω increases from Ω_m to Ω_c, the vortex at $+\sqrt{2}$ moves to infinity while the one at $-\sqrt{2}$ reaches the center and becomes stable there.

It is instructive to compare this result to that of Ref. [92], where the authors assume a condensate with an off-center vortex at position b close to the center, i.e., $\chi(z) \sim \sqrt{N}(z-b)$, and find perturbative corrections to the wave function using the Gross-Pitaevskii equation. Their new non-normalized wave function in the LLL up to $\mathcal{O}(b^2)$ is $\chi(z) \sim \sqrt{N}(z-b)(1+bz/2+\cdots)$ (see Eq. (15) of Ref. [92]) with the rotation frequency, to lowest order in b, being $\Omega \simeq \Omega_c$ (see Eq. (16) of Ref. [92]). This wave function represents two vortices at positions b and $-2/b$. Normalizing this wave function up to $\mathcal{O}(b^2)$ leads to

$$\chi(z) \sim \sqrt{N}\left[\frac{b}{2}z^2 + \Big(1 - \frac{3}{4}b^2\Big)z - b\right]. \tag{2.73}$$

We can repeat a similar procedure for the metastable state for which $u_m^< = \sqrt{2}\, v_m^<$. Then, the condensate wave function, Eq. (2.50), becomes

$$\psi(z) \sim \sqrt{N_1}\, z + u_m^< - \frac{u_m^<}{2}\, z^2. \tag{2.74}$$

Expanding for small $u_m^<$ and defining $\mathfrak{b} = -u_m^</\sqrt{N}$, we have

$$\psi(z) \sim \sqrt{N}\Big[\frac{\mathfrak{b}}{2}z^2 + \Big(1 - \frac{3}{4}\mathfrak{b}^2\Big)z - \mathfrak{b}\Big]. \tag{2.75}$$

Thus, $\chi(z)$ and $\psi(z)$ have the same form with $b \leftrightarrow \mathfrak{b}$. Since $\mathfrak{b}$ is small, $\psi(z)$ also represents two off-center vortices at positions $\mathfrak{b}$ (close to the origin) and $-2/\mathfrak{b}$ (much further away in the evanescent tail of the cloud). Using Eq. (2.59), we find the rotation rate of this two-vortex configuration in the lab frame to be

$$\Omega = \Omega_c - \frac{3}{16\hbar} N V_0 \, |\mathfrak{b}|^2 \tag{2.76}$$

which includes the next-order correction of $\mathcal{O}(|\mathfrak{b}|^2)$ to the result of Ref. [92]. Note that while the calculations of Ref. [92] are limited to the fast rotating regime and are valid only in the vicinity of Ω_c (due to their perturbative nature in the small parameter $\Omega - \omega_\perp$), the method presented here covers the entire region $0 \le \Omega \le \omega_\perp$ and is only limited by the number of states included in the condensate wave function.

2.5.1 The Energy Valley and the Metastable Point

The derivation of the local minimum of the energy in the metastable regime, $\Omega_m \leq \Omega \leq \Omega_c$, has so far been restricted to small values of u and v, i.e., when $\Omega \to \Omega_c$ according to Eq. (2.59). Ignoring the quartic term in Eq. (2.54) leads to a constant θ_m, representing a straight line in the u–v plane which the local minimum traverses as Ω varies. Including the quartic terms causes the valley in the energy landscape to curve, as shown in Fig. 2.3. In this section, we rederive the metastable state and its onset frequency, Ω_m, for larger values of u and v, keeping the quartic terms in the energy.

We first determine the equation governing the valley in the energy landscape. The valley is defined as a set of points, denoted here by $v(u)$, at which the change in the energy is extremum along (at least) one direction. We define

$$u = R\cos\eta \tag{2.77}$$

$$v = R\sin\eta \tag{2.78}$$

and write $\delta E' = E'(u+\delta u, v+\delta v) - E'(u,v) \simeq (\delta u\,\partial_u E' + \delta v\,\partial_v E')$. We find the direction that extremizes the change in the energy by keeping R constant while varying η; thus, $\delta u = -R\sin\eta\,\delta\eta$ and $\delta v = R\cos\eta\,\delta\eta$. Then, $\delta E'/\delta\eta = R(-\sin\eta\,\partial_u E' + \cos\eta\,\partial_v E') = 0$ which gives

$$\partial_v E'/\partial_u E' = \tan\eta = \delta v/\delta u \tag{2.79}$$

where the last equality is just the slope of the tangent to the curve $v(u)$, which can be seen by keeping the direction, η, fixed while varying R. Therefore, the differential equation for the bottom of the energy valley is

$$\frac{dv}{du} = \frac{\partial_v E'}{\partial_u E'} \qquad \text{with} \qquad v(u=0) = 0. \tag{2.80}$$

Its solution for $\Omega = \omega_\perp - \frac{3}{8\hbar}NV_0$ is the solid line in Fig. 2.3.

We rewrite $\tilde{E}'$ from Eq. (2.54) as $\zeta^2 A(\theta) + \zeta^4 B(\theta)$ where

$$A(\theta) = \frac{NV_0}{8}\left[\tilde{\Omega} + (3\cosh\theta - \sqrt{8}\sinh\theta)\right] \tag{2.81}$$

$$B(\theta) = \frac{V_0}{128}\left[-15 + 4\cosh\theta - 21\cosh(2\theta) + 16\sqrt{2}\sinh(2\theta)\right] \tag{2.82}$$

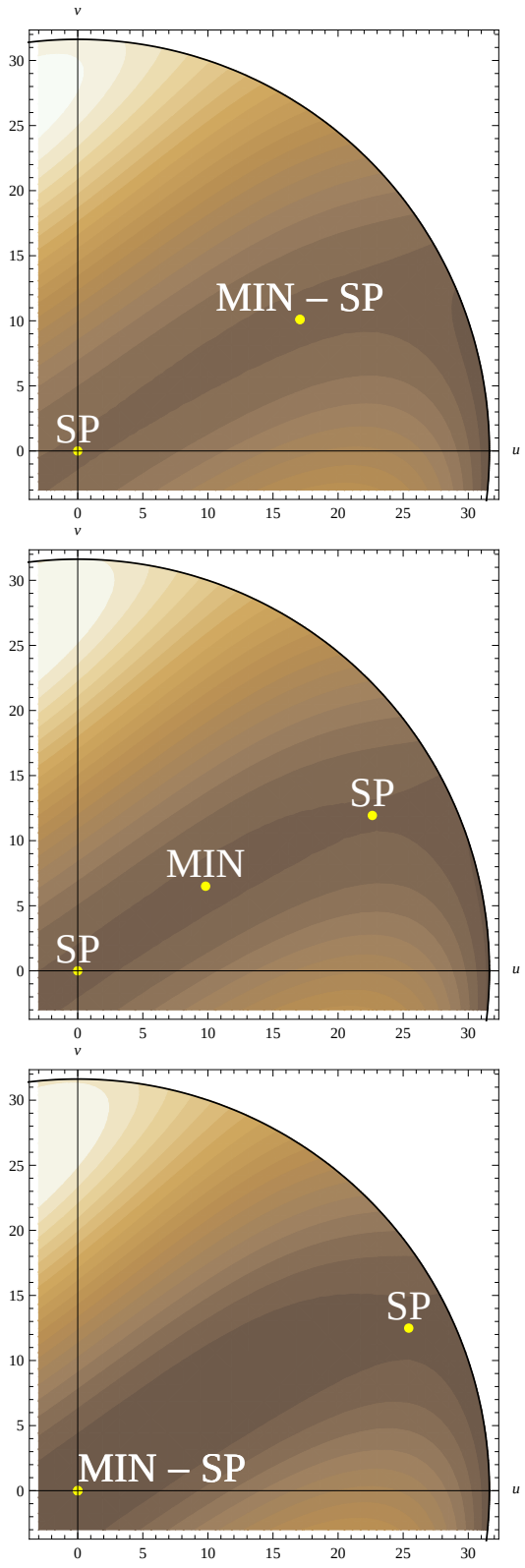

Figure 2.4: Energy landscapes for $\Omega = \omega_\perp - (2.1824/8\hbar)NV_0$ (top), $\omega_\perp - (2.1094/8\hbar)NV_0$ (middle), and $\omega_\perp - (1/4\hbar)NV_0$ (bottom), for $N = 10^3$ and $NV_0 = 0.1\,\hbar\omega_\perp$. The dots represent the critical points with `SP` and `MIN` indicating the saddle-points and minima respectively.

with

$$\tilde{\Omega} = \frac{\hbar(\Omega - \omega_\perp) + \frac{1}{8}NV_0}{\frac{1}{8}NV_0}. \tag{2.83}$$

At the critical points, $\partial\tilde{E}'/\partial\zeta = \partial\tilde{E}'/\partial\theta = 0$. The trivial solution, $\zeta = 0$, represents the center of the circle. Then, assuming $\zeta \neq 0$, we find

$$\frac{1}{A}\frac{\partial A}{\partial\theta} = \frac{1}{2B}\frac{\partial B}{\partial\theta} \tag{2.84}$$

which gives the critical points for all values of Ω.

For small Ω, the only critical point in the valley is at the origin. However, Fig. 2.4 shows that as Ω increases towards Ω_c, two other critical points (a saddle-point and a minimum of the energy) appear in the valley. It is also evident that the minimum moves towards the center as Ω increases. Thus, there should be a rotation frequency, namely the metastability frequency Ω_m, at which the saddle-point and the minimum lie on top of each other and, hence, the second derivative of the energy vanishes. Using Eq. (2.84), we find that at Ω_m,

$$\frac{1}{A}\frac{\partial^2 A}{\partial\theta^2} = \frac{1}{2B}\frac{\partial^2 B}{\partial\theta^2} - \left(\frac{1}{2B}\frac{\partial B}{\partial\theta}\right)^2. \tag{2.85}$$

The single critical point (apart from the origin) at Ω_m satisfies both Eqs. (2.84) and (2.85). Dividing Eq. (2.85) by Eq. (2.84) leads to an equation for θ independent of any other variable, namely

$$\frac{\partial^2 A/\partial\theta^2}{\partial A/\partial\theta} = \frac{\partial^2 B/\partial\theta^2}{\partial B/\partial\theta} - \frac{1}{2}\frac{\partial B/\partial\theta}{B}, \tag{2.86}$$

which, after some algebra, simplifies to

$$6\sqrt{2} + 55\sqrt{2}\cosh\theta - 48\sinh\theta + 42\sqrt{2}\cosh(2\theta) - 64\sinh(2\theta) - 103\sqrt{2}\cosh(3\theta) + 144\sinh(3\theta) = 0. \tag{2.87}$$

The solution is (using `MATHEMATICA`)

$$\begin{aligned}\cosh\theta_m = \frac{1}{241}\Bigg[& 50 + \sqrt{19129 + 6748\sqrt[3]{12} - 11568\sqrt[3]{18}} \\ & + \sqrt{2}\sqrt{19129 - 3374\sqrt[3]{12} + 5784\sqrt[3]{18} + \frac{3114605}{\sqrt{19129 + 6748\sqrt[3]{12} - 11568\sqrt[3]{18}}}}\Bigg] \\ \simeq\ & 2.0776\end{aligned} \tag{2.88}$$

at Ω_m or, using Eq. (2.84), $\tilde{\Omega}_m \simeq -1.1824$. Therefore, the frequency at which the first metastable state

appears is, in fact,

$$\Omega_m = \omega - \frac{2.1824}{8} N V_0 \tag{2.89}$$

which is much closer to the critical frequency Ω_c compared to the frequency given by Eq. (2.61). Contour plots of energy for rotation frequencies Ω_m and Ω_c can be seen in the top and bottom panels of Fig. 2.4, showing that the saddle-point at the origin (for $\Omega < \Omega_c$) turns into a minimum for $\Omega > \Omega_c$. Since the approximations of the previous section are valid for $\Omega \lesssim \Omega_c$, the minimum approaches the origin following the line $v = u/\sqrt{2}$, i.e., the slope of the valley at the origin is $1/\sqrt{2}$ near Ω_c.

The metastable state located at (u_m, v_m) represents two off-center vortices at the zeros of the condensate wave function, $z_m^{\pm}$, which satisfy

$$\frac{v_m}{\sqrt{2}} {z_m^{\pm}}^2 - \sqrt{N - (u_m^2 + v_m^2)}\, z_m^{\pm} - u_m = 0. \tag{2.90}$$

The positions of the two roots of this equation as functions of Ω are plotted in Fig. 2.5 for the metastable regime, $\Omega_m \leq \Omega \leq \Omega_c$. Just as before, one vortex approaches the center of the trap while the other moves to infinity as Ω increases. However, their initial positions are not symmetric with respect to the origin but are at $z_m^-(\Omega_m) = -0.5917$ and $z_m^+(\Omega_m) = +4.2506$ for the particular values of N and V_0 used in the figure. Since the vortices are stationary in the rotating frame, they precess around the origin with frequency Ω in the lab frame. Therefore, as seen in the lab frame, z_m^- spirals in towards the center of the trap while z_m^+ spirals out to infinity as Ω increases.

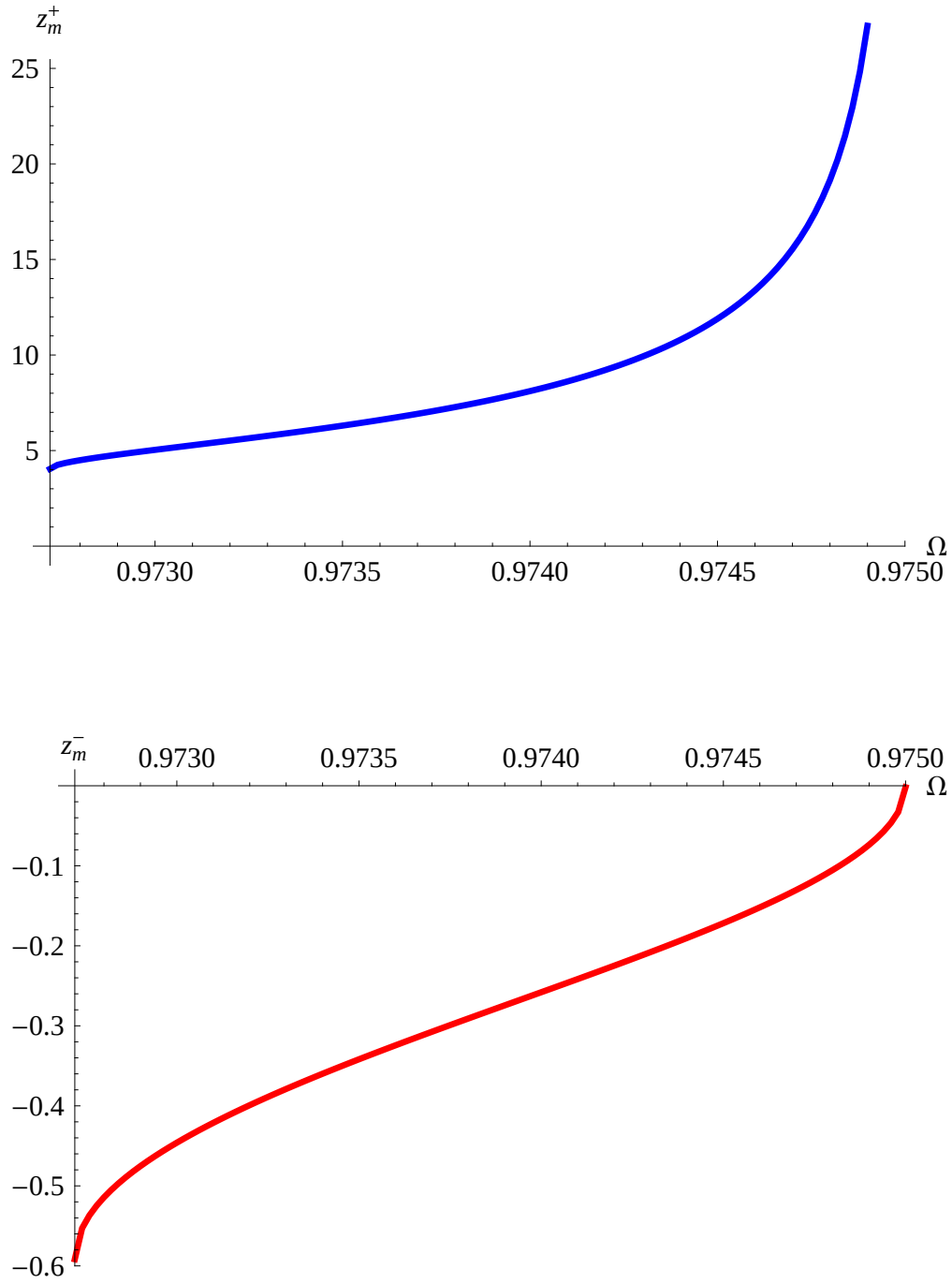

Figure 2.5: The position of the two off-center vortices for $N = 10^3$, $NV_0 = 0.1\,\hbar\omega_\perp$, and $\Omega_m \leq \Omega \leq \Omega_c$. Note the different vertical scales for z_m^+ and z_m^-.

Chapter 3

Correlations in lowest-Landau-level vortex states

3.1 Introduction

With increasing rotation, the ground state of an ultracold gas of bosons in a harmonic trap undergoes a transition from a vortex lattice with broken rotational symmetry, for which mean-field theory provides a good description (see Ref. [15] and references therein), to a series of symmetry-restored and strongly correlated states [45], bosonic analogs of quantum Hall states [40, 41, 86, 87, 88]. This transition is mediated by the correlations present in the interacting system which are absent in mean-field theory. Towards understanding how these correlations lead to more favorable states, we studied in Ref. [31] a condensate with a single vortex; including Bogoliubov fluctuations around the mean-field ground state, we showed that the correlations induced by these fluctuations lower the energy of the Bogoliubov ground state compared to that of the mean-field ground state and cause an uncertainty in the position of the vortex.

Here we take a first step in generalizing this earlier result to a vortex lattice, showing how correlating two particles in the wave function lowers the energy of the lattice. We focus on correlations described by simple bosonic Jastrow factors, $(z_i - z_j)^2$, in the wave function, where $z \sim x + \mathrm{i}y$ is the position of a particle in the complex plane. Such correlations tend to lower the interaction energy by keeping the particles apart and are, hence, favored by repulsive interactions. On the other hand, each factor carries two units of angular momentum and, therefore, tends to increase the kinetic energy of the system. With increasing angular momentum, more and more of these factors enter the wave function, and the states become more strongly correlated, e.g., as in the Read-Rezayi [43] and the bosonic Laughlin [21] states. The evolution of the system as its angular momentum increases towards and beyond the melting transition and the role that Jastrow correlations play in this phase transition is still an open problem [15]. With increasing angular momentum, particles begin to occupy single-particle states which previously were empty (or had vanishingly small occupations); this increase in the size of the configuration space of the particles can lead to possible quasi-degeneracies between states with different single-particle occupations and, consequently, to the onset of quantum fluctuations which ultimately destroy the vortex lattice. Even for low angular momenta, where

only a few vortices are present, correlations still play a significant role in redistributing the particles among single-particle states, as Cremon *et al.* find [48] by studying few-vortex ($N_{\rm v} \leq 4$) systems numerically and comparing the exact and mean-field ground states. This Chapter sheds a complementary light on such redistributions.

An informative example of how correlations function is the gas of attractive bosons studied in Ref. [21]. For a total (arbitrary) angular momentum $\hbar L$, the ground state wave function is

$$\psi_1(\mathbf{z}; L) = z_c^L \tag{3.1}$$

where $z_c = \sum_{i=1}^N z_i/N$ is the center of mass coordinate. This state has a total interaction energy $\sim -N(N-1)/2$. Moreover, the wave function

$$\psi_2(\mathbf{z}; L) = \sum_{i_1<i_2} (z_{i_1} - z_{i_2})^2 \, \psi_1(\mathbf{z}; L-2) \tag{3.2}$$

describes an excited state of the system with the same angular momentum and with a higher interaction energy $\sim -N(N-2)/2$. If we now change the nature of the interactions from attractive to repulsive, these two states switch places in the energy spectrum, with $|\psi_2(L)\rangle$ becoming lower in energy than $|\psi_1(L)\rangle$, although it does not become the ground state. Similar to the Bogoliubov single-vortex state (as we will show), the Jastrow correlations included in $|\psi_2(L)\rangle$ help to lower the now repulsive interaction energy.

In this Chapter, we first show how the real-space form of the Bogoliubov ground state of the single-vortex condensate [31] includes two-particle bosonic Jastrow factors and can be expanded as a sum over symmetric polynomials with successive number of Jastrow factors. The first term of the sum is just the original uncorrelated mean-field wave function, and the last term has $N/2$ simultaneous Jastrow factors. The effect of such Jastrow correlations is to reduce the total energy by a term $\mathcal{O}(N^{-1})$ which, although small, is a precursor of the more general expected effect of correlations. We then generalize the correlated single-vortex case to a vortex lattice, initially described as a mean-field condensate. Again, we find that the included Jastrow correlations lead to a relative reduction of the energy $\mathcal{O}(N^{-1})$. We also find that the inclusion of these correlations in the trial wave function leads to a nonvanishing density at the vortex cores, indicating the presence of quantum fluctuations of the vortices, similar to the case of the single-vortex system we previously studied [31].

In the next section, we delineate the basic model describing a condensate in terms of Landau levels. In Sec. 3.3, we expand the Bogoliubov ground state in terms of a series of N-particle Fock states with increasing number of particles in the two single-particle states connected to the mean-field ground state through the

interactions; we show that these Fock states are represented by *monomial symmetric polynomials* (which, in turn, can be expanded in terms of other symmetric polynomials containing Jastrow factors) and find the form of the correlations present in the wave function. In Sec. 3.4, we generalize this construction to a vortex lattice system. Finally, in Appendix D, we derive a general algebraic identity connecting the monomial symmetric polynomials encountered in this problem to symmetric polynomials with successive number of Jastrow factors, and in Appendix E, we lay out the details of the derivations used to arrive at the results of Sec. 3.3.

3.2 Basic Model

We consider a gas of N bosons of mass m in a harmonic trap of frequencies $\omega_\perp$ in the x–y plane and ω_z in the z direction, rotating around the z axis with angular velocity Ω. We assume weak two-body repulsive interactions of strength $g = 4\pi\hbar^2 a/m$, where a is the s-wave scattering length. The Hamiltonian in the rotating frame is thus

$$\mathcal{H}' = \sum_{i=1}^{N} \left[\frac{\mathbf{p}_i^2}{2m} + \frac{1}{2}m\big(\omega_\perp^2 x_i^2 + \omega_\perp^2 y_i^2 + \omega_z^2 z_i^2\big) - \Omega \ell_i \right] + g \sum_{i<j} \delta(\mathbf{r}_i - \mathbf{r}_j) \tag{3.3}$$

where $\ell = \hat{\mathbf{z}} \cdot (\mathbf{r} \times \mathbf{p})$ is the angular momentum along the z direction.

In the limit of fast rotation ($\Omega \lesssim \omega_\perp$) at zero temperature, the gas becomes quasi-two-dimensional and resides in the axial ground state of the harmonic trap. The single-particle eigenstates of the non-interacting system are the Landau levels, $|nm\rangle$, where n is the radial quantum number and $m \geq -n$ is the angular momentum along the rotation axis. The characteristic interaction energy scale is $V_0 = g/[(2\pi)^{3/2} d_\perp^2 d_z]$ where $d_{\perp,z} = \sqrt{\hbar/m\omega_{\perp,z}}$ are the characteristic oscillator lengths in the transverse and axial directions. We assume the interactions to be sufficiently weak that $V_0 \ll 2\hbar\omega_\perp$; therefore, as $\Omega \to \omega_\perp$, the system resides in the lowest-energy ($n = 0$) manifold of Landau levels. The wave function of a particle in the lowest Landau level (LLL) with m units of angular momentum, corresponding to the single-particle state $|0m\rangle$, is

$$\phi_m(z) \equiv \langle z\,|0m\rangle = \frac{1}{d_\perp \sqrt{\pi m!}}\, z^m e^{-|z|^2/2} \tag{3.4}$$

where $z = (x + \mathrm{i}y)/d_\perp$ is the dimensionless position in the complex plane. For brevity, we suppress, throughout this Chapter, the factor $\exp\big[-\sum_{i=1}^{N} |z_i|^2/2\big]/(d_\perp\sqrt{\pi})^N$ common to all N-particle LLL wave functions.

3.3 Correlations in the single-vortex Bogoliubov ground state

We studied in Ref. [31] the properties of a single-vortex system in the LLL by including small-amplitude Bogoliubov fluctuations about a mean-field condensate in $|01\rangle$. These fluctuations lower the energy of the Bogoliubov ground state by $-NV_0/4$ compared to the mean-field ground state; the relative reduction in the interaction energy is $\mathcal{O}(N^{-1})$. The vortex, which becomes energetically stable [91, 22] at the critical rotation frequency $\Omega_c = \omega_\perp - NV_0/4\hbar$, is on average slightly off-center by $\mathcal{O}(1/\sqrt{N})$ (in units of $d_\perp$) due to these quantum fluctuations. In this section, we investigate the nature, in real space, of correlations induced by Bogoliubov fluctuations.

The Bogoliubov ground state of a single-vortex LLL system at $\Omega = \Omega_c$ is [31]

$$|\mathrm{G}\rangle = \frac{1}{\sqrt{2}} \exp\big[-a_2^\dagger a_0^\dagger/\sqrt{2}\big]\,|N_1\rangle\,, \tag{3.5}$$

where a_m annihilates a particle with angular momentum m from the state $|0m\rangle$, and $|N_1\rangle$ is a coherent state with N_1 particles condensed in $|01\rangle$, satisfying the eigenvalue equation $a_1\,|N_1\rangle = \sqrt{N_1}\,|N_1\rangle$. This wave function does not conserve the particle number. In order to find its form in configuration space, we restrict the number of particles to N (assumed to be even) and project $|\mathrm{G}\rangle$ onto the N-particle Fock space. This new wave function, $|\mathrm{G};N\rangle$, can be approximated as a sum over states with $N-2m$ particles in $|01\rangle$ and m particles in $|00\rangle$ and $|02\rangle$,

$$|\mathrm{G};N\rangle \simeq \frac{1}{\sqrt{2}} \sum_{m=0}^{N/2} \big(-1/\sqrt{2}\big)^m\,|m, N-2m, m\rangle\,, \tag{3.6}$$

where $|n_0, n_1, n_2\rangle$ contains n_j particles in $|0j\rangle$ (with $j = 0, 1, 2$). The norm of this wave function is $\langle \mathrm{G};N\,|\mathrm{G};N\rangle = 1 - 2^{-(1+N/2)}$ and approaches unity when $N \to \infty$.

The first term in the sum ($m = 0$) is just the original mean-field many-body ground state

$$\langle \mathbf{z}\,|0, N, 0\rangle \sim z_1 \cdots z_N \tag{3.7}$$

where $\mathbf{z} = \{z_1, z_2, \ldots, z_N\}$. The $m = 1$ term includes first-order corrections and yields

$$\langle \mathbf{z}\,|1, N-2, 1\rangle \sim \mathcal{P}\big[z_1^0 z_2 \cdots z_{N-1}(z_N^2/\sqrt{2})\big] \tag{3.8}$$

where $\mathcal{P}$ denotes the sum of the distinct permutations with respect to the z_j's needed to symmetrize the wave function. After simplifying this expression (details in Appendix E), we find that the first-order Bogoliubov corrections take *one* pair of particles out of the condensate and correlate them through a bosonic Jastrow

factor,

$$\sum_{i_1<i_2}(z_{i_1}-z_{i_2})^2\prod_{k\neq i_1,i_2}z_k\equiv J_1(\mathbf{z}). \tag{3.9}$$

Similarly, the second-order Bogoliubov correction, the $m=2$ term in Eq. (3.6), leads to

$$\langle\mathbf{z}\,|2,N-4,2\rangle\sim\mathcal{P}\big[z_1^0z_2^0z_3\cdots z_{N-2}(z_{N-1}^2/\sqrt{2})(z_N^2/\sqrt{2})\big]. \tag{3.10}$$

Simplification of the resulting expression (details in Appendix E) shows that *two* pairs of particles are correlated through two simultaneous Jastrow factors, resulting in the following term in the wave function

$$\sum{}'\big(z_{i_1}-z_{i_2}\big)^2\big(z_{i_3}-z_{i_4}\big)^2\prod_{k\neq i_1\ldots i_4}z_k\equiv J_2(\mathbf{z}), \tag{3.11}$$

where the primed sum indicates the constraints $i_1<i_2,\ \ i_3<i_4,\ \ i_1<i_3,\ \ i_2\neq i_3,i_4$.

In fact, the real-space projection of the m^{th} term in the expansion (3.6) has up to m simultaneous Jastrow factors. To see this structure, we recast this term as

$$\begin{aligned}\langle\mathbf{z}\,|m,N-2m,m\rangle&\sim\mathcal{P}\big[z_1^0\cdots z_m^0(z_{m+1}^2/\sqrt{2})\cdots(z_{2m}^2/\sqrt{2})z_{2m+1}\cdots z_N\big]\\&=\frac{1}{2^{m/2}}\Big[\tbinom{N}{N-2m}\tbinom{2m}{m}\Big]^{-\frac{1}{2}}\mathcal{M}_{\{\underbrace{0\ldots0}_{m},\underbrace{2\ldots2}_{m},\underbrace{1\ldots1}_{N-2m}\}}(\mathbf{z}),\end{aligned} \tag{3.12}$$

where $\binom{N}{N-2m}\binom{2m}{m}$ is the number of distinct terms produced by the permutations. The monomial symmetric polynomial [97] $\mathcal{M}_{\boldsymbol{\alpha}}(\mathbf{z})$ is defined in Appendix D, and its representation in terms of symmetric polynomials with successive number of Jastrow factors, determined in Appendix E, is given by Eq. (D.29). Thus,

$$\langle\mathbf{z}\,|m,N-2m,m\rangle=\frac{1}{2^{m/2}}\left[\frac{1}{m!}\sqrt{\frac{N!}{(N-2m)!}}\,J_0(\mathbf{z})+\sqrt{\frac{(N-2m)!}{N!}}\sum_{j=1}^{m}2^{j-1}\,\frac{(2m-2j)!}{(m-j)!\,j!}\,J_j(\mathbf{z})\right] \tag{3.13}$$

where the N-variable symmetric polynomial $J_j(\mathbf{z})$, given by Eq. (D.14), includes j successive Jastrow factors. We immediately see up to m pairs of Jastrow-correlated particles in the m^{th}-order Bogoliubov correction to the mean-field ground state.

Substituting Eq. (3.13) into Eq. (3.6) and changing the order of summation using the identity

$$\sum_{m=0}^{N/2}\sum_{j=0}^{m}\cdots=\sum_{j=0}^{N/2}\sum_{m=j}^{N/2}\cdots, \tag{3.14}$$

we finally arrive at the expansion of the Bogoliubov ground state in terms of Jastrow polynomials,

$$\langle \mathbf{z} \,|\mathrm{G}; N\rangle = \frac{1}{\sqrt{2}} \sum_{j=0}^{N/2} A_j \, J_j(\mathbf{z}), \tag{3.15}$$

where

$$A_0 = \sum_{m=0}^{N/2} \frac{(-1)^m}{2^m \, m!} \sqrt{\frac{N!}{(N-2m)!}}\,, \tag{3.16}$$

$$A_{j\neq 0} = \sum_{m=j}^{N/2} \frac{(-1)^m \, (2m-2j)!}{2^{m-j+1} \, (m-j)! \, j!} \sqrt{\frac{(N-2m)!}{N!}}\,. \tag{3.17}$$

Equation (3.15) shows how incorporating Bogoliubov fluctuations in the mean-field ground state leads to pairs of particles being forced out of the condensate and correlated in the Jastrow form. The ratio of coefficients of successive terms decreases substantially with increasing j. The last term in the expansion above has correlations represented by $N/2$ Jastrow factors, and its coefficient is $\mathcal{O}(N^{-N})$ for large N.

Note that in the thermodynamic limit ($N \to \infty$), the mean-field ground state as described by the Gross-Pitaevskii equation is the true ground state of the system [98, 15]. In fact, the relative reduction in the energy between the Bogoliubov and the mean-field ground states is $\mathcal{O}(N^{-1})$ for large N [31]. In mesoscopic Bose-condensed systems, the role played by the correlations can be significant, with the Bogoliubov wave function energetically favored over the mean-field solution.

3.4 Extension to mean-field vortex lattices

As discussed above, the Bogoliubov ground state $|\mathrm{G}\rangle$, through the quantum fluctuations, has a lower energy than the mean-field ground state. It is clear from the form of the Jastrow polynomial $J_j(\mathbf{z})$ in Eq. (D.14) that this lower-energy state $|\mathrm{G}; N\rangle$ is constructed by correlating j pairs of particles through j distinct Jastrow factors, thereby leaving only $N-2j$ particles in the original mean-field condensate, $|01\rangle$. As a second example of the effect of Jastrow correlations, we argued, using the wave functions studied in Ref. [21] for a gas of attractive bosons, that correlating two particles through a Jastrow factor, Eq. (3.2), reduces the energy for repulsive bosons.

We now show that such Jastrow correlations also lower the energy of a vortex lattice state. In mean-field theory, an N-particle LLL condensate with N_v vortices at the positions $\{\xi_j\}$ (on a triangular lattice) takes the form

$$\psi_\mathrm{mf}(\mathbf{z}; N_\mathrm{v}) = \prod_{i=1}^{N} \prod_{j=1}^{N_\mathrm{v}} (z_i - \xi_j). \tag{3.18}$$

For large $N_{\rm v}$, the system is well described by the Thomas-Fermi approximation [25, 29], with the Thomas-Fermi radius R and rotation rate Ω given by the solution of the two equations

$$(R/d_\perp)^2 = \sqrt{\frac{4bNV_0}{\hbar(\omega_\perp - \Omega)}} = (\omega_\perp/\Omega)N_{\rm v}, \tag{3.19}$$

where $b \simeq 1.158$ is the Abrikosov lattice parameter. The state (3.18) is not an eigenstate of the total angular momentum operator $\mathcal{L}$, but has [29]

$$\langle \mathcal{L} \rangle_{\rm mf} = \hbar N \left[\frac{(R/d_\perp)^2}{3} - 1 \right]. \tag{3.20}$$

To study the effect of Jastrow correlations on the energetics of the vortex lattice, we construct a trial wave function by removing two particles from the mean-field condensate and simutaneously correlating them, arriving at the wave function

$$\psi_{\rm tr}(\mathbf{z}; N_{\rm v}) = \sum_{i_1<i_2} (z_{i_1} - z_{i_2})^2 \, \psi_{\rm mf}\big(\mathbf{z} - \{z_{i_1}, z_{i_2}\}; N_{\rm v}\big) \tag{3.21}$$

where $\psi_{\rm mf}\big(\mathbf{z}-\{z_{i_1}, z_{i_2}\}; N_{\rm v}\big)$ is an $(N-2)$-particle coherent state (with particles i_1 and i_2 removed) supporting the same vortices as the original state (3.18). Since the Jastrow factors in Eq. (3.21) force the particles away from each other, we expect the cloud for the correlated state to extend further in space compared to the mean-field one; in fact, the correlated state carrying the same total angular momentum as the mean-field one has a radius given by

$$R_{\rm tr}^2 \simeq R^2 \left(1 + \frac{4}{N}\right) \tag{3.22}$$

which can be easily seen by setting the two angular momentums (F.43) and (3.20) equal and solving for $R_{\rm tr}$.

The total interaction energy (found after a tedious calculation detailed in Appendix F) is given by

$$V_{\rm tr} \simeq V_0 \left(\frac{4b}{3}\right) \nu \, (N - 8), \tag{3.23}$$

where $\nu = N/N_{\rm v}$ is the filling factor; note this result is valid for large filling factors (in the vortex lattice regime). Including Jastrow correlations in the trial wave function indeed lowers the energy [albeit by a term $\mathcal{O}(N^{-1})$] compared to mean-field vortex lattice state, for which

$$V_{\rm mf} \simeq V_0 \left(\frac{4b}{3}\right) \nu \, (N - 1) \tag{3.24}$$

at the same value of the total angular momentum. The relative change in the interaction energy is similar to that for a single-vortex system as well as that for attractive bosons of Ref. [21]. Moreover, due to correlations, the average density at the vortex cores is non-zero for the trial state (3.21), similar to the behavior found in Ref. [31] for a single vortex. In the limit of large number of vortices and for $\nu \gg 1$, we find that the density at the vortex core is

$$n_{\rm tr}(\xi_j) \sim \nu^{-1} \, |\xi_j|^2 \, e^{-|\xi_j|^2} \tag{3.25}$$

(except for the central vortex).

We note that a relative $\mathcal{O}(N^{-1})$ change in the energy is not enough, in the thermodynamic limit, to drive the system towards the strongly correlated regime where the vortex lattice melts [45]. A detailed description of the melting of the lattice will involve states with large numbers of Jastrow-like correlations, e.g., as in Read-Rezayi states [43]. Therefore, vortex lattice wave functions of the form (3.21) are only good for large filling factors where the Gross-Pitaevskii equation is an excellent approximation.

3.5 Conclusion

This chapter described an initial study of the role of correlations in the ground state of a vortex lattice state, in the regime where the Gross-Pitaevskii equation is a good first description and quantum fluctuations are small. Although the advantages of including such interparticle correlations are clear – keeping the particles apart and reducing the interaction energy in the system – the detailed correlations in the exact ground state of the vortex lattice are not known analytically. Quantum fluctuations, driving the system towards a melting transition to strongly correlated quantum Hall states, become more pronounced as the angular momentum per particle approaches $\mathcal{O}(N)$ and the particle density becomes small, underlining the importance of interaction-induced correlations in this transition. The real-space form of the Bogoliubov ground state of a single-vortex condensate in the LLL studied here shows explicitly the Jastrow-like correlations of pairs of particles in this state. The Bogoliubov wave function is a superposition of the original uncorrelated mean-field ground state and correlated states with successive number of Jastrow pairs. As we showed, including Jastrow-correlated pairs (similar to those in the single-vortex Bogoliubov wave function) in a LLL system with $N_{\rm v}$ vortices on a triangular lattice lowers the energy compared to the mean-field wave function with no correlations; this state also exhibits non-zero density at the vortex cores, reflecting the quantum uncertainty in the vortex positions. Generally, interparticle interactions lead to the occupation of single-particle states that were originally unoccupied in the mean-field picture, allowing the system to explore larger regions of phase space, as effectively takes place in our trial wave function (3.21), as well as in Ref. [31] in the single-vortex Bogoliubov wave function. The next step needed is a systematic study of the evolution of the

populations of the single-particle states of the vortex lattice with increasing angular momentum.

Chapter 4

Bose-Einstein condensates in toroidal traps

4.1 Introduction

Superfluid flow in a toroidal trap is stabilized by a large energy barrier between the current-carrying state and a state with lower angular momentum [99, 16]. However, in mesoscopic systems, such as atomic Bose-Einstein condensates, the barrier can be sufficiently small that the system can tunnel quantum-mechanically to a state of lower angular momentum [100, 101]; furthermore, if the short-range interparticle interactions are attractive or very weakly repulsive, such a barrier does not exist, and the system can transition smoothly from the current-carrying state, to, e.g., the non-rotating ground state. Recent experiments in ultra-cold bosonic systems in toroidal traps, stimulated by the possibility of shining new light on the stability and decay of supercurrents [60, 6, 102] as well as by possible applications in other areas, e.g., interferometry [61, 62] and atomtronics [63], have seen such current decays [103, 66, 67, 68]. One such experimentally obtained toroidal condensate is shown in Fig. 4.1.

The stability of superflow depends on the interparticle interactions, the rotation rate of the trap, disorder in the trapping potential, and temperature. We consider a gas of interacting bosons at zero temperature in

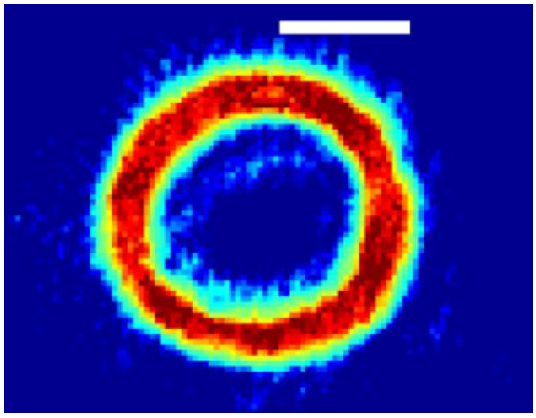

Figure 4.1: A toroidally trapped Bose-Einstein condensate of ^{87}Rb atoms, formed by imparting angular momentum to the atoms from a Laguerre-Gauss mode of the trapping laser. The white mark is 30 μm in length. Image from Phys. Rev. A **86**, 013629 (2012). Copyright (2012) by The American Physical Society.

a toroidal trap rotating at angular velocity Ω and address the question of how the single-vortex condensate with a metastable or unstable superflow evolves in the absence of dissipation, driven either by varying the rotation rate of the trap or by varying the interparticle interaction via a Feshbach resonance.

We consider, throughout this chapter, a quasi-one-dimensional gas of N bosons in a thin annulus of radius R and cross-sectional radius $r_0 \ll R$ at zero temperature. We discussed the basic physics of the metastability in Sec. 1.5 using a two-level system (with the non-rotating state, $|0\rangle$, and the state with azimuthal angular momentum $\hbar$ per particle, $|1\rangle$) with the Hamiltonian

$$\mathcal{H}_2 = \frac{\hbar^2}{2mR^2} N_1 + \frac{g}{2V}(N_0^2 + N_1^2 + 4N_0N_1) \tag{4.1}$$

where N_0 and N_1 are the number of particles in $|0\rangle$ and $|1\rangle$ respectively with $N = N_0 + N_1$ the total number of particles. As shown in Fig. 4.2, an energy barrier appears between the single-vortex state and the non-rotating ground state when

$$\frac{gN}{V} > \frac{\hbar^2}{2mR^2}. \tag{4.2}$$

With weakening interaction strength, the barrier decreases, and for

$$\frac{gN}{V} \leq \frac{\hbar^2}{2mR^2}, \tag{4.3}$$

it disappears, leading to instability of the single-vortex state.

We first delineate the regions of stability and the nature of instabilities of the full system as functions of the external rotation frequency of the trap, for both positive and negative interaction strengths. In general, the stability of the flow is manifest in the small-amplitude Bogoliubov fluctuations about the current-carrying condensate. Starting from a mean-field condensate, we include Bogoliubov fluctuations [96, 22] and find the eigenenergies of the quasiparticle excitations. With decreasing repulsion or trap rotational frequency, an energetic instability [22, 83] can appear in the system via excitations that decrease the angular momentum of the system by one unit; the system can lower its energy by exciting these quasiparticles. Moreover, we find a dynamical instability for sufficiently attractive interactions, where the quasiparticle eigenenergy becomes complex [22, 83] and the system is driven exponentially rapidly in time away from the initial state. For a system to evolve due to an energetic or a dynamical instability, the presence of dissipation is necessary in order to remove energy and angular momentum; in this section, we do not include dissipative effects. With a knowledge of the instabilities, we then study simple ground states that encompass the underlying physics, consisting of the two lowest-lying single-particle states. (Another example of how an instability indicates the

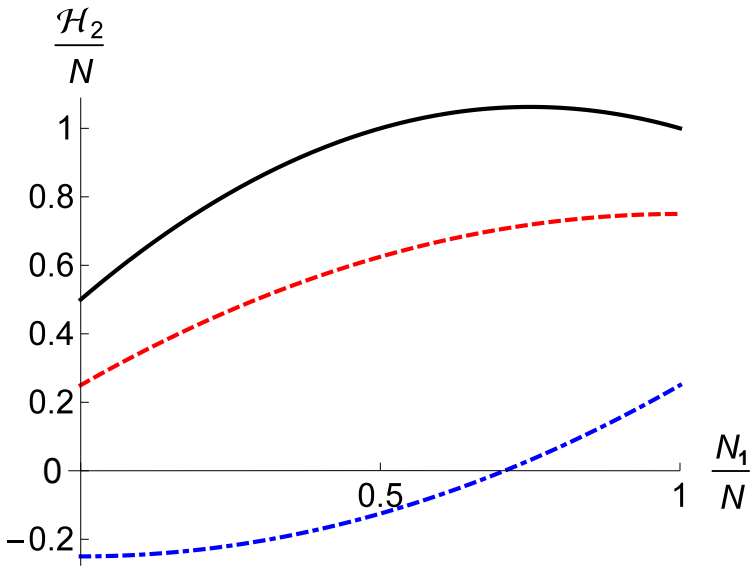

Figure 4.2: Energy landscape of the two-level model as a function of the number of particles in state $|1\rangle$. Note the energy barrier between the single-vortex and ground states for $gN/V > \hbar^2/2mR^2$ (solid line, in black); for $gN/V = \hbar^2/2mR^2$ (dashed line, in red), the slope vanishes at $N_1 = N$, while for $gN/V < \hbar^2/2mR^2$ (dot-dashed line, in blue) no barrier exists, indicating instability of the single-vortex state.

presence of a lower-energy metastable ground state is given in Ref. [31] where we studied a rapidly rotating trapped Bose gas in the lowest Landau level with a vortex at the center of the trap.)

For the system to feel the presence of the trap, the trapping potential must break the rotational symmetry. We describe the coupling of the system to the container by an asymmetric "disorder" potential stationary in the frame rotating at angular velocity Ω. Within mean-field theory, we determine the stationary states of the condensate formed from the single-particle states $|0\rangle$ and $|1\rangle$ and find that for sufficiently large interaction strengths, dependent on the disorder potential, the system exhibits a non-adiabatic response [76, 80] to variations of the rotation frequency, even if Ω is changed arbitrarily slowly. This behavior arises from the presence of multiple minima in the energy landscape (separated by a maximum or saddle-point which represents an unstable mode) and is characterized by the appearance of a *swallow-tail loop* in the lowest-lying adiabatic energy level and a fold-over in the occupation probability of the corresponding state as functions of the rotation frequency (see Fig. 4.6 and Fig. 4.7 below). The swallow-tail loop implies that the response of the system to external rotation exhibits hysteresis [76].

Moreover, we show that the quasi-one-dimensional Bose-Einstein condensate in a rotating annulus can be mapped onto the problem of a condensate trapped in a double-well potential with Josephson tunneling between the two wells. Therefore, macroscopic quantum phenomenon of self-trapping in double wells [104, 105, 106] also appears in such rotating Bose gases, where the system acquires a non-zero time-averaged

population difference between the two components. The onset of self-trapping, which is a steady-state population imbalance, exactly corresponds to the behavior of the energy levels discussed above.

We briefly note related theoretical studies in similar toroidally trapped systems: Bose condensates with dipolar interparticle interactions [107, 108] which induce an effective double-well Josephson junction, leading to self-trapping [109, 110, 111]; Bose-Einstein condensates with a modulated, spatially-dependent scattering length [112, 113, 114]; and hollow pipe optical waveguides with an azimuthally modulated refractive index which generates an effective double-well potential configuration [115].

In Sec. 4.2, we discuss the stability regime of the condensate by studying the energies of the Bogoliubov excitations. We then analyze the energy landscape of the two-mode system in Sec. 4.4 and demonstrate a swallow-tail loop in the energy of the ground state. We construct a mean-field description of this system in the presence of the disorder potential in Sec. 4.5. The appearance of swallow-tail loops and cusps in the energy levels and their relation to extrema in the energy landscape are studied in Sec. 4.5.1. Finally, in Sec. 4.5.2, we discuss the connection of this system to a trapped condensate tunneling in a double-well potential, and the corresponding connection of self-trapping in the double-well system to the behavior of the adiabatic energy levels discussed in the previous subsection.

4.2 Stability of the ground state

For a sufficiently thin annulus, the radial and axial excitations are frozen out, and the angle around the ring becomes the only effective degree of freedom. The normalized non-interacting single-particle eigenstates of this system are

$$\varphi_l(\theta) \equiv \langle \mathbf{r} | \, l \rangle = \frac{1}{\sqrt{2\pi R}} \, e^{\mathrm{i}l\theta} \tag{4.4}$$

with eigenenergies

$$\epsilon_l = \frac{(\hbar l)^2}{2mR^2} \tag{4.5}$$

where $\hbar l$ is the angular momentum and $\mathbf{r} = (R, \theta)$ is the position vector. The Hamiltonian in the laboratory frame is

$$\mathcal{H} = \sum_j \frac{(\hbar j)^2}{2mR^2} \, a_j^\dagger a_j + \frac{1}{2} \, \frac{g}{V} \sum_{j,k,m} a_{j-m}^\dagger a_{k+m}^\dagger a_k a_j \tag{4.6}$$

where a_j is the annihilation operator for a particle of angular momentum $\hbar j$, and $g = 4\pi\hbar^2 a/m$ is the two-body contact interaction strength with a the s-wave scattering length. The Hamiltonian in the frame

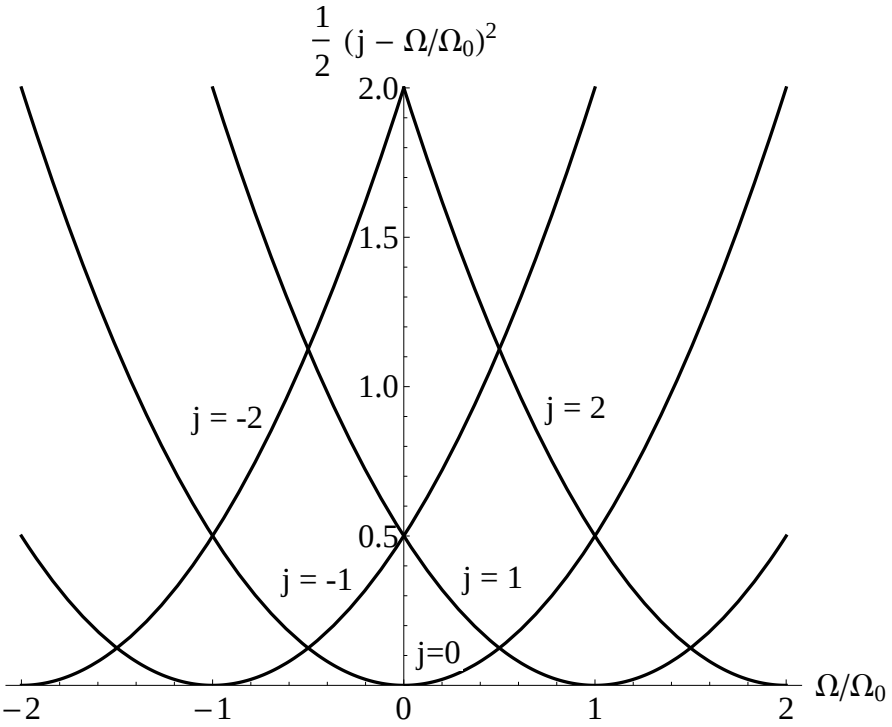

Figure 4.3: Single-particle energy levels in the rotating frame, measured in units of $\hbar\Omega_0$, as functions of Ω.

rotating at Ω (denoted by a prime) can be written as [116]

$$\mathcal{H}' = -N\frac{\hbar\Omega^2}{2\Omega_0} + \hbar\Omega_0 \sum_j \frac{1}{2}\Big(j - \tfrac{\Omega}{\Omega_0}\Big)^2 a_j^\dagger a_j + \frac{1}{2}\,\frac{g}{V} \sum_{j,k,m} a_{j-m}^\dagger a_{k+m}^\dagger a_k a_j \tag{4.7}$$

where

$$\Omega_0 = \frac{\hbar}{mR^2} \tag{4.8}$$

is the characteristic scale of rotation in the system. The non-interacting single-particle energy levels of $\mathcal{H}'$, depicted in Fig. 4.3, are periodic in Ω. At this stage, we do not include the disorder potential.

In the laboratory frame, the condensate $\psi_c(\theta, t)$ obeys the time-dependent Gross-Pitaevskii (GP) equation

$$\mathrm{i}\hbar\,\frac{\partial}{\partial t}\psi_c(\theta,t) = \left[-\frac{\hbar^2}{2mR^2}\,\frac{\partial^2}{\partial\theta^2} + \frac{g}{\pi r_0^2}\,|\psi_c(\theta,t)|^2\right]\psi_c(\theta,t). \tag{4.9}$$

To determine the stability of the system, we construct the normal modes of the condensate by perturbing the system around the stationary solution

$$\psi_c(\theta,t) = e^{-\mathrm{i}\mu t/\hbar}\,\psi_c(\theta) \tag{4.10}$$

where μ is the chemical potential. We expand the condensate wave function in terms of time-dependent modes with angular momentum ν measured relative to the condensate by writing

$$\psi(\theta,t) = e^{-\mathrm{i}\mu t/\hbar}\big[\psi_c(\theta) + \delta\psi(\theta,t)\big] \tag{4.11}$$

where

$$\delta\psi(\theta,t) = e^{\mathrm{i}S(\theta)}\sum_{\nu\neq 0}\big[u_\nu\,\varphi_\nu(\theta)\,e^{-\mathrm{i}\epsilon_v t/\hbar} - v_\nu^*\,\varphi_\nu^*(\theta)\,e^{\mathrm{i}\epsilon_v t/\hbar}\big] \tag{4.12}$$

with ϵ_v the eigenenergies, $S(\theta)$ the phase of $\psi_c(\theta)$, and u_ν and v_ν complex numbers to be determined. (Following Fetter's notation [22], we explicitly take the phase of the condensate out of the sum, whereas other authors include the exponential factor in the definition of excitation wave functions [117].) Note that Eq. (4.11) is equivalent to expanding the field operator as

$$\Psi(\theta) = \psi_c(\theta) + e^{\mathrm{i}S(\theta)}\sum_{\nu\neq 0}\big[u_\nu(\theta)\,\alpha_\nu - v_\nu^*(\theta)\,\alpha_\nu^\dagger\big] \tag{4.13}$$

where α_ν and $\alpha_\nu^\dagger$ are quasiparticle excitation annihilation and creation operators and $u_\nu(\theta) = u_\nu\,\varphi_\nu(\theta)$ and $v_\nu(\theta) = v_\nu\,\varphi_\nu(\theta)$. From now on, for brevity, we measure angular momentum in units of $\hbar$, time in units of Ω_0^{-1}, energy in units of $\hbar\Omega_0$, and define the dimensionless parameters $\eta = mRg/2\pi^2\hbar^2 r_0^2 = 2aR/\pi r_0^2$ and $\bar{\Omega} = \Omega/\Omega_0$.

We focus, in particular, on the lowest-energy single-vortex state, with a condensate of N_c atoms in the state $|1\rangle$, for which the GP equation implies that

$$\mu = \frac{1}{2} + \eta N_c. \tag{4.14}$$

The modes are described by the two coupled equations [96]

$$\begin{pmatrix} \nu + \left[\frac{1}{2}\nu^2 + \eta N_c\right] & -\eta N_c \\ \eta N_c & \nu - \left[\frac{1}{2}\nu^2 + \eta N_c\right] \end{pmatrix}\begin{pmatrix} u_\nu \\ v_\nu \end{pmatrix} = \epsilon_\nu \begin{pmatrix} u_\nu \\ v_\nu \end{pmatrix} \tag{4.15}$$

from which we find the eigenenergy

$$\epsilon_\nu = \nu \pm |\nu|\sqrt{\tfrac{1}{4}\nu^2 + \eta N_c}\,. \tag{4.16}$$

Note that for $\frac{1}{4}\nu^2 + \eta N_c < 0$, these energies are complex, indicating that the condensate is dynamically unstable [22, 83].

Since the transformation from the original bosonic operators to the quasiparticle ones is canonical, the bosonic commutation relations must also hold for the quasiparticle operators (see Appendix C). This means that physical quasiparticle states must be properly normalized [118, 22]. We find from Bogoliubov equations (see Eq. (2.23) of Ref. [96]) that

$$(\epsilon_\nu - \epsilon^*_{\nu'}) \int R\, d\theta \, [u^*_\nu(\theta) u_{\nu'}(\theta) - v^*_\nu(\theta) v_{\nu'}(\theta)] = 0. \tag{4.17}$$

This equation has some interesting consequences for $\nu = \nu'$. First, we find that if ϵ_ν is complex, the normalization constant has to be zero, i.e.,

$$\int R\, d\theta \, \left[\, |u_\nu(\theta)|^2 - |v_\nu(\theta)|^2 \,\right] = 0 \quad \rightarrow \quad |u_\nu|^2 = |v_\nu|^2 \,. \tag{4.18}$$

In other words, states with complex eigenenergies are not properly normalized. Second, if the normalization constant is non-zero (if, e.g., $|u_\nu|^2 - |v_\nu|^2 = 1$), then we find that ϵ_ν is real. Third, for a solution with real ϵ^+_ν and unit norm, assuming that ϵ^-_ν is also real yields

$$(\epsilon^+_\nu - \epsilon^-_\nu) \, (u^{+\,*}_\nu u^-_\nu - v^{+\,*}_\nu v^-_\nu) = 0. \tag{4.19}$$

Since $\epsilon^+_\nu \neq \epsilon^-_\nu$ (unless $\nu = 0$ which is prohibited), this means $v^-_\nu = (u^+_\nu / v^+_\nu)^* \, u^-_\nu$ which leads to $|u^-_\nu|^2 - |v^-_\nu|^2 = -\,|u^-_\nu|^2 \,/\, |v^+_\nu|^2$ which is always negative and is never equal to unity. This outcome indicates that ϵ^+_ν and ϵ^-_ν cannot both represent physical solutions at the same time. As long as the (+) branch represents a physical solution with positive norm, the (−) branch has to be unphysical. On the other hand, once one of the energies becomes complex, so does the other. The complex solutions always appear in a pair. Therefore, from now on, we pick the (+) branch in Eq. (4.16) as it is the only physical solution with positive norm. For a more general discussion on the mathematical properties of the Bogoliubov eigenstates, see the appendices in Refs. [83, 119].

The oscillations of the condensate can also be pictured in second-quantization as quasiparticle excitations of the condensate, as shown in Eq. (4.13). In the usual second-quantized Bogoliubov formalism, the coherence

factors are given in terms of ϵ_ν [118, 22] by

$$|u_\nu|^2 = \frac{1}{2}\left(\frac{\frac{1}{2}\nu^2 + \eta N_c}{|\nu|\sqrt{\frac{1}{4}\nu^2 + \eta N_c}} + 1\right) \tag{4.20}$$

$$|v_\nu|^2 = \frac{1}{2}\left(\frac{\frac{1}{2}\nu^2 + \eta N_c}{|\nu|\sqrt{\frac{1}{4}\nu^2 + \eta N_c}} - 1\right), \tag{4.21}$$

and the excitation energy in the rotating frame of a quasiparticle carrying ν units of angular momentum relative to the condensate becomes

$$\epsilon'_\nu(\bar{\Omega}) = \nu(1-\bar{\Omega}) + |\nu|\sqrt{\tfrac{1}{4}\nu^2 + \eta N_c}\,. \tag{4.22}$$

Self-consistency dictates that

$$N_c + \sum_{\nu\neq 0} |v_\nu|^2 = N. \tag{4.23}$$

We now analyze the stability of the ground state in terms of the normal modes. For weak interactions, $|\eta N_c| \ll \frac{1}{4}$, expansion to first order leads to

$$\epsilon'_\nu(\bar{\Omega}) \simeq \frac{1}{2}\,\nu^2 + \nu(1-\bar{\Omega}) + \eta N_c. \tag{4.24}$$

Thus, at $\bar{\Omega} = 0$ and for repulsive interactions, only $\epsilon_{-1} \simeq -\frac{1}{2} + \eta N_c$ is negative; the $\nu = -1$ mode is energetically unstable and anomalous, indicating that the correct ground state has lower angular momentum than the original single-vortex state. For attractive interactions, $\epsilon_{-2} \simeq \eta N_c$ is also negative, and the $\nu = -2$ mode is anomalous as well.

The general stability phase diagram of the $\nu = -1$ mode is shown in Fig. 4.4 in the interaction strength vs external rotation frequency plane. In the hashed region where $\eta N_c < -\frac{1}{4}$, the quasiparticle energy is complex. Note that the regions of dynamical instability and energetic instability are in agreement with the arguments in the appendix of Ref. [83]. In a dynamically unstable mode, where the eigenenergy is complex, one of the two components in Eq. (4.12) grows exponentially in time while the other decays exponentially. An unstable mode, living around a maximum or a saddle-point in the energy landscape, hints at the existence of a stable lower-energy state, corresponding to a modified condensate. However, a small-amplitude analysis does not, in general, reveal the nature of the new stable state (see, e.g., Refs. [31, 120] where such modified condensates are explicitly discussed). The solid black line, the solution of $\epsilon'_\nu = 0$, shows the critical values of interaction strength and rotation frequency needed for stability. For a non-interacting system, the $\nu = -1$

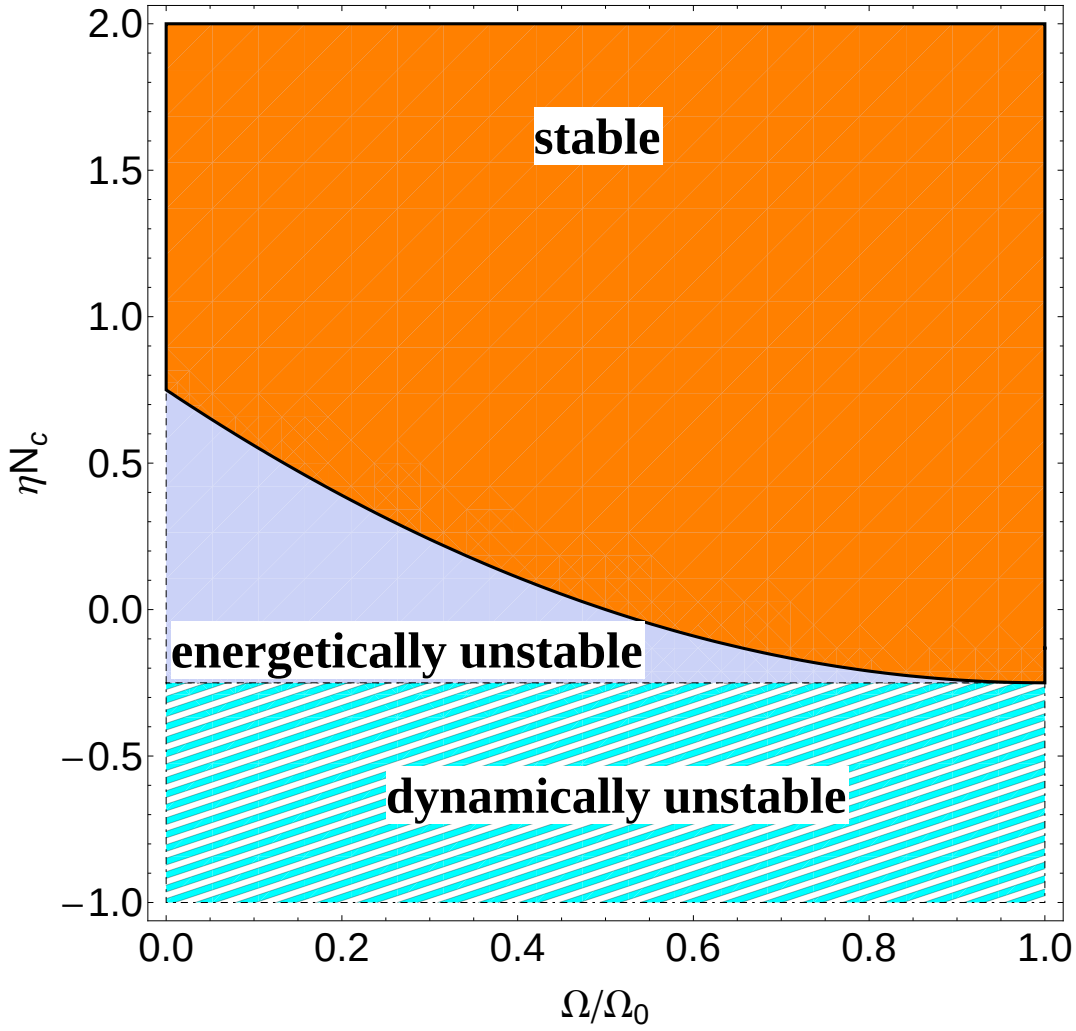

Figure 4.4: Stability phase diagram in the rotation rate vs interaction strength plane, for the $\nu = -1$ normal mode of a condensate with one unit of angular momentum per particle. Energetic instabilities are caused by excitations with negative energy, whereas those with complex energies lead to dynamical instabilities.

mode becomes stable at $\bar{\Omega} = \frac{1}{2}$. Interestingly, faster rotations shrink the energetically unstable region and stabilize this mode even for weakly attractive interactions. At $\bar{\Omega} = 1$, the energetically unstable region completely vanishes, and the gas becomes stable for $\eta N_c > -\frac{1}{4}$. As mentioned before, due to the absence of dissipation in our model, the energy is conserved, and the instabilities (although present) fail to change the state of the system into one with lower energy and lower angular momentum.

In the experiment in Ref. [68], where $N \sim 8 \times 10^4$ atoms of ^{87}Rb with unit circulation were held in a ring trap of radius $R \sim 9\,\mu$m, we find

$$\eta N \sim 1.8 \times 10^3. \tag{4.25}$$

Also, the experiment in Ref. [67], with $N \sim 8 \times 10^4$ atoms of ^{23}Na in a ring trap of radius $R \sim 20\,\mu$m, has

$$\eta N \sim 2.9 \times 10^3. \tag{4.26}$$

The initial states in current experiments [67, 68] are within the stable regime discussed here, far from encountering any energetical or dynamical instabilities (see Fig. 4.4). However, by suddenly changing the strength of the interparticle interaction from repulsive to sufficiently attractive via a Feshbach resonance, thereby bringing the system from the stable region into the dynamically unstable region, one would be able to investigate experimentally the evolution of the system in the presence of a dynamical instability.

The above stability analysis was done for an initial condensate in $|1\rangle$. Due to the periodicity of the single-particle energy levels with respect to the external rotation frequency (see Fig. 4.3), we can extend the same arguments easily to condensates in higher angular momentum states. For a condensate in $|j\rangle$, the chemical potential is

$$\mu = \frac{1}{2}\, j^2 + \eta N_c, \tag{4.27}$$

and the quasiparticle energies become

$$\epsilon'_\nu(\bar{\Omega}) = \nu(j - \bar{\Omega}) + |\nu| \sqrt{\tfrac{1}{4}\nu^2 + \eta N_c}. \tag{4.28}$$

Thus, the anomalous $\nu = -1$ mode (which connects $|j-1\rangle$ and $|j+1\rangle$ to the condensate) becomes stable at $\bar{\Omega} = j - \frac{1}{2}$ for a non-interacting system; its regions of stability in the presence of interactions, for $j - 1 < \bar{\Omega} < j$, are identical to those shown in Fig. 4.4.

4.3 Depletion of the condensate

We now find the depletion of the condensate due to the interactions. Using Eq. (4.23), we find that the depletion of the condensate is given by

$$\delta N = \sum_{\nu\neq 0} |v_\nu|^2 = 2\sum_{\nu=1}^{\infty} |v_\nu|^2 = \int_1^\infty d\nu \left(\frac{\frac{1}{2}\nu^2 + \eta N_c}{\sqrt{\frac{1}{4}\nu^4 + \eta N_c\, \nu^2}} - 1 \right). \tag{4.29}$$

The difference between this case and the three-dimensional one (see, for example, Chapter 8 of Ref. [9]) is the absence of a factor of ν^2 in the integrand (originating from the latter case's infinitesimal volume element) and also the fact that the lower limit of the integral here cannot be extended to zero. We define $\nu^2 = 2\eta N_c\, x^2$ and find

$$\delta N = \sqrt{2\eta N_c} \int_{1/\sqrt{2\eta N_c}}^\infty dx \left(\frac{x^2+1}{\sqrt{x^4+2x^2}} - 1 \right). \tag{4.30}$$

Unlike the three-dimensional problem, the value of the integral here *does* depend on the parameters of the system through the non-analytic combination $\sqrt{2\eta N_c}$ in the lower limit of the integral. This integral has a closed form with the following limits

$$\int_{1/t}^\infty dx \left(\frac{x^2+1}{\sqrt{x^4+2x^2}} - 1 \right) \xrightarrow{t\gg 1} \frac{\ln t}{\sqrt{2}} + \mathcal{O}(t^{-1}), \tag{4.31}$$

$$\int_{1/t}^\infty dx \left(\frac{x^2+1}{\sqrt{x^4+2x^2}} - 1 \right) \xrightarrow{t\ll 1} \frac{t^3}{6} + \mathcal{O}(t^5). \tag{4.32}$$

For a condensate in a ring trap, the dimensionless parameter $\eta N_c = 2aRN_c/\pi r_0^2$ is actually a large number; for example, for the two experiments discussed previously, $\sqrt{2\eta N_c} \sim 100$. Therefore, for large N and R, we should use the first approximation above. Thus, we find the fractional depletion (in proper units)

$$\frac{\delta N}{N} \sim \sqrt{\frac{a}{N}}\, \ln\sqrt{aN} \tag{4.33}$$

which is non-analytical in the scattering length. Note that even for these large empirical values, the condensate depletion is very small; for example, for the experiments referenced here, we find $\delta N/N \sim 3\times 10^{-3}$. Hence, a very large fraction of the particles are condensed into the state $|1\rangle$.

4.4 Two-mode approximation

As discussed above, when the energy of the $\nu = -1$ mode becomes negative, the system, condensed in $|1\rangle$, prefers a ground state with smaller angular momentum than $\hbar$ per particle. As shown in Fig. 4.3, over the

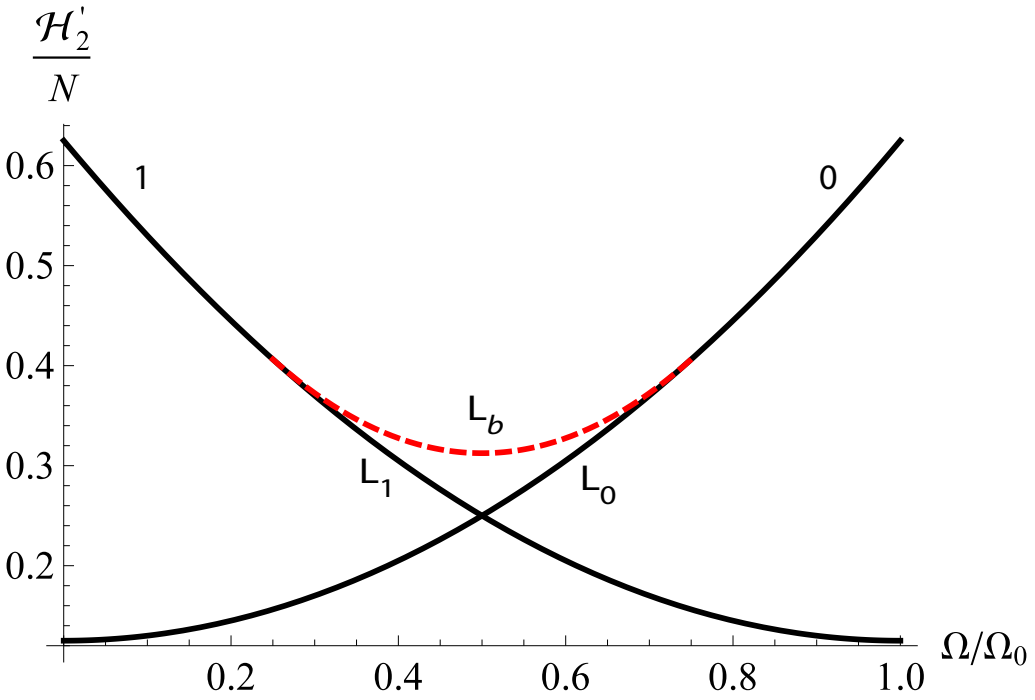

Figure 4.5: The energy per particle, in units of $\hbar\Omega_0$, of the states $|N,0\rangle$ (labeled 0) and $|0,N\rangle$ (labeled 1) and that of the barrier state $|b\rangle$ (dashed line) as functions of the rotation frequency, for $\eta N = 1/4$. An energy loop (labeled by L_b, L_0, and L_1) emerges due to the existence of a maximum in the energy landscape.

entire range $0 < \bar{\Omega} < 1$, the lowest-lying single-particle states are $|0\rangle$ and $|1\rangle$. The states $|-1\rangle$ and $|2\rangle$ have, in general, much higher energies and are not mixed in with the ground state by weak interactions; only for $\eta N \gtrsim 1$ is the mixing significant at $\bar{\Omega} \simeq 0$ and $\bar{\Omega} \simeq 1$. Hence, for sufficiently weak interactions ($\eta N \lesssim 1$), we can keep only $|0\rangle$ and $|1\rangle$ in the description of the system and work in a two-mode approximation with the truncated Hamiltonian in the frame rotating at $\bar{\Omega}$,

$$\mathcal{H}_2' = \left(\frac{1}{2} - \bar{\Omega}\right) N_1 + \frac{1}{2}\eta\big(N_0^2 + N_1^2 + 4N_0N_1\big) \tag{4.34}$$

where $N_j = a_j^\dagger a_j$. The eigenstates of $\mathcal{H}_2'$ are the Fock states

$$|N_0, N_1\rangle = \frac{1}{\sqrt{N_0!\,N_1!}}\big(a_0^\dagger\big)^{N_0}\big(a_1^\dagger\big)^{N_1}|\text{vac}\rangle \tag{4.35}$$

where $|\text{vac}\rangle$ is the vacuum.

This system has been studied extensively in Ref. [76]; we briefly recap the results here. Similar to the non-interacting case, in the ground state for $\bar{\Omega} < \frac{1}{2}$, all the particles are condensed into $|0\rangle$, while for $\bar{\Omega} > \frac{1}{2}$, they are condensed into $|1\rangle$. As one finds by extremizing the energy, the spectrum also acquires an energy

maximum when

$$\left|\bar{\Omega} - \tfrac{1}{2}\right| < \eta N, \tag{4.36}$$

corresponding to the state

$$|b\rangle = \left|\tfrac{1}{2}N + (\bar{\Omega} - \tfrac{1}{2})/2\eta, \tfrac{1}{2}N - (\bar{\Omega} - \tfrac{1}{2})/2\eta\right\rangle. \tag{4.37}$$

This state can be seen as the maximum in Fig. 4.2 for $\bar{\Omega} = 0$ and $\eta N > \frac{1}{2}$; as ηN decreases below $\frac{1}{2}$, the region in $\bar{\Omega}$ for which such a maximal state exists shrinks, as depicted by the dashed line in Fig. 4.5 for $\eta N = \frac{1}{4}$. This state acts as a barrier between the two ground states, making it energetically expensive for density modulations (vortex-induced phase slips) to drive the system from one minimum to the other, even as $\bar{\Omega}$ is varied. Note the loop structure in Fig. 4.5 indicated by the lines labeled L_b, L_0, and L_1, whose effect on the response of the system to changes in $\bar{\Omega}$ will be discussed in the next section.

4.5 Symmetry breaking in mean-field theory

We now turn to the question of how the condensate responds dynamically to changes in its rotation rate. In realistic experiments, the potentials felt by the particles are never fully rotationally invariant (see, e.g., Ref. [68]); the breaking of rotational invariance changes the way single-particle states of given angular momentum are mixed. In order to couple the system to rotations of the trap, we include in the Hamiltonian a small "disorder" potential, $v(\theta - \Omega t)$, which is stationary in the frame rotating at Ω. Such a potential favors a coherent superposition of states (a single condensate) over a fragmented (Fock) state [116, 121, 122]; we assume the following variational form for the time-dependent two-mode condensate wave function

$$|\psi_c(t)\rangle = \sqrt{N}\left[c_0(t)\,|0\rangle + c_1(t)\,|1\rangle\right] \tag{4.38}$$

with the following normalization condition

$$|c_0(t)|^2 + |c_1(t)|^2 = 1. \tag{4.39}$$

The time-evolution of the condensate wave function in the rotating frame is governed by the GP equation

$$\mathrm{i}\frac{\partial}{\partial t}\psi_c(\theta,t) = \left[-\frac{1}{2}\frac{\partial^2}{\partial\theta^2} + \mathrm{i}\bar{\Omega}\frac{\partial}{\partial\theta} + \eta\,|\psi_c(\theta,t)|^2 + v(\theta)\right]\psi_c(\theta,t).$$

In the two-mode model, we can, with no loss of generality, take

$$v(\theta) = 2v\cos\theta \tag{4.40}$$

with v real and positive, corresponding to a coupling between the states $|0\rangle$ and $|1\rangle$ of the form $2Nv\,\mathrm{Re}\big[c_1^* c_0\big]$, so that the mean-field Hamiltonian becomes

$$\frac{\mathcal{H}_2'}{N} = \left(\frac{1}{2} - \bar{\Omega}\right)|c_1|^2 + \frac{1}{2}\eta N\big(1 + 2\,|c_0|^2\,|c_1|^2\big) + 2v\,\mathrm{Re}\big[c_1^* c_0\big]. \tag{4.41}$$

With this coupling, the amplitudes obey the two coupled differential equations

$$\begin{aligned} \mathrm{i}\frac{\partial}{\partial t}c_0 &= \eta N\big[2 - |c_0|^2\big]c_0 + vc_1, \\ \mathrm{i}\frac{\partial}{\partial t}c_1 &= \eta N\big[2 - |c_1|^2\big]c_1 + vc_0 + \left(\frac{1}{2} - \bar{\Omega}\right)c_1. \end{aligned} \tag{4.42}$$

The angular momentum per particle of the system changes according to

$$\frac{\partial}{\partial t}\langle \ell \rangle = -\mathrm{i}\frac{\partial}{\partial t}\int d\theta\,\psi_c^*(\theta,t)\frac{\partial}{\partial\theta}\psi_c(\theta,t) = 2v\,\mathrm{Im}\big[c_1^* c_0\big] \tag{4.43}$$

which vanishes, as it should, in the absence of v and also when the phase of $c_1^* c_0$ equals 0 or π.

4.5.1 Swallow-tail loops

We now ask how the system responds dynamically as the external rotation rate is varied. As we show, the non-linearity inherent in the GP equation leads to forced tunneling between the energy levels of the system in the presence of v. To see this behavior, we first construct the steady-state solutions of the GP equation in the form

$$|\psi_c(t)\rangle = e^{-\mathrm{i}\mu t}\,|\psi_c(0)\rangle \tag{4.44}$$

where μ is the chemical potential, a function of N; then, Eq. (4.42) gives

$$\begin{aligned} \mu c_0 &= \Big[\eta N\big(2 - |c_0|^2\big)\Big]c_0 + vc_1, \\ \mu c_1 &= \Big[\big(\tfrac{1}{2} - \bar{\Omega}\big) + \eta N\big(2 - |c_1|^2\big)\Big]c_1 + vc_0. \end{aligned} \tag{4.45}$$

The occupation probabilities of $|0\rangle$ and $|1\rangle$ as functions of μ are

$$\begin{aligned} |c_0|^2 &= \frac{\left(\frac{1}{2} - \bar{\Omega}\right) + \eta N - \mu}{\left(\frac{1}{2} - \bar{\Omega}\right) + 2(\eta N - \mu)} \\ |c_1|^2 &= \frac{\eta N - \mu}{\left(\frac{1}{2} - \bar{\Omega}\right) + 2(\eta N - \mu)} \end{aligned} \tag{4.46}$$

The eigenstates, then, have the form

$$\begin{aligned} |\mathrm{I}\rangle &= \begin{pmatrix} |c_0| \\ -|c_1| \end{pmatrix} \\ |\mathrm{II}\rangle &= \begin{pmatrix} |c_0| \\ |c_1| \end{pmatrix} \end{aligned} \tag{4.47}$$

where $|\mathrm{I}\rangle$ denotes the ground state branch and $|\mathrm{II}\rangle$ the excited state branch, since a phase difference of π between c_0 and c_1 minimizes the coupling energy $2N\upsilon\,\mathrm{Re}\left[c_1^* c_0\right]$ whereas a phase difference of 0 maximizes it.

The chemical potential (the "adiabatic energy level" in the sense of Refs. [83, 80]) is found from the determinant

$$\begin{vmatrix} \eta N\left(2 - |c_0|^2\right) - \mu & \upsilon \\ \upsilon & \left(\frac{1}{2} - \bar{\Omega}\right) + \eta N\left(2 - |c_1|^2\right) - \mu \end{vmatrix} = 0 \tag{4.48}$$

together with Eqs. (4.46). The result is a fourth-order equation for μ, with two to four real solutions depending on the values of $\eta N/2\upsilon \equiv \Lambda$ and $\bar{\Omega}$. The chemical potential is simply related to the energy per particle in the rotating frame by

$$E' = \mu - \frac{1}{2}\eta N\Big(1 + 2\,|c_0|^2\,|c_1|^2\Big). \tag{4.49}$$

The energy levels corresponding to states $|\mathrm{I}\rangle$ and $|\mathrm{II}\rangle$, in general, exhibit an avoided crossing as a function of Ω due to the presence of disorder. Since μ and E' are simply related by Eq. (4.49), the physical content of their corresponding plots is identical. To illustrate the physics, we plot the behavior in terms of μ since it is graphically clearer. Figure 4.6 shows the real solutions for μ as functions of $\bar{\Omega}$ for selected values of ηN and υ. As shown in the figure, and as we will prove at the end, for $\Lambda < 1$, the two energy levels have an avoided crossing at the critical value of the rotation rate

$$\bar{\Omega}_c = \frac{1}{2}; \tag{4.50}$$

at $\Lambda = 1$, a cusp appears in the lower branch at this frequency; and for $\Lambda > 1$, the cusp gives birth to a loop in the lower branch. The loop discussed earlier in Sec. 4.4 in the absence of the disorder potential (see Fig. 4.5) evolves into the present loop as the disorder is turned on. Note that at a given rotation frequency, Fig. 4.5 shows either two or three states, while Fig. 4.6 shows two or four states; the extra state arises from mixing of the upper maximum-energy state with lower-energy states (not shown in Fig. 4.5).

As seen in Fig. 4.7, the derivative of the occupation, $|c_0|^2$, of $|0\rangle$ with respect to $\bar{\Omega}$ diverges as the cusp appears in the lowest energy band, and the occupation folds over itself (the characteristic 'S' shape seen in fold catastrophes [77, 84, 85]) as the loop emerges for $\Lambda > 1$. The swallow-tail loop indicates hysteresis [76] and a lack of adiabatic evolution with $\bar{\Omega}$ [83, 80, 82, 79, 123] in a condensate in an annulus.

To see the physics of the swallow-tail loop, imagine that we prepare the system, with $\Lambda > 1$, on the lower branch at $\bar{\Omega} = 0$ and very slowly increase $\bar{\Omega}$ to avoid any tunneling to the other branch. The system will, then, follow this branch adiabatically until the point where the branch terminates and folds back on itself (at $\bar{\Omega} > \frac{1}{2}$). Upon further increase of $\bar{\Omega}$, the system is forced to make a discontinuous jump either to the lower part of branch I (indicated by the arrow A in Fig. 4.6) or to the upper branch II (indicated by the arrow B). Similarly, the occupation probability of $|0\rangle$ adiabatically follows the change in $\bar{\Omega}$ until the branch starts to fold over itself, at which point a sudden change in the population of that state becomes inevitable with further increase of the rotation frequency, as indicated by the arrows in Fig. 4.6. In other words, a fraction of the particles in $|0\rangle$ are forced to tunnel to $|1\rangle$. Sweeping $\bar{\Omega}$ in the other direction forces a similar behavior on the system as well.

The folded-over section of branch I of the occupation probability and the respective top part of the swallow-tail loop of the lowest-energy level (in the bottom panels of Figs. 4.7 and 4.6) are inaccessible through a sweep of Ω and correspond to unstable states. In direct analogy with the barrier state discussed earlier, they indicate the presence of more than one minimum in the energy landscape, separated by a maximum or a saddle-point [76, 84]. As we show in the next subsection, the appearance of the cusp (along with the corresponding divergence of $\partial |c_0|^2 / \partial \bar{\Omega}$ at $\bar{\Omega}_c$) and the swallow-tail loop (along with the corresponding fold-over in the level population) are related to the macroscopic quantum phenomenon of self-trapping or self-locked population imbalance.

4.5.2 Self-trapping

Interesting quantum phenomena, including Josephson effects analogous to those in superconductors and also chaotic dynamical behaviors, arise from the dynamical behavior of the macroscopic phase difference between the two components of the time-dependent condensate (4.38). To see this connection, we recast the

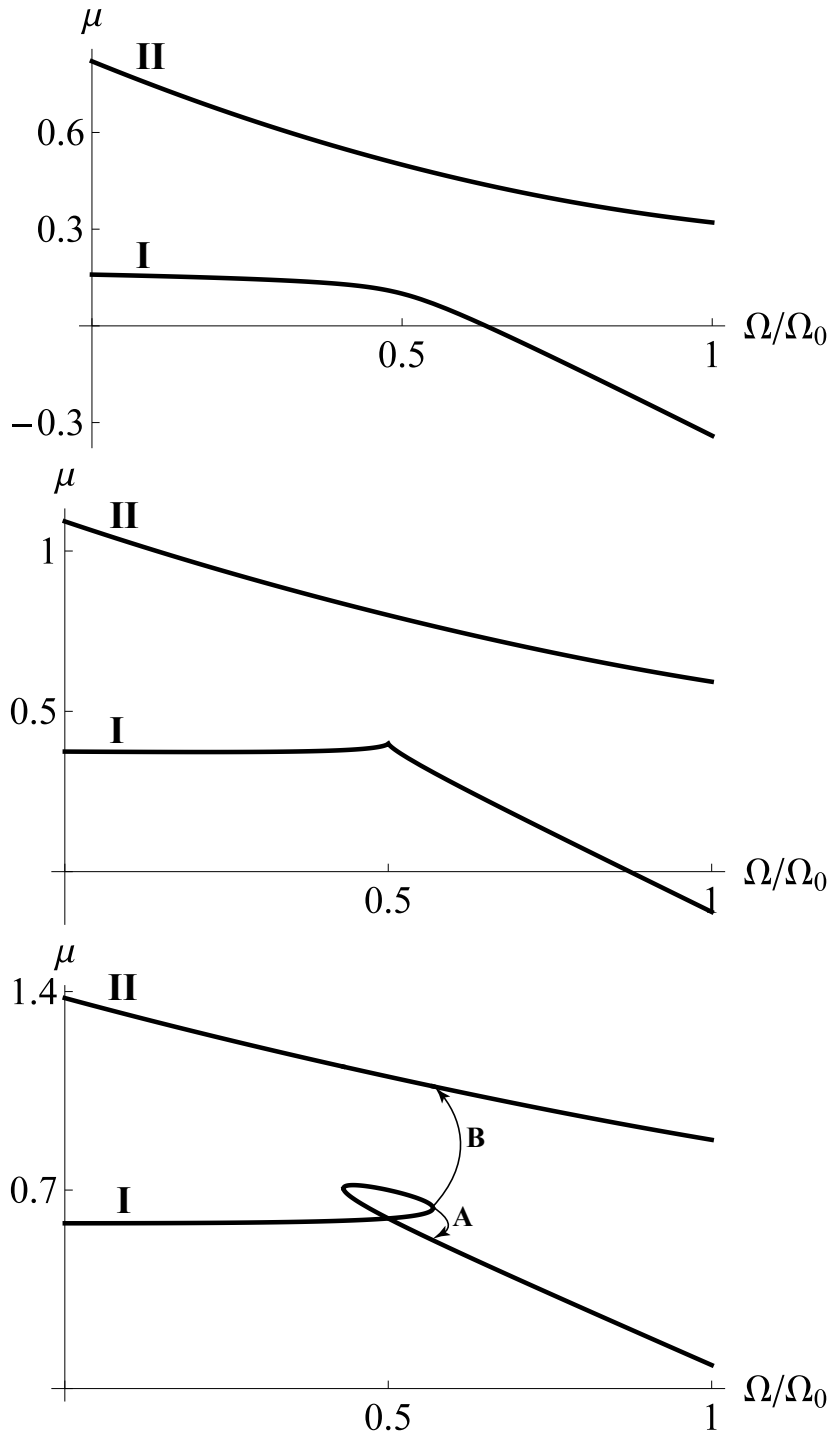

Figure 4.6: Adiabatic energy levels, measured in units of $\hbar\Omega_0$, as functions of $\bar{\Omega}$ for $\eta N = v$ (top), $\eta N = 2v$ (middle), and $\eta N = 3v$ (bottom), with $v = 1/5$. In all plots, the lowest-energy branch is indicated by I and the top energy level by II. The arrows A and B in the right column indicate the discontinuous change in the population of $|0\rangle$ and the forced tunneling of particles to $|1\rangle$ as $\bar{\Omega}$ is changed past the folding point.

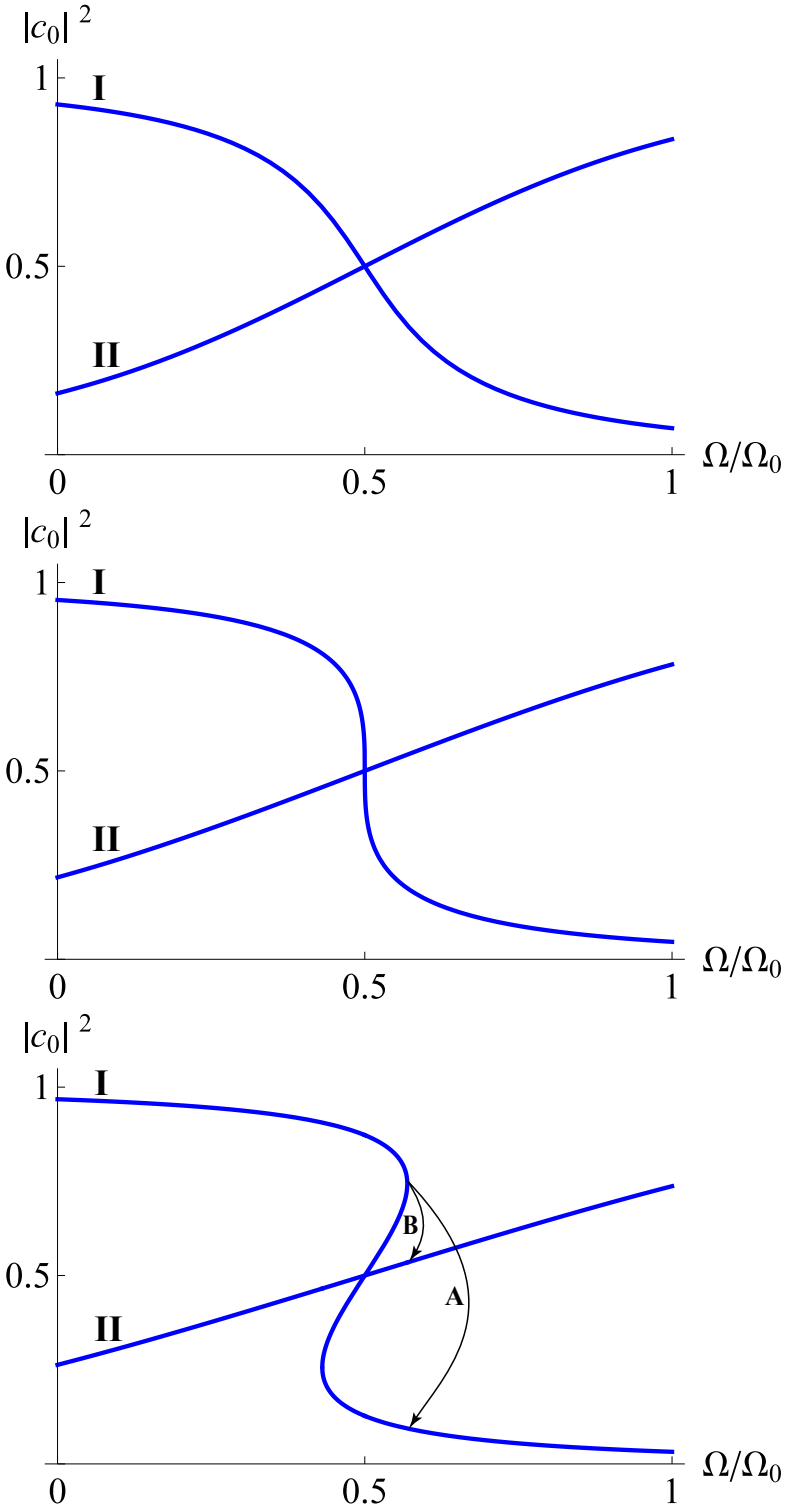

Figure 4.7: Occupation probabilities of $|0\rangle$ as functions of $\bar{\Omega}$ for $\eta N = v$ (top), $\eta N = 2v$ (middle), and $\eta N = 3v$ (bottom), with $v = 1/5$. In all plots, the population branch corresponding to the lowest-energy level is indicated by I, and the one corresponding to the higher-energy level by II. The arrows A and B in the bottom plot indicate the discontinuous change in the population of $|0\rangle$ and the forced tunneling of particles to $|1\rangle$ as $\bar{\Omega}$ is changed past the folding point.

time-evolution equations (4.42) in terms of the population difference

$$z = |c_0|^2 - |c_1|^2 , \tag{4.51}$$

where $-1 \leq z \leq 1$, and the phase difference

$$\phi = \alpha_0 - \alpha_1 \tag{4.52}$$

between the two constituent states, where $\alpha_j = \arg[c_j]$. Then, we find

$$\frac{\partial}{\partial \tau} z = -\sqrt{1 - z^2}\, \sin\phi \tag{4.53}$$

$$\frac{\partial}{\partial \tau} \phi = \Delta E + \Lambda z + \frac{z}{\sqrt{1 - z^2}}\, \cos\phi \tag{4.54}$$

where we rescale the time to

$$\tau = 2 v t \tag{4.55}$$

and set

$$\Delta E = \frac{\frac{1}{2} - \bar{\Omega}}{2v}. \tag{4.56}$$

These equations are identical to Eqs. (3a) and (3b) of Ref. [104] which describes coherent tunneling between two Bose-Einstein condensates in a double-well potential; therefore, all the results of that paper directly apply to the present system. The two levels, $|0\rangle$ and $|1\rangle$, correspond to the two wells. In the double-well system, an applied DC voltage between the two wells induces tunneling and, therefore, an AC particle current

$$\mathcal{I} = 2N v \frac{\partial}{\partial \tau} z \tag{4.57}$$

between the two condensates [106]. Analogously, in a toroidal trap, an external rotation induces a population transfer between the two levels.

The Hamiltonian (4.41) written in terms of ϕ and z is given, to within a constant term, by

$$\frac{\mathcal{H}_2'}{N v} = -\Delta E\, z - \frac{1}{2}\Lambda z^2 + \sqrt{1 - z^2}\, \cos\phi \tag{4.58}$$

and is a conserved quantity. Given that the dynamics is Hamiltonian, the quantum analog of the Poincaré recurrence theorem holds [124, 125], and, therefore, the system is inherently periodic in time.

The time evolution of the system, calculated numerically, is shown in Fig. 4.8 for different Λ. With

increase of Λ for a given initial population imbalance, $z(0)$, the oscillations in $z(\tau)$ change from purely harmonic (see Fig. 4.8a) to anharmonic (see Fig. 4.8b)and a plateau appears in $z(\tau)$ (the nearly flat part of the curve in Fig. 4.8c). At a critical value of Λ, dependent on $z(0)$, the oscillation period becomes infinite, and the population imbalance becomes time-independent at $z(\tau) = z_s$ (see Fig. 4.8d). For Λ larger than this critical value, $z(\tau)$ oscillates in time entirely above z_s (not shown in Fig. 4.8). Similarly, for fixed ΔE and Λ, there exists a critical value z_c of the initial population difference for which the oscillations cease and $z(\tau)$ becomes constant after a finite time (the plateau continues indefinitely). This evolution to a state with a non-zero time-averaged value of $z(\tau)$ (independent of ΔE and for Λ greater than or equal to the critical value discussed above) is the analog of the phenomenon of self-trapping in the double-well system [104, 105, 106].

The condition to develop self-trapping is that the two time derivatives, $\partial z/\partial\tau$ and $\partial\phi/\partial\tau$, vanish simultaneously. From Eq. (4.53), this requires $\phi = 0$ or π (although it appears that the singular point $z = 1$ also makes $z(\tau)$ time-independent, the correct solution is actually time-dependent [106], as can be deduced from Eq. (4.42), and is thus unacceptable). From Eq. (4.54), the steady-state value z_s is given in terms of ΔE and Λ by

$$\Delta E + \Lambda z_s \pm \frac{z_s}{\sqrt{1 - z_s^2}} = 0. \tag{4.59}$$

Once the system reaches this plateau, it must stay there forever, since the equations of motion are first-order in time. The critical initial population difference z_c that leads to self-trapping can be found from energy conservation. For an initial phase difference, $\phi(0)$, we find

$$\Delta E\, z_c + \frac{1}{2}\Lambda z_c^2 - \sqrt{1 - z_c^2}\,\cos\phi(0) = \Delta E\, z_s + \frac{1}{2}\Lambda z_s^2 \mp \sqrt{1 - z_s^2}\,. \tag{4.60}$$

As illustrated in Fig. 4.8, the stationary self-trapped population imbalance z_s is, in general, non-zero and only vanishes for $\Delta E = 0$.

The steady-state self-trapped solution is, in fact, related to the adiabatic energy levels discussed above. The stationary value $\phi = \pi$ leads to the ground state (branch I in Fig. 4.6), whereas $\phi = 0$ gives the excited state (branch II in Fig. 4.6). We focus first on the point $\bar{\Omega} = \bar{\Omega}_c$ at which the cusp and the tip of the swallow-tail loop appear and for which $\Delta E = 0$; choosing the minus sign in Eq. (4.59) (corresponding to the ground state), we find three solutions

$$z_s = \begin{cases} -\sqrt{1 - \Lambda^{-2}}\,, \\ 0, \\ +\sqrt{1 - \Lambda^{-2}}\,. \end{cases} \tag{4.61}$$

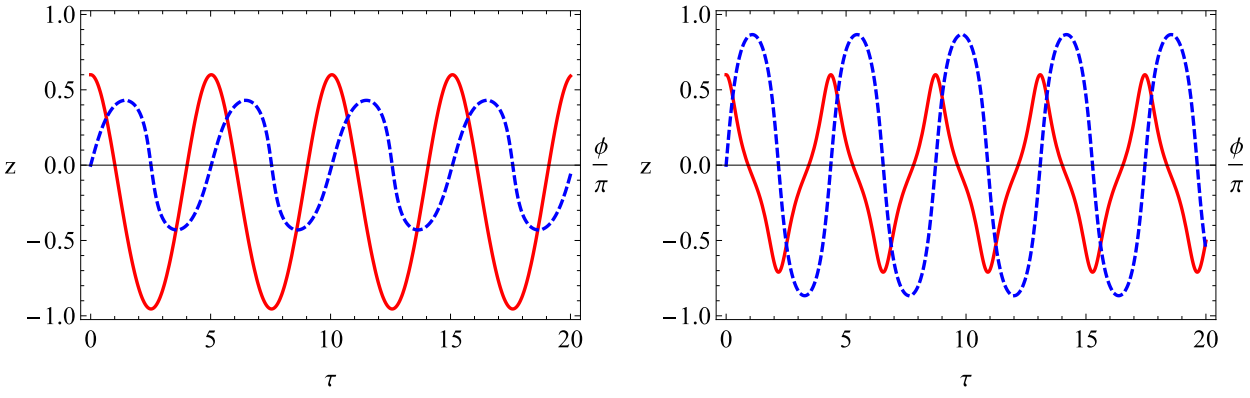

(a) $\Lambda = 1$

(b) $\Lambda = 7.75$

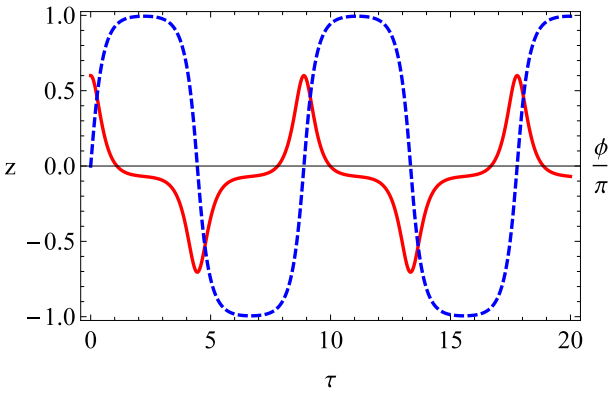

(c) $\Lambda = 8.2365$

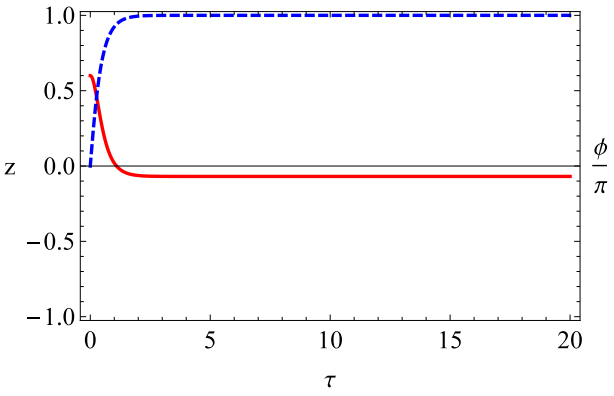

(d) $\Lambda = 8.2374$

Figure 4.8: Population difference z (solid line, in red) and phase difference ϕ/π (dashed line, in blue) as functions of τ for $\Delta E = 1/2$ and (a) $\Lambda = 1$ below the critical value, (b) 7.75, (c) 8.2365 just below the critical value, and (d) 8.2374 the critical value. The initial conditions are $z(\tau = 0) = 0.6$ and $\phi(\tau = 0) = 0$. Note how the oscillatory behavior of $z(\tau)$ changes from purely harmonic to anharmonic as Λ increases; finally, $z(\tau)$ and $\phi(\tau)$ both become time-independent as Λ reaches the critical value.

For $\Lambda < 1$, two solutions are complex and unphysical; however, when $\Lambda = 1$, all three solutions become degenerate at $z_s = 0$; and for $\Lambda > 1$, we have three distinct solutions. This change in the number of solutions at the critical point $\Lambda = 1$ is another indication of the occurence of the catastrophe [77, 84] when a swallow-tail loop appears. Moreover, Eq. (4.59) also yields

$$\frac{\partial z_s}{\partial \bar{\Omega}} = -\frac{1}{\Lambda\left(1-\Lambda^2\right)} = 2\,\frac{\partial \left|c_0\right|^2}{\partial \bar{\Omega}} \tag{4.62}$$

for $\Delta E = 0$. For $\Lambda = 1$, this quantity diverges; for $\Lambda < 1$, it is negative; and for $\Lambda > 1$, it is positive. Together, these two quantities exhibit the exact behavior, with varying Λ, seen in Fig. 4.7 at $\bar{\Omega} = \bar{\Omega}_c$. In general, for non-zero ΔE, finding z_s as a function of Ω by solving Eq. (4.59), we indeed see the behavior for $|c_0|^2$ depicted in Fig. 4.7. Hence, the ceasing of the coherent oscillation between the two components of the condensate (as the system becomes self-trapped) and the appearance of a cusp or a swallow-tail loop in the lowest-lying adiabatic energy level are in one-to-one correspondence. This proves our previous statement that the critical disorder strength for which a cusp or a loop first appears is $\Lambda = 1$ or, in other words, $v = \eta N/2$.

4.6 Summary

In this chapter, we analyzed the stability of a Bose-Einstein condensate in a rotating toroidal trap in terms of the normal modes of small-amplitude deviations from a metastable current-carrying state. We identified regions of energetic and dynamical instabilities in the phase space as functions of the interparticle interaction strength and rotation rate of the trap. Describing the coupling of the system to the rotation of the trap by a symmetry-breaking disorder perturbation to the original Hamiltonian, we investigated the steady-state and the general dynamics of this system in a two-mode mean-field model. We found that in the presence of these disorders, swallow-tail loops appear in the lowest-lying energy band for sufficiently strong interaction strengths and, as the rotation rate is varied, force a sudden, non-adiabatic change in the state of the system and the population of the two constituent states. Next, we investigated the connection of this system with a system of two condensates tunneling in a double-well potential and showed that these two systems have identical dynamics; therefore, the analog of the phenomenon of self-trapping also appears in the system studied in this chapter. Finally, we calculated the onset and the properties of self-trapping and showed how the steady-state self-trapped states are described in terms of the energy eigenstates.

Chapter 5

Discussion

We now discuss some possible extensions to the methods and results presented in this dissertation. The material in this chapter is preliminary and unpublished.

5.1 Other correlated states

Having discussed the effect of quantum fluctuations and interparticle correlations on the energetics of a vortex lattice, we now look at other forms of correlated states. Using the notation introduced in Appendix F, we write the mean-field GP condensate wave function in terms of the elementary symmetric polynomials (see Appendix D) defined on the set of vortices $\boldsymbol{\xi}' = \{\xi_j | j = 1, \ldots, N_\mathrm{v} - 1\}$ (excluding the vortex at the center of the trap, $\xi_0 = 0$) as

$$\psi(z) = C \sum_{j=0}^{N_\mathrm{v}'/6} \mathcal{S}_{N_\mathrm{v}'-6j}(\boldsymbol{\xi}')\, z^{6j+1} \tag{5.1}$$

where $N_\mathrm{v}' = N_\mathrm{v} - 1$ and the normalization constant is determined through $|C|^{-2} = \pi \sum_{j=0}^{N_\mathrm{v}'/6} (6j+1)! \left|\mathcal{S}_{N_\mathrm{v}'-6j}\right|^2$. Note how the 6-fold symmetry of the lattice is manifested in sum above. The occupations of the LLLs become

$$n_{6j+1} = N \frac{(6j+1)! \left|\mathcal{S}_{N_\mathrm{v}'-6j}\right|^2}{\sum_{j'=0}^{N_\mathrm{v}'/6} (6j'+1)! \left|\mathcal{S}_{N_\mathrm{v}'-6j'}\right|^2} \quad \text{for} \quad 0 \le j \le N_\mathrm{v}'/6 \tag{5.2}$$

with other states having zero occupation. These occupation probabilities are shown in Fig. 5.1 for triangular lattices with different number of vortices.

We see that the occupations of most of the single-particle LLLs are of the same order. However, the system does not form a fragmented condensate but, instead, can be described by a coherent sum of all the occupied states; the mean-field many-body state can be written in the general form

$$|\mathrm{C}\rangle = \frac{1}{\sqrt{N!}} \left[\sum_j \sqrt{\frac{n_j}{N}}\, a_j^\dagger \right]^N |\mathrm{vac}\rangle \tag{5.3}$$

where $|\mathrm{vac}\rangle$ is the vacuum, $n_j \in \mathbb{R}$, and $\sum_j n_j = N$. This state is not an eigenstate of the angular momentum

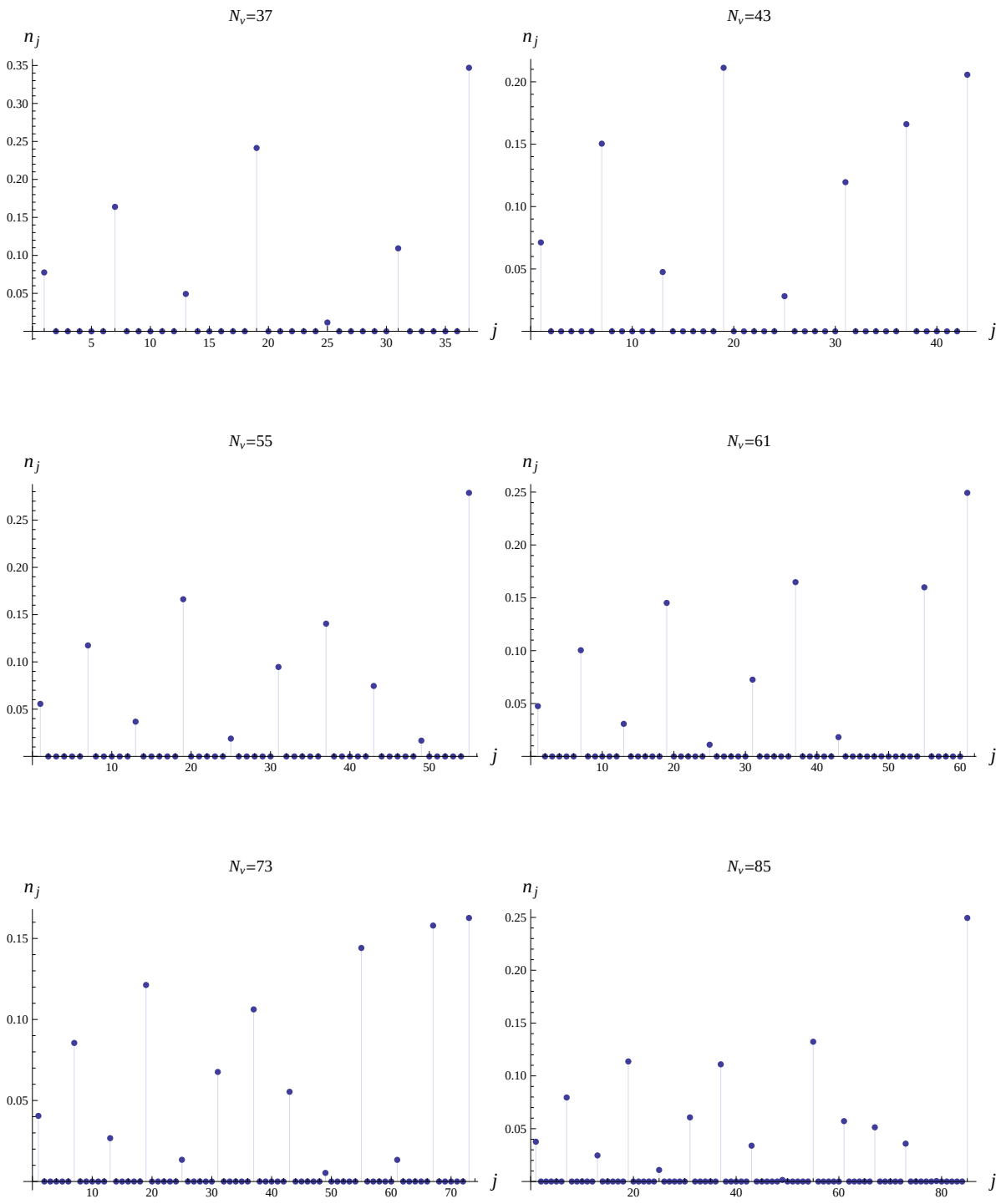

Figure 5.1: Occupations of LLLs (normalized to unity) for different triangular lattices with intervortex separation $a_{\rm v} = d_\perp \sqrt{2\pi/\sqrt{3}}$ achieved for $\Omega = \omega_\perp$.

operator (due to its broken rotational symmetry), but has $\langle \mathrm{C}| \mathcal{L} |\mathrm{C}\rangle = \sum_j \hbar j\, n_j$. However, we know that as the angular momentum of the system increases, the ground state will eventually lose its coherence and will cease to be a single condensate. We investigate the possibility of the system achieving this transition by forming a fragmented condensate, written generally as the Fock state

$$|\mathrm{F}\rangle = \left[\prod_j \frac{\left(a_j^\dagger\right)^{n_j}}{\sqrt{n_j!}}\right] |\mathrm{vac}\rangle \tag{5.4}$$

where $n_j \in \mathbb{N}$ and $\sum_j n_j = N$. Such a state is an eigenstate of angular momentum with eigenvalue $\sum_j \hbar j\, n_j$. Note that $\{n_j\}$ for the coherent and Fock states are not necessarily equal.

W rewrite the two-body interaction matrix element (2.11) as

$$\mathrm{V}^m_{m_1 m_2} = V_0 \frac{(m_1+m_2)!}{2^{m_1+m_2}\sqrt{(m_1-m)!(m_2+m)!m_2!m_1!}} \tag{5.5}$$

where $\hbar m$ is the transfered angular momentum during a scattering process (with $m_2+m \geq 0$ and $m_1-m \geq 0$). The interaction energies of the coherent and Fock states, then, are

$$V_\mathrm{C} = \frac{1}{2}\left(1-\frac{1}{N}\right)\left[\sum_i V^0_{ii}\, n_i^2 + 2\sum_{i\neq j} V^0_{ij}\, n_i n_j + \sum_{\substack{i,j,k \\ (k\neq 0)}}{}' V^k_{ij}\sqrt{n_{i-k}n_{j+k}n_j n_i}\right] \tag{5.6}$$

$$V_\mathrm{F} = \frac{1}{2}\left[\sum_i V^0_{ii}\, n_i(n_i-1) + 2\sum_{i\neq j} V^0_{ij}\, n_i n_j\right] \tag{5.7}$$

where the prime on the sum indicates the conditions $j+k \geq 0$ and $i-k \geq 0$.

Let us assume, for the sake of argument, that the occupations in the Fock state can take real values and are equal to those in the coherent state. Given that the angular momentum of both states would then be equal, comparing the two interaction energies determines the energetically-favorable state. The difference between the two interaction energies is

$$V_\mathrm{C} - V_\mathrm{F} = \frac{1}{2}\left[\sum_i V^0_{ii}\, n_i\left(1-\frac{n_i}{N}\right) + \left(1-\frac{1}{N}\right)\sum_{\substack{i,j,k \\ (k\neq 0)}}{}' V^k_{ij}\sqrt{n_{i-k}n_{j+k}n_j n_i} - \frac{2}{N}\sum_{i\neq j} V^0_{ij}\, n_i n_j\right]. \tag{5.8}$$

Since there are many more positive (although relatively small) terms in the interaction energy of the coherent state (the $k \neq 0$ terms) compared to that of the Fock state, the last term in Eq. (5.8) would have a hard time canceling their effect if a lot of single-particle states are populated. It would, thus, be possible for the Fock state – a fragmented condensate – to have a lower energy than the coherent state for large angular

momenta.

In the following, we discuss two situations where the Fock state could lead to an energetically favorable state. We have to mention beforehand that these are just pedagogical examples and will never be encountered in an experiment. The first example considers the extreme case of $n_i = 1$ for $i = 0, 1, \ldots, N-1$. We find

$$V_{\mathrm{C}} - V_{\mathrm{F}} = \frac{1}{2}\left(1 - \frac{1}{N}\right)\left[\sum_i V^0_{ii} + \sum_{\substack{i,j,k \\ (k\neq 0)}}{}' V^k_{ij} - \frac{2}{N-1}\sum_{i\neq j} V^0_{ij}\right]. \tag{5.9}$$

The leading-order behaviors of the sums are $\sum_i V^0_{ii} \sim \sqrt{N}$ and $\sum_{i\neq j} V^0_{ij} \sim 2N - \mathcal{O}(1)\sqrt{N}$ for large N. It is now obvious that this configuration favors the Fock state over the coherent state. Although the system described in this extreme case is not what one sees in a rapidly rotating Bose gas (the Laughlin state is not a fragmented condensate), it shows that a transition from a coherent state to a state with no coherence is likely to happen as more and more LLLs get populated by increasing the rotation rate.

As the second example, we look at the energies of a coherent state versus a Fock state with the occupations given by Eq. (5.2) for a triangular lattice. Below, we give the procedure to achieve this comparison.

1. We fix the number of vortices N_{v} while the number of particles N is allowed to change.

2. We construct a *perfect* triangular lattice of N_{v} vortices with intervortex separation a_{v} (a function of N_{v}, to be determined) using `MATHEMATICA`. Then, according to Eq. (5.2), the LLL occupations $\{n_j\}_{\mathrm{C,F}}$ (normalized to unity) are now only functions of a_{v}. We find these occupations through forming the respective elementary symmetric polynomials.

3. Using the fact that $L_{\mathrm{C,F}}/N = \sum_{j=0}^{N_{\mathrm{v}}} \hbar j\, n_j$, the angular momentum per particle (in units of $\hbar$), $\ell \equiv L/(\hbar N)$, of each state also becomes only a function of a_{v}.

4. Given that $\Omega = \omega_\perp + \partial V/\partial L$, we find for the triangular lattice, using Eqs. (3.19) and (3.24), that $N_{\mathrm{v}} = 3(\ell+1) - (V_0/\hbar\omega_\perp)\, 4b(N-1)/[3(\ell+1)]$. We then solve this equation for the angular momentum per particle ℓ of the coherent (mean-field) state in terms of the number of vortices N_{v}.

5. Setting the two angular momenta (from steps 3 and 4) equal determines self-consistently the intervortex separation a_{v} in terms of the number of vortices N_{v}.

6. Knowing a_{v} (and, hence, $\{n_j\}$), we calculate V_{F} using Eq. (5.7). For the energy of the coherent state, we use the value given by Eq. (3.24) (note that this value, obtained for a slightly distorted lattice, is 8/9 times the interaction energy for a perfect lattice with the same angular momentum [29]).

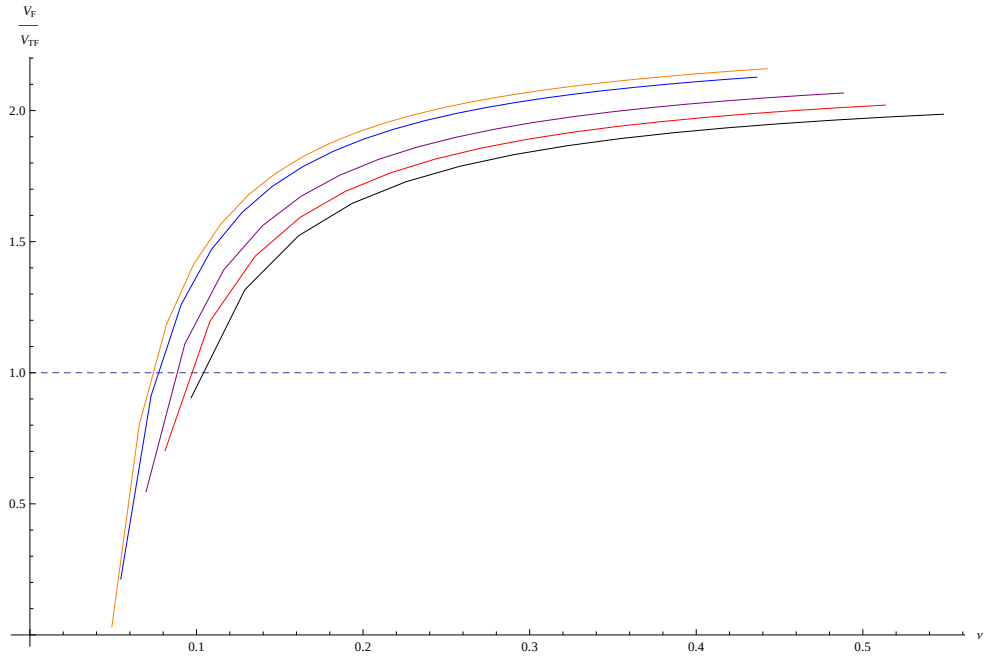

Figure 5.2: The ratio of the interaction energy of the Fock state to that of the coherent (mean-field) state as a function of the filling factor for $V_0/\hbar\omega_\perp \simeq 9 \times 10^{-4}$. Different colors represent different number of vortices with $N_v = 31$ (black), 37 (red), 43 (purple), 55 (blue), and 61 (orange).

7. The only free parameter in the system is the number of particles N. By changing N (while N_v is fixed), we compare the two energies at the same filing factor ν.

We show in Fig. 5.2 the ratio of these two interaction energies as a function of the filling factor. As shown, the energy of the Fock state eventually falls below that of the coherent state, although this happens at very small filling factors $\nu \lesssim 0.1$, corresponding to the case of very few particles, $N \sim 4$. For such few-particle systems, the assumption of being in the thermodynamic limit ($N \to \infty$) clearly fails, and it is not surprising that the mean-field GP state, the vortex lattice, is no longer the ground state [98]. Again, we should emphasize the pedagogical nature of this example, reflected in the fact that at such small filling factors, even the Fock state is not the ground state.

In the two examples presented above, we set the single-particle occupations of the LLLs for the Fock state equal to those for the coherent state. This was an artificial constraint, removing which could lead to a lower-energy Fock state. To investigate this possibility systematically, we need to find the optimum level occupations for a given total number of particles N and angular momentum L. Then, minimizing

$V_{\rm F} - \mu N - \Omega L$ with respect to $\{n_j\}$ leads to the following matrix (linear) equation

$$\begin{pmatrix} V^0_{00} & 2V^0_{01} & 2V^0_{02} & \dots \\ 2V^0_{10} & V^0_{11} & 2V^0_{12} & \dots \\ 2V^0_{20} & 2V^0_{21} & V^0_{22} & \dots \\ \vdots & \vdots & \vdots & \ddots \end{pmatrix} \begin{pmatrix} n_0 \\ n_1 \\ n_2 \\ \vdots \end{pmatrix} = \begin{pmatrix} \mu + 0\,\Omega + \frac{1}{2}V^0_{00} \\ \mu + 1\,\Omega + \frac{1}{2}V^0_{11} \\ \mu + 2\,\Omega + \frac{1}{2}V^0_{22} \\ \vdots \end{pmatrix}. \tag{5.10}$$

For the coherent state, minimizing $V_{\rm C} - \mu N - \Omega L$ gives a set of nonlinear equations

$$V^0_{ll}\, n_l + 2 \sum_{\substack{i \\ (i\neq l)}} V^0_{il}\, n_i + \frac{1}{4\sqrt{n_l}} \Bigg[\sum_{\substack{j,k \\ (k\neq 0)}}{}' V^k_{lj} \sqrt{n_j n_{j+k} n_{l-k}} + \sum_{\substack{i,k \\ (k\neq 0)}}{}' V^k_{il} \sqrt{n_i n_{l+k} n_{i-k}} + \sum_{\substack{i,k \\ (k\neq 0)}}{}' V^k_{i,l-k} \sqrt{n_i n_{l-k} n_{i-k}} + \sum_{\substack{j,k \\ (k\neq 0)}}{}' V^k_{l+k,j} \sqrt{n_{l+k} n_j n_{j+k}} \Bigg] = \frac{\mu + l\Omega}{1 - 1/N}. \tag{5.11}$$

Even though for very large particle numbers, the distribution that minimizes $V_{\rm C}$ is that of a triangular vortex lattice, the situation could be significantly different for few-particle systems (see below). The best distributions can be obtained by solving both equations numerically; we can then study the energetics of these states in detail for different angular momenta and different particle numbers.

For small number of particles ($N \sim 5 - 10$), other classes of correlated states have been shown to be superior to the GP mean-field states, namely the rotating boson molecules (RBM) [126, 127] and rotating vortex clusters (RVC) [128]. These states, with their rotational symmetry restored via projection techniques [47], are eigenstates of the angular momentum (unlike the GP state) and describe localized particles and vortices respectively. For example, a RVC state is formed through projecting out states with definite angular momentum out of the GP state [128]

$$|\psi_{\rm RVC}(L)\rangle = \int_0^{2\pi} \frac{d\theta}{2\pi}\, e^{{\rm i}L\theta}\, |\psi_{\rm GP}(\theta)\rangle \tag{5.12}$$

where $|\psi_{\rm GP}(\theta)\rangle$ is obtained through rotating the GP state by the angle θ. The GP state can be thought of as a wave packet formed by the superposition of the RVC states. Out of these constituent states, the one with the largest coefficient turns out to have the lowest energy and is the closest in angular momentum to the GP state; the energy of this RVC state is lower than that of the GP state [128]. In a RBM, bosons crystallize on a lattice, whereas vortices form a lattice in a RVC. However, by restoring the rotational symmetry, this localization is completely hidden from the density. In both cases, the (hidden) lattice configurations represent the point-group symmetry corresponding to the underlying angular momentum selection rule [47].

It would be very interesting to compare such rotating clusters of bosons or vortices with the Fock states discussed in this section for small number of particles and low angular momentum per particle.

5.2 Effects of non-zero temperature

All the discussion up to now has been constrained to zero temperature, for which almost all the particles are condensed and the effect of non-condensate particles can be safely ignored. However, in reality, experiments are performed at non-zero temperatures where the possibility of the thermal cloud playing an important role in the dynamics of the system cannot be readily dismissed (see, e.g., Ref. [129] for a quantitative study of vortex nucleation due to the effects of the thermal cloud). In this part, we briefly discuss non-zero temperature phenomena using the self-consistent theory of Zaremba, Nikuni, and Griffin (ZNG) [130, 131] which itself is based on the non-equilibrium Green's function formalism of Baym and Kadanoff [132].

The Heisenberg equation of motion for the bosonic field operator is

$$\mathrm{i}\hbar\frac{\partial\Psi(\mathbf{r},t)}{\partial t} = \hbar^0\Psi(\mathbf{r},t) + g\Psi^\dagger(\mathbf{r},t)\Psi(\mathbf{r},t)\Psi(\mathbf{r},t) \tag{5.13}$$

where $\hbar^0$ is the single-particle part of the Hamiltonian. We can decompose the field operator as $\Psi(\mathbf{r},t) = \psi(\mathbf{r},t) + \tilde{\Psi}(\mathbf{r},t)$ where $\psi = \langle\Psi\rangle$ corresponds to the condensate wave function and $\tilde{\Psi}$ denotes the non-condensate (fluctuation) part. Using this, we find the *exact* equation of motion for the condensate [130]

$$\mathrm{i}\hbar\frac{\partial\psi(\mathbf{r},t)}{\partial t} = \left[-\frac{\hbar^2\boldsymbol{\nabla}^2}{2m} + V(\mathbf{r}) + g\,n(\mathbf{r},t) + 2g\,\tilde{n}(\mathbf{r},t)\right]\psi(\mathbf{r},t) + g\,\tilde{m}(\mathbf{r},t)\psi^*(\mathbf{r},t) + g\left\langle\tilde{\Psi}^\dagger(\mathbf{r},t)\tilde{\Psi}(\mathbf{r},t)\tilde{\Psi}(\mathbf{r},t)\right\rangle \tag{5.14}$$

where $V(\mathbf{r})$ is the external (trapping) potential, $n = |\psi|^2$ is the condensate density, $\tilde{n} = \langle\tilde{\Psi}^\dagger\tilde{\Psi}\rangle$ is the non-condensate density, and $\tilde{m} = \langle\tilde{\Psi}\tilde{\Psi}\rangle$ is the anomalous density.

There exist several approximations in the literature to simplify this equation [131]; the ZNG theory uses the so-called Popov approximation [133, 134] where the anomalous density $\tilde{m}$ is ignored. It can be shown that both $\tilde{m}$ and $\langle\tilde{\Psi}^\dagger\tilde{\Psi}\tilde{\Psi}\rangle$ are $\mathcal{O}(g)$ with the latter being imaginary [135]; the ZNG theory only keeps imaginary terms of order g^2 in Eq. (5.14) [130]. Hence, we arrive at a generalized GP equation for the time evolution of the condensate

$$\mathrm{i}\hbar\frac{\partial\psi(\mathbf{r},t)}{\partial t} = \left[-\frac{\hbar^2\boldsymbol{\nabla}^2}{2m} + V(\mathbf{r}) + g\,n(\mathbf{r},t) + 2g\,\tilde{n}(\mathbf{r},t) - \mathrm{i}R(\mathbf{r},t)\right]\psi(\mathbf{r},t) \tag{5.15}$$

where $R = \mathrm{i}g\langle\tilde{\Psi}^\dagger\tilde{\Psi}\tilde{\Psi}\rangle/\psi \sim \mathcal{O}(g^2)$ represents the effect of collisions of the condensate and non-condensate atoms which lead to the removal (or addition) of atoms from (to) the condensate; in other words, the

condensate and non-condensate are now allowed to exchange particles. Within the ZNG theory, this quantity is given by

$$R(\mathbf{r},t) = 2\pi g^2 \int \frac{d^3\mathbf{p}_2}{(2\pi\hbar)^3}\frac{d^3\mathbf{p}_3}{(2\pi\hbar)^3}\frac{d^3\mathbf{p}_4}{(2\pi\hbar)^3}\big[f_2(1+f_3)(1+f_4)-(1+f_2)f_3f_4\big] \times (2\pi\hbar)^3\delta(m\mathbf{v}+\mathbf{p}_2-\mathbf{p}_3-\mathbf{p}_4)\,\delta(\epsilon+\tilde{\epsilon}_2-\tilde{\epsilon}_3-\tilde{\epsilon}_4). \tag{5.16}$$

Here, the condensate particles have momentum $m\mathbf{v}$ with

$$\mathbf{v}(\mathbf{r},t) = \left(\frac{\mathrm{i}\hbar}{2m}\right)\frac{\psi(\mathbf{r},t)\boldsymbol{\nabla}\psi^*(\mathbf{r},t)-\psi^*(\mathbf{r},t)\boldsymbol{\nabla}\psi(\mathbf{r},t)}{|\psi(\mathbf{r},t)|^2} \tag{5.17}$$

and energy $\epsilon = \mu + \frac{1}{2}m\mathbf{v}^2$ where

$$\mu(\mathbf{r},t) = -\frac{\hbar^2\boldsymbol{\nabla}^2\sqrt{n(\mathbf{r},t)}}{2m\sqrt{n(\mathbf{r},t)}} + V(\mathbf{r}) + g\big[n(\mathbf{r},t)+2\tilde{n}(\mathbf{r},t)\big] \tag{5.18}$$

is the condensate chemical potential. The non-condensate particles, on the other hand, have excitation energies given by the Hartree-Fock expression

$$\tilde{\epsilon}_i \equiv \tilde{\epsilon}(\mathbf{p}_i,\mathbf{r}_i,t) = \frac{\mathbf{p}_i^2}{2m} + V(\mathbf{r}_i) + 2g\big[n(\mathbf{r}_i,t)+\tilde{n}(\mathbf{r}_i,t)\big] \tag{5.19}$$

and are distributed according to $f_i \equiv f(\mathbf{p}_i,\mathbf{r}_i,t)$ with

$$\tilde{n}(\mathbf{r},t) = \int \frac{d^3\mathbf{p}}{(2\pi\hbar)^3} f(\mathbf{p},\mathbf{r},t). \tag{5.20}$$

Having found the equation of motion of the condensate, we now show how the non-condensate evolves in time in the presence of the condensate. According to the kinetic theory of gases, the distribution functions, in the presence of an effective mean-field potential $U(\mathbf{r},t) = V(\mathbf{r}) + 2g\big[n(\mathbf{r},t)+\tilde{n}(\mathbf{r},t)\big]$, behave as

$$\frac{\mathrm{d}f(\mathbf{p},\mathbf{r},t)}{\mathrm{d}t} = \frac{\partial f(\mathbf{p},\mathbf{r},t)}{\partial t} + \frac{\mathbf{p}}{m}\cdot\boldsymbol{\nabla}_{\mathbf{r}} f(\mathbf{p},\mathbf{r},t) - [\boldsymbol{\nabla}_{\mathbf{r}}U(\mathbf{r},t)]\cdot\boldsymbol{\nabla}_{\mathbf{p}} f(\mathbf{p},\mathbf{r},t) \tag{5.21}$$

where $\partial\mathbf{r}/\partial t = \partial\tilde{\epsilon}(\mathbf{p},\mathbf{r},t)/\partial\mathbf{p}$ and $\partial\mathbf{p}/\partial t = -\partial\tilde{\epsilon}(\mathbf{p},\mathbf{r},t)/\partial\mathbf{r}$ due to the Hamiltonian dynamics of the system. In the ZNG formalism, the collisions are quantitatively represented by

$$\frac{\mathrm{d}f(\mathbf{p},\mathbf{r},t)}{\mathrm{d}t} = C_{12}[f,\psi] + C_{22}[f] \tag{5.22}$$

where C_{12} and C_{22} denote, respectively, the interaction between condensate and non-condensate atoms and that between non-condensate atoms alone. Thus, the equation of motion for the distribution functions of thermal atoms is

$$\frac{\partial f(\mathbf{p},\mathbf{r},t)}{\partial t}+\frac{\mathbf{p}}{m}\cdot\boldsymbol{\nabla}_{\mathbf{r}}f(\mathbf{p},\mathbf{r},t)-[\boldsymbol{\nabla}_{\mathbf{r}}U(\mathbf{r},t)]\cdot\boldsymbol{\nabla}_{\mathbf{p}}f(\mathbf{p},\mathbf{r},t)=C_{12}[f,\psi]+C_{22}[f] \tag{5.23}$$

where the collisional integrals (implicit functions of $\mathbf{r}$, $\mathbf{p}$, and t) are given by

$$\begin{aligned}C_{12}[f,\psi]=\frac{4\pi}{\hbar}g^2\left|\psi\right|^2\int\frac{d^3\mathbf{p}_2}{(2\pi\hbar)^3}\frac{d^3\mathbf{p}_3}{(2\pi\hbar)^3}\frac{d^3\mathbf{p}_4}{(2\pi\hbar)^3}\big[(1+f_2)f_3f_4-f_2(1+f_3)(1+f_4)\big]\\ \times(2\pi\hbar)^3\delta(m\mathbf{v}+\mathbf{p}_2-\mathbf{p}_3-\mathbf{p}_4)\,\delta(\epsilon+\tilde{\epsilon}_2-\tilde{\epsilon}_3-\tilde{\epsilon}_4)\\ \times(2\pi\hbar)^3\big[\delta(\mathbf{p}-\mathbf{p}_2)-\delta(\mathbf{p}-\mathbf{p}_3)-\delta(\mathbf{p}-\mathbf{p}_4)\big]\end{aligned} \tag{5.24}$$

and

$$\begin{aligned}C_{22}[f]=\frac{4\pi}{\hbar}g^2\int\frac{d^3\mathbf{p}_2}{(2\pi\hbar)^3}\frac{d^3\mathbf{p}_3}{(2\pi\hbar)^3}\frac{d^3\mathbf{p}_4}{(2\pi\hbar)^3}\big[(1+f)(1+f_2)f_3f_4-ff_2(1+f_3)(1+f_4)\big]\\ \times(2\pi\hbar)^3\delta(\mathbf{p}+\mathbf{p}_2-\mathbf{p}_3-\mathbf{p}_4)\,\delta(\tilde{\epsilon}+\tilde{\epsilon}_2-\tilde{\epsilon}_3-\tilde{\epsilon}_4).\end{aligned} \tag{5.25}$$

Finally, we need to connect the two equations of motion for $\psi(\mathbf{r},t)$ and $f(\mathbf{p},\mathbf{r},t)$. This is done via

$$R(\mathbf{r},t)=\frac{\hbar}{2\left|\psi(\mathbf{r},t)\right|^2}\int\frac{d^3\mathbf{p}}{(2\pi\hbar)^3}\,C_{12}[f(\mathbf{p},\mathbf{r},t),\psi(\mathbf{r},t)]. \tag{5.26}$$

These equations provide a self-consistent second-order theory of the dynamics of a BEC in contact with thermal atoms. The former obeys a dissipative GP equation while the latter follows a quantum Boltzmann equation [136]. Theoretical predictions of the ZNG formalism are in excellent agreement with the observations in cold atoms experiments (see Ref. [131] for a review).

As a first and the simplest step in studying non-zero temperature effects, we employ the static thermal cloud approximation [130] which ignores the dynamics of the thermal cloud completely and assumes the time-independent thermal-equilibrium distribution

$$f^0(\mathbf{p},\mathbf{r})=\frac{1}{e^{\beta[\mathbf{p}^2/2m+U_0(\mathbf{r})-\tilde{\mu}_0(\mathbf{r})]}-1} \tag{5.27}$$

for the thermal atoms where $U_0(\mathbf{r})=V(\mathbf{r})+2g\big[n_0(\mathbf{r})+\tilde{n}_0(\mathbf{r})\big]$ is the equilibrium mean-field potential experienced by the atoms, $\beta=1/k_{\mathrm{B}}T$, and $\tilde{\mu}_0(\mathbf{r})$ is the equilibrium value of the thermal cloud local chemical

potential; we assume that the thermal atoms are at rest. This distribution yields $C_{22}[f^0] = 0$, and the thermal cloud local density $\tilde{n}_0(\mathbf{r})$ does not change in time. The condensate, therefore, is now coupled to a static reservoir (thermal atoms). The effect of collisions between the condensate and thermal atoms, given by Eq. (5.16), reduces to

$$R_0(\mathbf{r},t) = \frac{\hbar}{2\tau_0(\mathbf{r},t)} \left(e^{\beta[\epsilon(\mathbf{r},t)-\tilde{\mu}_0(\mathbf{r})]} - 1\right) \tag{5.28}$$

where

$$\epsilon(\mathbf{r},t) = \mu(\mathbf{r},t) + \frac{1}{2}m[\mathbf{v}(\mathbf{r},t)]^2 \tag{5.29}$$

is the condensate atom energy. The collision time is defined by

$$\frac{1}{\tau_0(\mathbf{r},t)} = \frac{4\pi}{\hbar}g^2 \int \frac{d^3\mathbf{p}_2}{(2\pi\hbar)^3}\frac{d^3\mathbf{p}_3}{(2\pi\hbar)^3}\frac{d^3\mathbf{p}_4}{(2\pi\hbar)^3}(1+f_2^0)f_3^0 f_4^0\,(2\pi\hbar)^3\delta(m\mathbf{v}+\mathbf{p}_2-\mathbf{p}_3-\mathbf{p}_4)\,\delta(\epsilon+\tilde{\epsilon}_2^0-\tilde{\epsilon}_3^0-\tilde{\epsilon}_4^0) \tag{5.30}$$

where the equilibrium thermal atom energy $\tilde{\epsilon}^0(\mathbf{r}) = \mathbf{p}^2/2m + U_0(\mathbf{r})$ is time-independent. The time-dependence of the collision time τ_0 is, thus, entirely due to that of the condensate variables $\mathbf{v}(\mathbf{r},t)$ and $\epsilon(\mathbf{r},t)$. In complete local equilibrium, the thermal atom chemical potential satisfies $\tilde{\mu}_0(\mathbf{r}) = \epsilon_0(\mathbf{r})$ which implies that the condensate and thermal cloud do not exchange particles, $R_0(\mathbf{r},t) \to 0$.

To further simplify the matter, we now apply this method to the case of the toroidally trapped condensate studied in Chapter 4, an effectively quasi-one-dimensional system living in a torus of radius R and cross-sectional radius r_0. We assume that the condensate is initially in the state with unit angular momentum per particle, $|\ell = 1\rangle$. Therefore, the (one-dimensional) equilibrium condensate density becomes uniform $n_0(\theta) = N_{\mathrm{c},0}(T)/2\pi R$ which, in turn, implies that the (one-dimensional) equilibrium thermal cloud density is also uniform $\tilde{n}_0(\theta) = N_{\mathrm{t},0}(T)/2\pi R$ (note the constraint $N_{\mathrm{c},0}(T)+N_{\mathrm{t},0}(T) = N$). Similarly, other equilibrium quantities are also position-independent; defining the effective interaction strength in one dimension $g_{1\mathrm{D}} = g/\pi r_0^2$, we find $U_0 = g_{1\mathrm{D}}N/\pi R$ and $\tilde{\mu}_0 = \epsilon_0 = U_0 - g_{1\mathrm{D}}N_{\mathrm{c},0}(T)/2\pi R + \hbar^2/2mR^2$. The equilibrium thermal distribution becomes

$$f^0(\mathbf{p}) = \frac{1}{e^{\beta[\mathbf{p}^2/2m+g_{1\mathrm{D}}N_{\mathrm{c},0}(T)/2\pi R-\hbar^2/2mR^2]}-1}. \tag{5.31}$$

Note that since the system is one-dimensional, the thermal excitation momentum $\mathbf{p}$ is directed along the tangential direction and, given the periodic boundary conditions, is quantized, i.e., $\mathbf{p} = (\hbar\nu/R)\hat{\boldsymbol{\theta}}$ with $\nu \in \mathbb{Z}$. The number of particles in the condensate and the thermal cloud at temperature T are, then, determined self-consistently through

$$\frac{N - N_{\mathrm{c},0}(T)}{2\pi R} = \int \frac{d\mathbf{p}}{2\pi\hbar}\, f^0(\mathbf{p}). \tag{5.32}$$

In Chapter 4, we defined the characteristic rotation rate $\Omega_0 = \hbar/mR^2$ and the dimensionless interaction energy scale $\eta = (g_{1\mathrm{D}}/2\pi R)/\hbar\Omega_0$. With these, we can rewrite the thermal distribution as

$$f^0(\nu) = \frac{1}{\exp\left\{\frac{1}{2}\beta\hbar\Omega_0\left[\nu^2 - 1 + 2\eta N_{\mathrm{c},0}(T)\right]\right\} - 1}. \tag{5.33}$$

We now consider dynamics of the system due to small deviations from the state of equilibrium. We define the changes in condensate density and velocity through

$$n(\theta, t) = n_0 + \delta n(\theta, t) \tag{5.34}$$

$$\mathbf{v}(\theta, t) = \mathbf{v}_0 + \delta\mathbf{v}(\theta, t) \tag{5.35}$$

where $\mathbf{v}_0 = (\hbar/mR)\hat{\boldsymbol{\theta}}$ is the equlibrium condensate velocity (in $|\ell = 1\rangle$). Given that the deviations are small, we linearize the collision term and find

$$\delta R_0(\theta, t) = \frac{\hbar\beta}{2\tau_0}\left[-\frac{\hbar^2}{4mR^2}\,\frac{1}{n_0}\,\frac{\partial^2}{\partial\theta^2}\delta n(\theta, t) + g_{1\mathrm{D}}\delta n(\theta, t) + m\mathbf{v}_0\cdot\delta\mathbf{v}(\theta, t)\right] \tag{5.36}$$

where the first term in the square brackets is due to the change in the quantum pressure and the collision time, defined by

$$\begin{aligned}\frac{1}{\tau_0} = \frac{4\pi}{\hbar}g_{1\mathrm{D}}^2\int\frac{d\mathbf{p}_2}{2\pi\hbar}\,\frac{d\mathbf{p}_3}{2\pi\hbar}\,\frac{d\mathbf{p}_4}{2\pi\hbar}\left(1 + f^0(\mathbf{p}_2)\right)f^0(\mathbf{p}_3)f^0(\mathbf{p}_4)\,(2\pi\hbar)\,\delta\big((\hbar/R)\hat{\boldsymbol{\theta}} + \mathbf{p}_2 - \mathbf{p}_3 - \mathbf{p}_4\big)\\ \times\,\delta\left(\left(\frac{\hbar^2}{2mR^2} - \frac{g_{1\mathrm{D}}N_{\mathrm{c},0}(T)}{2\pi R}\right) + \frac{\mathbf{p}_2^2 - \mathbf{p}_3^2 - \mathbf{p}_4^2}{2m}\right)\\ = 8\pi\Omega_0\eta^2\int d\nu_2\,d\nu_3\,d\nu_4\left(1 + f^0(\nu_2)\right)f^0(\nu_3)f^0(\nu_4)\,\delta\big(\nu_2 - \nu_3 - \nu_4 + 1\big)\,\delta\big(\nu_2^2 - \nu_3^2 - \nu_4^2 + 1 - 2\eta N_{\mathrm{c},0}(T)\big),\end{aligned} \tag{5.37}$$

is now time- and position-independent. In the current experiments, $\eta \sim 2\times10^{-2}$ (cf. Ref. [68]); therefore, the collision rate $1/\tau_0$ (measured in units of Ω_0) is a very small number. Nevertheless, due to the collisions between the condensate and thermal atoms, the dynamics of the system is dissipative. The small changes in the density and velocity are related to a respective small change in the condensate wave function, namely

$$\psi(\theta, t) = e^{-\mathrm{i}\epsilon_0 t/\hbar}\big[\psi_0(\theta) + \delta\psi(\theta, t)\big] \tag{5.38}$$

where $\psi_0(\theta) = \sqrt{n_0}\, e^{\mathrm{i}\theta}$ corresponds to the current-carrying state $|\ell = 1\rangle$. This yields

$$\delta n(\theta, t) = \sqrt{n_0}\left[e^{-\mathrm{i}\theta}\delta\psi(\theta, t) + e^{\mathrm{i}\theta}\delta\psi^*(\theta, t)\right], \tag{5.39}$$

$$\delta \mathbf{v}(\theta, t) = \left(\frac{-\mathrm{i}\hbar}{2mR}\right)\frac{\hat{\boldsymbol{\theta}}}{\sqrt{n_0}}\frac{\partial}{\partial\theta}\left[e^{-\mathrm{i}\theta}\delta\psi(\theta, t) - e^{\mathrm{i}\theta}\delta\psi^*(\theta, t)\right]. \tag{5.40}$$

Using these relations, we finally arrive at the linearized dissipative GP equation

$$\mathrm{i}\hbar\frac{\partial}{\partial t}\delta\psi(\theta, t) = -\frac{\hbar^2}{2mR^2}\frac{\partial}{\partial\theta^2}\delta\psi(\theta, t) + (2g_{1\mathrm{D}}n - \epsilon_0)\delta\psi(\theta, t) + g_{1\mathrm{D}}[\psi_0(\theta)]^2\delta\psi^*(\theta, t) - \mathrm{i}\,\delta R_0(\theta, t)\psi_0(\theta) \tag{5.41}$$

where $\delta R_0(\theta, t)$ is given by Eq. (5.36) and $n = N/2\pi R$ is the total (constant) density.

Apart from the last term which arises from the collisions, the above linearized equation is identical to the linearized GP equation in the Popov approximation [134]. Thus, we look for Bogoliubov-like solutions of the form (see also Eq. (4.12))

$$\delta\psi(\theta, t) = e^{\mathrm{i}\theta}\sum_{\nu\neq 0}\left[u_\nu(\theta)e^{-\mathrm{i}\omega_\nu t} - v_\nu^*(\theta)\, e^{\mathrm{i}\omega_\nu t}\right]. \tag{5.42}$$

Since $\delta R_0 \sim 1/\tau_0 \sim \mathcal{O}(\eta^2)$, the last term in Eq. (5.41), which results in the damping of the normal modes, can be treated perturbatively. We therefore expect the mode frequency ω_ν to acquire a small, but complex, correction [129, 137]

$$\omega_\nu = \omega_\nu^0 - \mathrm{i}\gamma_\nu \tag{5.43}$$

where $\gamma_\nu \sim 1/\tau_0$ is the damping rate due to the collisions of condensate and thermal atoms and ω_ν^0, the mode frequency in the absence of collisional effects, is derived from Eq. (4.16), taking into account the temperature dependence of the number of particles in the condensate, namely

$$\omega_\nu^0 = \Omega_0\left[\nu + |\nu|\sqrt{\tfrac{1}{4}\nu^2 + \eta N_{\mathrm{c},0}(T)}\right]. \tag{5.44}$$

The detailed form of γ_ν requires solving Eq. (5.41) (and its complex conjugate) using the mode expansion (5.42). Nonetheless, the fact that the normal modes have now acquired a complex part indicates that they have a finite lifetime. Therefore, we expect a current-carrying state to eventually decay, under appropriate conditions, to another state with lower energy and angular momentum. We find from Eqs. (5.42) and (5.39) that

$$\delta n(\theta, t) = 2\sqrt{n_0}\sum_{\nu\neq 0}\mathrm{Re}\left[[u_\nu(\theta) - v_\nu(\theta)]\, e^{-\mathrm{i}\omega_\nu^0 t}\right] e^{-\gamma_\nu t} \tag{5.45}$$

which indicates that density fluctuations will die out if $\gamma_\nu > 0$, hinting at the stability of the current-carrying state towards fluctuations. However, an exponential growth of the density fluctuations, $\delta n_\nu(\theta, t) \sim e^{|\gamma_\nu| t}$, becomes possible when γ_ν changes sign and becomes negative, indicating a dynamical instability in the system towards states with different angular momentum.

We note that due to the highly nonlinear nature of the dissipative GP equation, the full dynamics of the system can only be solved numerically. Moreover, our use of the static thermal cloud approximation should be viewed as a mere first step towards studying effects of the thermal cloud on the condensate. In reality, a change in the condensate density will induce a change in the thermal cloud density which will act back on the condensate through the mean-field HF potential (as used in the ZNG theory). This complex interplay between the two components makes the problem analytically intractable.

Appendix A

Two-dimensional harmonic oscillator in polar coordinates

In this Appendix, we solve the Schrödinger equation for a two-dimensional harmonic oscillator,

$$\left(-\frac{\hbar^2}{2m}\boldsymbol{\nabla}^2 + \frac{1}{2}m\omega_\perp^2\mathbf{r}^2\right)\psi(\mathbf{r}) = E\psi(\mathbf{r}), \tag{A.1}$$

and find its eigenenergies and eigenfunctions in polar coordinates.

We start by rescaling the original Schrödinger equation by defining $d_\perp^2 = \hbar/m\omega_\perp$ and $k^2 = 2mE/\hbar^2$; then, $2\epsilon \equiv k^2 d_\perp^2 = 2E/\hbar\omega_\perp$ is the unitless "eigenenergy" and $\mathbf{x} \equiv \mathbf{r}/d_\perp$ is the unitless "position" vector. We then have

$$\left(-\boldsymbol{\nabla}^2 + \mathbf{x}^2\right)\psi(\mathbf{x}) = 2\epsilon\,\psi(\mathbf{x}) \tag{A.2}$$

where the derivatives are now taken with respect to $\mathbf{x}$.

Since in polar coordinates,

$$\boldsymbol{\nabla}^2 = \frac{1}{x}\frac{\partial}{\partial x}\left(x\,\frac{\partial}{\partial x}\right) + \frac{1}{x^2}\frac{\partial^2}{\partial\varphi^2} = \frac{\partial^2}{\partial x^2} + \frac{1}{x}\frac{\partial}{\partial x} + \frac{1}{x^2}\frac{\partial^2}{\partial\varphi^2}, \tag{A.3}$$

we assume that

$$\psi(\mathbf{x}) = R(x)\,e^{\mathrm{i}m\varphi}; \tag{A.4}$$

therefore, m should be an integer for $\psi(\mathbf{x})$ to be single-valued. Plugging Eq. (A.4) into Eq. (A.2) yields

$$-\left(\frac{\partial^2 R}{\partial x^2} + \frac{1}{x}\frac{\partial R}{\partial x} - \frac{m^2}{x^2}\,R\right) + x^2 R = 2\epsilon R. \tag{A.5}$$

We know that as $|\mathbf{r}| \to \infty$, we should have $\psi(\mathbf{r}) \to 0$. In this limit, the above ODE reduces to $-\partial^2 R/\partial x^2 + x^2 R = 0$. Thus, $\lim_{x\to\infty} R(x) \sim e^{-x^2/2}$, and we write

$$R(x) = u(x)\,e^{-x^2/2} \tag{A.6}$$

with the derivatives

$$\frac{\partial R}{\partial x} = \left(\frac{\partial u}{\partial x} - x\,u\right) e^{-x^2/2}, \tag{A.7}$$

$$\frac{\partial^2 R}{\partial x^2} = \left[\frac{\partial^2 u}{\partial x^2} - 2x\,\frac{\partial u}{\partial x} + (x^2-1)u\right] e^{-x^2/2}. \tag{A.8}$$

Using Eq. (A.6) and the derivatives above, we recast Eq. (A.5) as an ODE for $u(x)$,

$$\frac{\partial^2 u}{\partial x^2} + \left(\frac{1}{x} - 2x\right)\frac{\partial u}{\partial x} + \left(2\epsilon - 2 - \frac{m^2}{x^2}\right) u = 0. \tag{A.9}$$

Since this ODE is invariant with respect to the sign of m, we define

$$u(x) = x^{|m|}\, v(x) \tag{A.10}$$

which leads to

$$\frac{\partial u}{\partial x} = \left(|m|\, v + x\,\frac{\partial v}{\partial x}\right) x^{|m|-1}, \tag{A.11}$$

$$\frac{\partial^2 u}{\partial x^2} = \left[x^2\,\frac{\partial^2 v}{\partial x^2} + 2\,|m|\,x\,\frac{\partial v}{\partial x} + |m|\,(|m|-1)v\right] x^{|m|-2}. \tag{A.12}$$

Using these derivatives and Eq. (A.10), we rewrite Eq. (A.9) as another ODE for $v(x)$ as follows

$$x\,\frac{\partial^2 v}{\partial x^2} + \big(2\,|m| + 1 - 2x^2\big)\frac{\partial v}{\partial x} + 2[\epsilon - (|m|+1)]x\,v = 0. \tag{A.13}$$

Dividing this equation by x and using the fact that $x\,dx = d(x^2/2)$, we find

$$4x^2\frac{\partial^2 v}{\partial (x^2)^2} + 4\big(\,|m| + 1 - x^2\big)\frac{\partial v}{\partial (x^2)} + 2[\epsilon - (|m|+1)]\,v = 0 \tag{A.14}$$

or, with $y \equiv x^2$,

$$y\,\frac{\partial^2 v}{\partial y^2} + \big(\,|m| + 1 - y\big)\frac{\partial v}{\partial y} + \frac{1}{2}[\epsilon - (|m|+1)]\,v = 0. \tag{A.15}$$

This is the ODE for the associated Laguerre polynomials [138] and has a non-singular solution only if the coefficient of $v(y)$ is a non-negative integer. Therefore, we have

$$v(y) = L_n^{(|m|)}(y) \tag{A.16}$$

where $n = \frac{1}{2}[\epsilon-(|m|+1)] \in \mathbb{N}_0$. In other words, the eigenenergies of this two-dimensional harmonic oscillator are

$$E = \hbar\omega_\perp(2n + |m| + 1) \quad \text{with} \quad n \geq 0,\ m \in \mathbb{Z} \tag{A.17}$$

where n is the radial quantum number and m is the angular momentum. The non-normalized eigenfunctions corresponding to the above eigenvalues are, therefore,

$$\psi_{nm}(x, \varphi) = e^{-x^2/2}\, x^{|m|}\, L_n^{(|m|)}\big(x^2\big)\, e^{\mathrm{i}m\varphi}\,. \tag{A.18}$$

Using Eq. (13.48) of Ref. [138], namely

$$\int_0^\infty dy\, e^{-y}\, y^k\, L_i^{(k)}(y) L_j^{(k)}(y) = \delta_{ij}\, \frac{(i+k)!}{i!}, \tag{A.19}$$

we write

$$\begin{aligned}
\langle \psi_{nm} | \, \psi_{nm} \rangle &= \int_0^\infty \int_0^{2\pi} e^{-x^2}\, x^{2|m|}\, L_n^{(|m|)}\big(x^2\big) L_n^{(|m|)}\big(x^2\big)\, x\, dx d\varphi \\
&= \pi \int_0^\infty dy\, e^{-y}\, y^{|m|}\, L_n^{(|m|)}(y) L_n^{(|m|)}(y) \\
&= \frac{\pi\,(n+|m|)!}{n!}.
\end{aligned} \tag{A.20}$$

Thus, the normalized eigenfunctions become

$$\psi_{nm}(x, \varphi) = \sqrt{\frac{n!}{\pi\,(n+|m|)!}}\, e^{-x^2/2}\, x^{|m|}\, L_n^{(|m|)}\big(x^2\big)\, e^{\mathrm{i}m\varphi} \tag{A.21}$$

where $x = |\mathbf{r}|\,/d_\perp$.

Appendix B

Bogoliubov approximation in the Landau level manifold

The many-body Hamiltonian of an N-body system in a harmonic trap with pairwise contact interaction is

$$\mathcal{H} = \sum_{i=1}^{N} \hbar_i^0 + \sum_{i<j} v_{ij} \tag{B.1}$$

where

$$\hbar_i^0 = \frac{\mathbf{p}_i^2}{2m} + \frac{1}{2} m\omega_\perp^2 \mathbf{r}_i^2 \tag{B.2a}$$

$$v_{ij} = g_{2\mathrm{D}}\, \delta(\mathbf{r}_i - \mathbf{r}_j) \tag{B.2b}$$

are the non-interacting and two-body interaction parts. The eigenstates of the non-interacting, single-particle Hamiltonian, Eq. (B.2a), are given by Eq. (A.21), i.e.,

$$\phi_{nm}(z) \equiv \langle \mathbf{r} \,|nm\rangle = \frac{1}{d_\perp} \sqrt{\frac{n!}{\pi(n+|m|)!}}\, e^{-|z|^2/2}\, |z|^{|m|}\, L_n^{(|m|)}\big(\,|z|^2\,\big)\, e^{\mathrm{i}m\varphi}, \tag{B.3}$$

and have energies given by Eq. (A.17), i.e.,

$$\epsilon_{nm} = \hbar\omega_\perp(2n + |m| + 1), \tag{B.4}$$

where $z = (x + \mathrm{i}y)/d_\perp$ and $L_n^{(k)}(x)$ is the associated Laguerre polynomial [138]. We define $\mathcal{L} = \sum_{i=1}^{N} \ell_i$ as the z component of the total angular momentum, and the Hamiltonian in the rotating frame, $\mathcal{H}' = \mathcal{H} - \Omega\mathcal{L}$, becomes

$$\mathcal{H}' = \sum_{i=1}^{N} \left[\frac{\mathbf{p}_i^2}{2m} + \frac{1}{2} m\omega_\perp^2 \mathbf{r}_i^2 - \Omega \ell_i \right] + \sum_{i<j} g_{2\mathrm{D}}\, \delta(\mathbf{r}_i - \mathbf{r}_j). \tag{B.5}$$

Since $|nm\rangle$ is also an eigenstate of ℓ_i with eigenvalue m, the non-interacting, single-particle part of Eq. (B.5) has the eigenvalue $\epsilon'_{nm} = \hbar\big[(2n + |m| + 1)\omega_\perp - m\Omega\big]$. Defining the creation (annihilation) operators $a_{nm}^\dagger$

(a_{nm}) corresponding to $|nm\rangle$, this Hamiltonian in the second quantization language becomes

$$\mathcal{H}' = \sum_{nm} \epsilon'_{nm} a^\dagger_{nm} a_{nm} + \frac{1}{2} \sum_{\substack{\{n_i m_i\} \\ (i=1\ldots4)}} \mathrm{V}^{n_4 n_3 n_2 n_1}_{m_4 m_3 m_2 m_1} a^\dagger_{n_4 m_4} a^\dagger_{n_3 m_3} a_{n_2 m_2} a_{n_1 m_1} \tag{B.6}$$

where, using Eq. (B.2b), we have

$$\begin{aligned} \mathrm{V}^{n_4 n_3 n_2 n_1}_{m_4 m_3 m_2 m_1} \equiv \langle n_4 m_4; n_3 m_3 |\, v \,| n_2 m_2; n_1 m_1 \rangle &= \int d^2\mathbf{r}_i d^2\mathbf{r}_j \, \phi^*_{n_4 m_4}(\mathbf{r}_i) \phi^*_{n_3 m_3}(\mathbf{r}_j) v_{ij} \phi_{n_2 m_2}(\mathbf{r}_j) \phi_{n_1 m_1}(\mathbf{r}_i) \\ &= g_{2\mathrm{D}} \int d^2\mathbf{r} \, \phi^*_{n_4 m_4}(\mathbf{r}) \phi^*_{n_3 m_3}(\mathbf{r}) \phi_{n_2 m_2}(\mathbf{r}) \phi_{n_1 m_1}(\mathbf{r}). \end{aligned} \tag{B.7}$$

Since $\phi_{nm}(z) \sim e^{\mathrm{i}m\varphi}$, it follows from Eq. (B.7) that in order for $\mathrm{V}^{n_4 n_3 n_2 n_1}_{m_4 m_3 m_2 m_1}$ to be non-zero, we should have $m_1 + m_2 = m_3 + m_4$; in other words, the angular momentum is conserved by two-body interactions. Thus, one can write

$$m_3 = m_2 + m \tag{B.8}$$

$$m_4 = m_1 - m \tag{B.9}$$

where m is the transfered angular momentum in a two-body scattering process.

We now proceed with the Bogoliubov approximation to the Hamiltonian (B.6) in the limit of weak interactions. Assume that N_{01} particles are condensed into the state with a vortex at the center with winding number 1; therefore, the condensate wave function is $\psi(\mathbf{r}) = \sqrt{N_{01}}\, \phi_{01}(\mathbf{r})$. If $N_{01} \lesssim N$, one can substitute the operators corresponding to $|01\rangle$ (that is, $a^\dagger_{01}$ and a_{01}) with $\sqrt{N_{01}}$ in Eq. (B.6). Interactions cause the number of particles in the condensate, N_{01}, to fluctuate, but the total number of particles is fixed, i.e.,

$$N = \sum_{nm} a^\dagger_{nm} a_{nm}. \tag{B.10}$$

Moreover, the energy difference between higher Landau level (HLL) states $|nm\rangle$ and $|n+1, m\rangle$ is $2\hbar\omega_\perp$, which is much greater, in the limit $\Omega \to \omega_\perp$, than that between successive states in the lowest Landau level (LLL) manifold ($|0m\rangle$ and $|0, m+1\rangle$) which is $\mathcal{O}(\hbar[\omega_\perp - \Omega])$. Therefore, whenever there is a sum over HLL states $|nm\rangle$, we pick the values of n according to

$$n = \begin{cases} 0 & \text{if } m \geq 0 \\ |m| & \text{if } m < 0 \end{cases}. \tag{B.11}$$

This ensures that for negative values of single-particle angular momentum ($m < 0$), only the lowest-energy HLL state, a state of the form $||m|, m\rangle$, is mixed; other HLL states with the same m are separated from this one by an energy gap which is an integer multiple of $2\hbar\omega_\perp$, and mixing them costs a lot of extra energy.

Substituting the number operator with its expectation value and using Eq. (B.11) leads to

$$N_{01} = N - \sum_{\substack{nm \\ (|nm\rangle \neq |01\rangle)}} a^\dagger_{nm} a_{nm} \simeq N - \sum_m{}' \left(a^\dagger_{0m} a_{0m} + a^\dagger_{m,-m} a_{m,-m}\right) \tag{B.12}$$

where the prime on the sum means that the $m = 0$ contribution comes *only* from the first ($|0m\rangle$) term and the $m = 1$ contribution comes *only* from the second ($|m, -m\rangle$) term in the parentheses, whereas both terms contribute to the $m \geq 2$ part of the sum (the state $|01\rangle$ is excluded from the sum). Squaring Eq. (B.12), using the bosonic commutation relation $\left[a_{nm}, a^\dagger_{n'm'}\right] = \delta_{nn'}\delta_{mm'}$, and keeping up to quadratic order in $a^\dagger$'s and a's together yield

$$\begin{aligned} N_{01}^2 &= N^2 - 2N \sum_m{}' \left(a^\dagger_{0m} a_{0m} + a^\dagger_{m,-m} a_{m,-m}\right) + \left[\sum_m{}' \left(a^\dagger_{0m} a_{0m} + a^\dagger_{m,-m} a_{m,-m}\right)\right]^2 \\ &\simeq N^2 - 2N \sum_m{}' \left(a^\dagger_{0m} a_{0m} + a^\dagger_{m,-m} a_{m,-m}\right) + \sum_{m,m'}{}' \left(a^\dagger_{0m} a_{0m} a^\dagger_{0m'} a_{0m'} + a^\dagger_{m,-m} a_{m,-m} a^\dagger_{m',-m'} a_{m',-m'}\right) \\ &\simeq N^2 - (2N-1) \sum_m{}' \left(a^\dagger_{0m} a_{0m} + a^\dagger_{m,-m} a_{m,-m}\right). \end{aligned} \tag{B.13}$$

The first term of the Hamiltonian in the rotating frame, Eq. (B.6), can be written as

$$\sum_{nm} \epsilon'_{nm} a^\dagger_{nm} a_{nm} \simeq N_{01}\epsilon'_{01} + \sum_m{}' \left(\epsilon'_{0m} a^\dagger_{0m} a_{0m} + \epsilon'_{m,-m} a^\dagger_{m,-m} a_{m,-m}\right). \tag{B.14}$$

The sum in the interaction term, the second term in Eq. (B.6), is more involved, but the summand can be categorized as

$$\begin{aligned} &\overbrace{\mathrm{V}^{0000}_{1111} a^\dagger_{01} a^\dagger_{01} a_{01} a_{01}}^{\textbf{I: } m_1=1, m_2=1, m=0} + \overbrace{\mathrm{V}^{n_4 00 n_1}_{m_1 11 m_1} a^\dagger_{n_4 m_1} a^\dagger_{01} a_{01} a_{n_1 m_1}}^{\textbf{II: } m_1\neq 1, m_2=1, m=0} + \overbrace{\mathrm{V}^{0 n_3 n_2 0}_{1 m_2 m_2 1} a^\dagger_{01} a^\dagger_{n_3 m_2} a_{n_2 m_2} a_{01}}^{\textbf{III: } m_1=1, m_2\neq 1, m=0} \\ &+ \overbrace{\mathrm{V}^{n_4 n_3 n_2 n_1}_{m_1 m_2 m_2 m_1} a^\dagger_{n_4 m_1} a^\dagger_{n_3 m_2} a_{n_2 m_2} a_{n_1 m_1}}^{\textbf{IV: } m_1\neq 1, m_2\neq 1, m=0} + \overbrace{\mathrm{V}^{n_4 n_3 00}_{1-m,1+m,11} a^\dagger_{n_4,1-m} a^\dagger_{n_3,1+m} a_{01} a_{01}}^{\textbf{V: } m_1=1, m_2=1, m\neq 0} \\ &+ \underbrace{\mathrm{V}^{n_4 n_3 0 n_1}_{m_1-m,1+m,1 m_1} a^\dagger_{n_4, m_1-m} a^\dagger_{n_3,1+m} a_{01} a_{n_1 m_1}}_{\textbf{VI: } m_1\neq 1, m_2=1, m\neq 0} + \underbrace{\mathrm{V}^{n_4 n_3 n_2 0}_{1-m, m_2+m, m_2 1} a^\dagger_{n_4,1-m} a^\dagger_{n_3, m_2+m} a_{n_2 m_2} a_{01}}_{\textbf{VII: } m_1=1, m_2\neq 1, m\neq 0} \\ &+ \underbrace{\mathrm{V}^{n_4 n_3 n_2 n_1}_{m_1-m, m_2+m, m_2 m_1} a^\dagger_{n_4, m_1-m} a^\dagger_{n_3, m_2+m} a_{n_2 m_2} a_{n_1 m_1}}_{\textbf{VIII: } m_1\neq 1, m_2\neq 1, m\neq 0} \end{aligned}$$

which becomes, upon setting $n_i = 0$ if the corresponding $m_i = 1$, up to quadratic order in the operators

$$\overbrace{N_{01}^2 \mathrm{V}^{0000}_{1111}}^{\mathbf{I}} + N_{01}\big(\overbrace{\mathrm{V}^{n_4 0 0 n_1}_{m_1 1 1 m_1} a^\dagger_{n_4 m_1} a_{n_1 m_1}}^{\mathbf{II}:\, m_1\neq 1} + \overbrace{\mathrm{V}^{0 n_3 n_2 0}_{1 m_2 m_2 1} a^\dagger_{n_3 m_2} a_{n_2 m_2}}^{\mathbf{III}:\, m_2\neq 1} + \overbrace{\mathrm{V}^{0 n_3 0 n_1}_{1 m_1 1 m_1} a^\dagger_{n_3 m_1} a_{n_1 m_1}}^{\mathbf{VI}:\, m_1-m=1, m\neq 0} + \overbrace{\mathrm{V}^{n_4 0 n_2 0}_{m_2 1 m_2 1} a^\dagger_{n_4 m_2} a_{n_2 m_2}}^{\mathbf{VII}:\, m_2+m=1, m\neq 0}\big)$$
$$+ N_{01}\big(\underbrace{\mathrm{V}^{n_4 n_3 0 0}_{1-m,1+m,1 1} a^\dagger_{n_4,1-m} a^\dagger_{n_3,1+m}}_{\mathbf{V}:\, m\neq 0} + \underbrace{\mathrm{V}^{00 n_2 n_1}_{11,1-m,1+m} a_{n_2,1-m} a_{n_1,1+m}}_{\mathbf{VIII}:\, m_1-m=1, m_2+m=1, m\neq 0}\big).$$

Since m_i's are dummy variables, separating the LLL ($m \geq 0$) and HLL ($m < 0$) states using the selection rule (B.11) explicitly gives the following form for the summand above

$$N_{01}^2 \mathrm{V}^{0000}_{1111} + N_{01}\Big[\overbrace{\big(\mathrm{V}^{0000}_{m11m} + \mathrm{V}^{0000}_{1mm1} + \mathrm{V}^{0000}_{1m1m} + \mathrm{V}^{0000}_{m1m1}\big) a^\dagger_{0m} a_{0m}}^{\text{for } m=0,2,3,4,\ldots \text{ above}}$$
$$+ \overbrace{\big(\mathrm{V}^{m00m}_{-m,1,1,-m} + \mathrm{V}^{0mm0}_{1,-m,-m,1} + \mathrm{V}^{0m0m}_{1,-m,1,-m} + \mathrm{V}^{m0m0}_{-m,1,-m,1}\big) a^\dagger_{m,-m} a_{m,-m}}^{\text{for } m=-1,-2,-3,-4,\ldots \text{ above}}\Big]$$
$$+ N_{01}\Big[\big(\underbrace{\mathrm{V}^{m-1,000}_{1-m,1+m,11} a^\dagger_{m-1,1-m} a^\dagger_{0,1+m} + \mathrm{V}^{00,m-1,0}_{11,1-m,1+m} a_{m-1,1-m} a_{0,1+m}}_{\text{for } m=1,2,3,4,\ldots \text{ above}}\big)$$
$$+ \big(\underbrace{\mathrm{V}^{0,m-1,00}_{1+m,1-m,11} a^\dagger_{0,1+m} a^\dagger_{m-1,1-m} + \mathrm{V}^{000,m-1}_{11,1+m,1-m} a_{0,1+m} a_{m-1,1-m}}_{\text{for } m=-1,-2,-3,-4,\ldots \text{ above}}\big)\Big].$$

Note that the sign of m is explicitly shown, and we then used $m \geq 0$ everywhere. We now use the fact that

$$\mathrm{V}^{0000}_{m11m} = \mathrm{V}^{0000}_{1mm1} = \mathrm{V}^{0000}_{1m1m} = \mathrm{V}^{0000}_{m1m1} \tag{B.15}$$

$$\mathrm{V}^{m00m}_{-m,1,1,-m} = \mathrm{V}^{0mm0}_{1,-m,-m,1} = \mathrm{V}^{0m0m}_{1,-m,1,-m} = \mathrm{V}^{m0m0}_{-m,1,-m,1} \tag{B.16}$$

$$\mathrm{V}^{m-1,000}_{1-m,1+m,11} = \mathrm{V}^{00,m-1,0}_{11,1-m,1+m} = \mathrm{V}^{0,m-1,00}_{1+m,1-m,11} = \mathrm{V}^{000,m-1}_{11,1+m,1-m} \tag{B.17}$$

to simplify the summand and, finally, arrive at

$$N_{01}^2 V^{0000}_{1111} + 4N_{01}\big(\overbrace{\mathrm{V}^{0000}_{m11m} a^\dagger_{0m} a_{0m}}^{m=0,2,3,4,\ldots} + \overbrace{\mathrm{V}^{m00m}_{-m,1,1,-m} a^\dagger_{m,-m} a_{m,-m}}^{m=1,2,3,4,\ldots}\big)$$
$$+ 2N_{01} \overbrace{\mathrm{V}^{m-1,000}_{1-m,1+m,11}\big(a^\dagger_{m-1,1-m} a^\dagger_{0,1+m} + a_{m-1,1-m} a_{0,1+m}\big)}^{m=1,2,3,4,\ldots}. \tag{B.18}$$

It should be emphasized that in the term proportional to $4N_{01}$ (the second term above), the $m = 0$ and $m = 1$ contributions come *only* from the first ($|0m\rangle$) and second ($|m, -m\rangle$) terms in parentheses respectively, whereas both terms contribute to the $m \geq 2$ part of the sum (the state $|01\rangle$ is excluded). Hence, the primed sum defined previously will be used for this term.

Using Eqs. (B.14) and (B.18), the rotating frame Hamiltonian, Eq. (B.6), can be rewritten in a quadratic form as

$$\begin{aligned}\mathcal{H}' = &\left(N_{01}\epsilon'_{01} + \frac{1}{2}N_{01}^2\mathrm{V}_{1111}^{0000}\right)\\ &+ \sum_m{}' \left[\left(\epsilon'_{0m} + 2N_{01}\mathrm{V}_{m11m}^{0000}\right)a_{0m}^\dagger a_{0m} + \left(\epsilon'_{m,-m} + 2N_{01}\mathrm{V}_{-m,1,1,-m}^{m00m}\right)a_{m,-m}^\dagger a_{m,-m}\right]\\ &+ \sum_{m\geq 1} N_{01}\mathrm{V}_{1-m,1+m,11}^{m-1,000}\left(a_{m-1,1-m}^\dagger a_{0,1+m}^\dagger + a_{m-1,1-m}a_{0,1+m}\right). \end{aligned} \tag{B.19}$$

The Bogoliubov Hamiltonian (B.19) is written in terms of the number of particles in the condensate, N_{01}, which is a fluctuating quantity rather than the total number of particles, which is fixed. To find $\mathcal{H}'$ as a function of N, we substitute Eqs. (B.12) and (B.13) into Eq. (B.19) and find

$$\begin{aligned}\mathcal{H}' =&\left\{\left[N - \sum_l{}'\left(a_{0l}^\dagger a_{0l} + a_{l,-l}^\dagger a_{l,-l}\right)\right]\epsilon'_{01} + \frac{1}{2}\left[N^2 - (2N-1)\sum_l{}'\left(a_{0l}^\dagger a_{0l} + a_{l,-l}^\dagger a_{l,-l}\right)\right]\mathrm{V}_{1111}^{0000}\right\}\\ &+\sum_m{}'\left\{\left(\epsilon'_{0m} + 2\left[N - \sum_l{}'\left(a_{0l}^\dagger a_{0l} + a_{l,-l}^\dagger a_{l,-l}\right)\right]\mathrm{V}_{m11m}^{0000}\right)a_{0m}^\dagger a_{0m} +\right.\\ &\qquad\left.\left(\epsilon'_{m,-m} + 2\left[N - \sum_l{}'\left(a_{0l}^\dagger a_{0l} + a_{l,-l}^\dagger a_{l,-l}\right)\right]\mathrm{V}_{-m,1,1,-m}^{m00m}\right)a_{m,-m}^\dagger a_{m,-m}\right\}\\ &+\sum_{m\geq 1}\left[N - \sum_l{}'\left(a_{0l}^\dagger a_{0l} + a_{l,-l}^\dagger a_{l,-l}\right)\right]\mathrm{V}_{1-m,1+m,11}^{m-1,000}\left(a_{m-1,1-m}^\dagger a_{0,1+m}^\dagger + a_{m-1,1-m}a_{0,1+m}\right).\end{aligned}$$

The quartic terms in the second line above (with the primed sum) can be approximated up to quadratic order in the operators using the bosonic commutation relations as follows

$$\begin{aligned}\sum_m{}'\sum_l{}'\left(a_{0l}^\dagger a_{0l} + a_{l,-l}^\dagger a_{l,-l}\right)a_{0m}^\dagger a_{0m} &\simeq \sum_m{}'\sum_l{}' a_{0l}^\dagger a_{0l}a_{0m}^\dagger a_{0m}\\ &= \sum_m{}'\sum_l{}' a_{0l}^\dagger\left(\delta_{lm} + a_{0m}^\dagger a_{0l}\right)a_{0m}\\ &\simeq \sum_m{}' a_{0m}^\dagger a_{0m}\end{aligned}$$

and

$$\begin{aligned}\sum_m{}'\sum_l{}'\left(a_{0l}^\dagger a_{0l} + a_{l,-l}^\dagger a_{l,-l}\right)a_{m,-m}^\dagger a_{m,-m} &\simeq \sum_m{}'\sum_l{}' a_{l,-l}^\dagger a_{l,-l}a_{m,-m}^\dagger a_{m,-m}\\ &= \sum_m{}'\sum_l{}' a_{l,-l}^\dagger\left(\delta_{lm} + a_{m,-m}^\dagger a_{l,-l}\right)a_{m,-m}\\ &\simeq \sum_m{}' a_{m,-m}^\dagger a_{m,-m}\end{aligned}$$

whereas those in the last line can be approximated as

$$
\begin{aligned}
&\sum_{m\geq 1}{\sum_{l}}' \big(a^\dagger_{0l}a_{0l} + a^\dagger_{l,-l}a_{l,-l}\big)\big(a^\dagger_{m-1,1-m}a^\dagger_{0,1+m} + a_{m-1,1-m}a_{0,1+m}\big)\\
&\simeq \sum_{m\geq 1}{\sum_{l}}' \big(a^\dagger_{0l}a_{0l} + a^\dagger_{l,-l}a_{l,-l}\big)a^\dagger_{m-1,1-m}a^\dagger_{0,1+m}\\
&= \sum_{m\geq 1}{\sum_{l}}' \big[a^\dagger_{0l}\big(\delta_{0,m-1}\delta_{l,1-m} + a^\dagger_{m-1,1-m}a_{0l}\big)a^\dagger_{0,1+m} + a^\dagger_{l,-l}\big(\delta_{l,m-1} + a^\dagger_{m-1,1-m}a_{l,-l}\big)a^\dagger_{0,1+m}\big]\\
&= \sum_{m\geq 1}{\sum_{l}}' \Big\{\big[\delta_{m1}\delta_{l0}a^\dagger_{00}a^\dagger_{02} + a^\dagger_{0l}a^\dagger_{m-1,1-m}\big(\delta_{l,1+m} + a^\dagger_{0,1+m}a_{0l}\big)\big]\\
&\qquad\qquad + \big[\delta_{l,m-1}a^\dagger_{m-1,1-m}a^\dagger_{0,1+m} + a^\dagger_{l,-l}a^\dagger_{m-1,1-m}\big(\delta_{l0}\delta_{-l,1+m} + a^\dagger_{0,1+m}a_{l,-l}\big)\big]\Big\}\\
&\simeq \sum_{m\geq 1}{\sum_{l}}' \big[\big(\delta_{m1}\delta_{l0}a^\dagger_{00}a^\dagger_{02} + \delta_{l,1+m}a^\dagger_{0,1+m}a^\dagger_{m-1,1-m}\big) + \big(\delta_{l,m-1}a^\dagger_{m-1,1-m}a^\dagger_{0,1+m} + \delta_{l0}\delta_{m,-1}a^\dagger_{00}a^\dagger_{-2,2}\big)\big].
\end{aligned}
$$

However, in the primed sum above over l, we have $l_+ = 0, 2, 3, 4, \ldots$ for the first parentheses, whereas we need $l_- = 1, 2, 3, 4, \ldots$ for the second one. Hence, since $m \geq 1$, we can write the above sum as follows

$$
\begin{aligned}
&\Big(\sum_{l_+}\left(\delta_{l0} + \delta_{l2}\right)a^\dagger_{00}a^\dagger_{02} + \sum_{m>1}\sum_{l_+}\delta_{l,1+m}a^\dagger_{0,1+m}a^\dagger_{m-1,1-m}\Big) + \Big(\sum_{m>1}\sum_{l_-}\delta_{l,m-1}a^\dagger_{m-1,1-m}a^\dagger_{0,1+m}\Big)\\
=&\Big(2a^\dagger_{00}a^\dagger_{02} + \sum_{m>1}a^\dagger_{0,1+m}a^\dagger_{m-1,1-m}\Big) + \Big(\sum_{m>1}a^\dagger_{m-1,1-m}a^\dagger_{0,1+m}\Big)\\
=&2\sum_{m\geq 1}a^\dagger_{m-1,1-m}a^\dagger_{0,1+m}.
\end{aligned}
$$

Therefore, the Hamiltonian in the rotating frame as a function of the total number of particles becomes

$$
\begin{aligned}
\mathcal{H}' = &\left(N\epsilon'_{01} + \frac{1}{2}N^2\mathrm{V}^{0000}_{1111}\right)\\
&+ {\sum_{m}}'\Big\{\Big[\epsilon'_{0m} - \epsilon'_{01} + \frac{1}{2}\mathrm{V}^{0000}_{1111} - 2\mathrm{V}^{0000}_{m11m} + N\big(2\mathrm{V}^{0000}_{m11m} - \mathrm{V}^{0000}_{1111}\big)\Big]a^\dagger_{0m}a_{0m} +\\
&\qquad\Big[\epsilon'_{m,-m} - \epsilon'_{01} + \frac{1}{2}\mathrm{V}^{0000}_{1111} - 2\mathrm{V}^{m00m}_{-m,1,1,-m} + N\big(2\mathrm{V}^{m00m}_{-m,1,1,-m} - \mathrm{V}^{0000}_{1111}\big)\Big]a^\dagger_{m,-m}a_{m,-m}\Big\}\\
&+ \sum_{m\geq 1}\mathrm{V}^{m-1,000}_{1-m,1+m,11}\big[(N-2)a^\dagger_{m-1,1-m}a^\dagger_{0,1+m} + Na_{m-1,1-m}a_{0,1+m}\big].
\end{aligned}
\tag{B.20}
$$

In the thermodynamic limit ($N \to \infty$ provided that $NV_0 = \text{const.} \ll 1$), terms of $\mathcal{O}(V_0)$ in the equation above, e.g., $\frac{1}{2}\mathrm{V}^{0000}_{1111} - 2\mathrm{V}^{0000}_{m11m}$, are $\mathcal{O}(N^{-1})$ smaller compared to other interaction terms and, hence, will be ignored. Thus, the rotating frame Bogoliubov Hamiltonian finally becomes, up to quadratic order in the

Landau level creation and annihilation operators,

$$\begin{aligned}\mathcal{H}' = &\left(N\epsilon'_{01} + \frac{1}{2}N^2\mathrm{V}^{0000}_{1111}\right) \\ &+ {\sum_m}' \Big\{ \Big[\epsilon'_{0m} - \epsilon'_{01} + N\big(2\mathrm{V}^{0000}_{m11m} - \mathrm{V}^{0000}_{1111}\big)\Big] a^\dagger_{0m} a_{0m} \\ &\qquad + \Big[\epsilon'_{m,-m} - \epsilon'_{01} + N\big(2\mathrm{V}^{m00m}_{-m,1,1,-m} - \mathrm{V}^{0000}_{1111}\big)\Big] a^\dagger_{m,-m} a_{m,-m} \Big\} \\ &+ \sum_{m\geq 1} N\mathrm{V}^{m-1,000}_{1-m,1+m,11}\big(a^\dagger_{m-1,1-m} a^\dagger_{0,1+m} + a_{m-1,1-m} a_{0,1+m}\big). \end{aligned} \tag{B.21}$$

The first term in Eq. (B.21) (a constant) is just the energy of a condensate when no fluctuations are present, that is, with all N particles condensed into the state $|01\rangle$. It is now clear that in the presence of a condensate in $|01\rangle$, the interparticle interactions connect $|00\rangle$ with $|02\rangle$, $|1,-1\rangle$ with $|03\rangle$, $|2,-2\rangle$ with $|04\rangle$, etc.

Appendix C

The canonical transformations

Assume a quadratic Hamiltonian of the form

$$\mathcal{H} = \epsilon_a\, a^\dagger a + \epsilon_b\, b^\dagger b + \bar{\epsilon}\big(a^\dagger b^\dagger + ab\big) \tag{C.1}$$

where a and b are two bosonic annihilation operators and $\epsilon_a, \epsilon_b, \bar{\epsilon} \in \mathbb{R}$.

We define two new annihilation operators

$$\begin{aligned} \alpha &= u\, a + v\, b^\dagger \\ \beta &= u\, b + v\, a^\dagger \end{aligned} \tag{C.2}$$

with $u, v \in \mathbb{C}$ and require that they be bosonic by satisfying $[\alpha, \alpha^\dagger] = [\beta, \beta^\dagger] = 1$, i.e.,

$$\begin{aligned} [\alpha, \alpha^\dagger] &= [u\, a + v\, b^\dagger, u^*\, a^\dagger + v^*\, b] = |u|^2 \overbrace{[a, a^\dagger]}^{1} + |v|^2 \overbrace{[b^\dagger, b]}^{-1} + \big(uv^* \overbrace{[a, b]}^{0} + u^* v \overbrace{[b^\dagger, a^\dagger]}^{0}\big) = |u|^2 - |v|^2\,, \\ [\beta, \beta^\dagger] &= [u\, b + v\, a^\dagger, u^*\, b^\dagger + v^*\, a] = |u|^2 \overbrace{[b, b^\dagger]}^{1} + |v|^2 \overbrace{[a^\dagger, a]}^{-1} + \big(uv^* \overbrace{[b, a]}^{0} + u^* v \overbrace{[a^\dagger, b^\dagger]}^{0}\big) = |u|^2 - |v|^2\,. \end{aligned}$$

Hence, we should have

$$|u|^2 - |v|^2 = 1, \tag{C.3}$$

using which we can invert Eq. (C.2) to get

$$\begin{aligned} a &= u^*\, \alpha - v\, \beta^\dagger, \\ b &= u^*\, \beta - v\, \alpha^\dagger. \end{aligned} \tag{C.4}$$

Therefore, we can rewrite the diagonal and off-diagonal parts of the Hamiltonian, $\mathcal{H}$, in terms of the new

operators as

$$\begin{aligned}
\epsilon_a\, a^\dagger a + \epsilon_b\, b^\dagger b &= \epsilon_a\big(u\,\alpha^\dagger - v^*\,\beta\big)\big(u^*\,\alpha - v\,\beta^\dagger\big) + \epsilon_b\big(u\,\beta^\dagger - v^*\,\alpha\big)\big(u^*\,\beta - v\,\alpha^\dagger\big) \\
&= \epsilon_a\big[\,|u|^2\,\alpha^\dagger\alpha + |v|^2\,\beta\beta^\dagger - \big(uv\,\alpha^\dagger\beta^\dagger + u^*v^*\,\beta\alpha\big)\big] \\
&\quad + \epsilon_b\big[\,|u|^2\,\beta^\dagger\beta + |v|^2\,\alpha\alpha^\dagger - \big(uv\,\beta^\dagger\alpha^\dagger + u^*v^*\,\alpha\beta\big)\big] \\
&= (\epsilon_a + \epsilon_b)\,|v|^2 + \big(\epsilon_a\,|u|^2 + \epsilon_b\,|v|^2\,\big)\alpha^\dagger\alpha + \big(\epsilon_a\,|v|^2 + \epsilon_b\,|u|^2\,\big)\beta^\dagger\beta \\
&\quad - (\epsilon_a + \epsilon_b)\big(uv\,\alpha^\dagger\beta^\dagger + u^*v^*\,\alpha\beta\big)
\end{aligned}$$

and

$$\begin{aligned}
\bar\epsilon\big(a^\dagger b^\dagger + ab\big) &= \bar\epsilon\big[\big(u\,\alpha^\dagger - v^*\,\beta\big)\big(u\,\beta^\dagger - v^*\,\alpha\big) + \big(u^*\,\alpha - v\,\beta^\dagger\big)\big(u^*\,\beta - v\,\alpha^\dagger\big)\big] \\
&= \bar\epsilon\Big\{\big[u^2\,\alpha^\dagger\beta^\dagger + v^{*2}\,\beta\alpha - uv^*\big(\alpha^\dagger\alpha + \beta\beta^\dagger\big)\big] + \big[u^{*2}\,\alpha\beta + v^2\,\beta^\dagger\alpha^\dagger - u^*v\big(\alpha\alpha^\dagger + \beta^\dagger\beta\big)\big]\Big\} \\
&= \bar\epsilon\big[-(uv^* + u^*v) - (uv^* + u^*v)\big(\alpha^\dagger\alpha + \beta^\dagger\beta\big) + (u^2 + v^2)\alpha^\dagger\beta^\dagger + (u^{*2} + v^{*2})\alpha\beta\big].
\end{aligned}$$

The Hamiltonian in terms of the new operators becomes

$$\begin{aligned}
\mathcal{H} =& \big[(\epsilon_a + \epsilon_b)\,|v|^2 - \bar\epsilon(uv^* + u^*v)\big] \\
&+ \Big\{\big[\epsilon_a\,|u|^2 + \epsilon_b\,|v|^2 - \bar\epsilon(uv^* + u^*v)\big]\alpha^\dagger\alpha + \big[\epsilon_a\,|v|^2 + \epsilon_b\,|u|^2 - \bar\epsilon(uv^* + u^*v)\big]\beta^\dagger\beta\Big\} \\
&+ \Big\{\big[\bar\epsilon(u^2 + v^2) - (\epsilon_a + \epsilon_b)uv\big]\alpha^\dagger\beta^\dagger + \big[\bar\epsilon(u^{*2} + v^{*2}) - (\epsilon_a + \epsilon_b)u^*v^*\big]\alpha\beta\Big\}. \qquad \text{(C.5)}
\end{aligned}$$

For $\mathcal{H}$ to be diagonal in the new operators, the coefficients of the off-diagonal terms in the last line above (which are complex conjugates of each other) should be zero; hence,

$$\bar\epsilon\,(u^2 + v^2) - (\epsilon_a + \epsilon_b)\,uv = 0. \qquad \text{(C.6)}$$

With $u = |u|\,e^{\mathrm{i}\theta_u}$ and $v = |v|\,e^{\mathrm{i}\theta_v}$, we rewrite Eq. (C.6) as

$$\bar\epsilon\,\Big(\,|u|^2\,e^{2\mathrm{i}\theta_u} + |v|^2\,e^{2\mathrm{i}\theta_v}\Big) - (\epsilon_a + \epsilon_b)\,|u|\,|v|\,e^{\mathrm{i}(\theta_u + \theta_v)} = 0. \qquad \text{(C.7)}$$

Dividing this by $e^{\mathrm{i}(\theta_u + \theta_v)}$, we find

$$\bar\epsilon\,\Big(\,|u|^2\,e^{\mathrm{i}(\theta_u - \theta_v)} + |v|^2\,e^{-\mathrm{i}(\theta_u - \theta_v)}\Big) - (\epsilon_a + \epsilon_b)\,|u|\,|v| = 0 \qquad \text{(C.8)}$$

which clearly depends only on the relative phase between u and v. The imaginary part of this equation yields

$$\bar{\epsilon}\left(|u|^2 - |v|^2\right)\sin(\theta_u - \theta_v) = 0. \tag{C.9}$$

Since $\bar{\epsilon} \neq 0$ and $|u|^2 - |v|^2 = 1$, we have

$$\theta_u - \theta_v = n\pi, \quad n \in \mathbb{Z}. \tag{C.10}$$

In other words, $e^{\mathrm{i}\theta_v} = (-1)^n e^{\mathrm{i}\theta_u}$. Therefore, the relative phase between u and v is not completely random, and the quasiparticle operators α and β can take only two forms depending on the relative sign of u and v in Eq. (C.2).

We now proceed to solve Eqs. (C.3) and (C.6) as follows. Defining $|u| = \cosh\tau$ and $|v| = \sinh\tau$ with $\tau \geq 0$, we see that Eq. (C.3) is automatically satisfied. Thus, substituting in Eq. (C.6) leads to

$$e^{2\mathrm{i}\theta_u}\left[\bar{\epsilon}\left(\cosh^2\tau + \sinh^2\tau\right) - (-1)^n(\epsilon_a + \epsilon_b)\cosh\tau\sinh\tau\right] = 0 \tag{C.11}$$

or, in other words,

$$\tanh(2\tau) = (-1)^n \frac{\bar{\epsilon}}{\left(\dfrac{\epsilon_a + \epsilon_b}{2}\right)}. \tag{C.12}$$

Given that $\tau \geq 0$ by definition, we see that n should be even if $\mathrm{sgn}[\bar{\epsilon}/(\epsilon_a + \epsilon_b)] = 1$ and should be odd if $\mathrm{sgn}[\bar{\epsilon}/(\epsilon_a + \epsilon_b)] = -1$. Using the identity

$$\cosh^2\tau = \frac{1}{2}\left[\cosh(2\tau) + 1\right] = \frac{1}{2}\left(\frac{1}{\sqrt{1 - \tanh^2(2\tau)}} + 1\right) \tag{C.13}$$

and defining $\epsilon_\pm \equiv (\epsilon_a \pm \epsilon_b)/2$, together with Eq. (C.12), lead to

$$|u|^2 = \frac{1}{2}\left(\frac{1}{\sqrt{1 - (\bar{\epsilon}/\epsilon_+)^2}} + 1\right) = \frac{1}{2}\left(\sqrt{\frac{\epsilon_+^2}{\epsilon_+^2 - \bar{\epsilon}^2}} + 1\right). \tag{C.14}$$

Therefore, for a solution to exist, we should have $|\epsilon_+| > |\bar{\epsilon}|$; we define $\epsilon^2 = \epsilon_+^2 - \bar{\epsilon}^2$ and find

$$\begin{aligned} |u|^2 &= \frac{1}{2}\left(\left|\frac{\epsilon_+}{\epsilon}\right| + 1\right), \\ |v|^2 &= \frac{1}{2}\left(\left|\frac{\epsilon_+}{\epsilon}\right| - 1\right). \end{aligned} \tag{C.15}$$

With these values of u and v, the Hamiltonian (C.5) will be diagonal.

With the above values for the coherence factors u and v, we find

$$|u|^2\,|v|^2 = \frac{1}{4}\left(\frac{\epsilon_+^2}{\epsilon^2}-1\right) = \left(\frac{\bar\epsilon}{2\epsilon}\right)^2 \quad\rightarrow\quad |u|\,|v| = \left|\frac{\bar\epsilon}{2\epsilon}\right|. \tag{C.16}$$

Thus, we have

$$\begin{aligned}
(\epsilon_a+\epsilon_b)\,|v|^2 - \bar\epsilon\,(uv^*+u^*v) &= \frac{1}{2}\left(\left|\frac{\epsilon_+}{\epsilon}\right|-1\right)(\epsilon_a+\epsilon_b) - 2(-1)^n\left|\frac{\bar\epsilon}{2\epsilon}\right|\bar\epsilon \\
&= \left(\left|\frac{\epsilon_+}{\epsilon}\right|-1\right)\epsilon_+ - (-1)^n\left|\frac{\bar\epsilon}{\epsilon}\right|\bar\epsilon \\
&= \epsilon_+\left\{\left(\left|\frac{\epsilon_+}{\epsilon}\right|-1\right) - \left|\frac{\bar\epsilon}{\epsilon}\right|\left[(-1)^n\,\frac{\bar\epsilon}{\epsilon_+}\right]\right\} \\
&= \epsilon_+\left\{\left(\left|\frac{\epsilon_+}{\epsilon}\right|-1\right) - \left|\frac{\bar\epsilon}{\epsilon}\right|\left|\frac{\bar\epsilon}{\epsilon_+}\right|\right\} \\
&= \mathrm{sgn}[\epsilon_+]\left(\frac{\epsilon_+^2-\bar\epsilon^2}{|\epsilon|} - |\epsilon_+|\right) \\
&= \mathrm{sgn}[\epsilon_+]\;|\epsilon| - \epsilon_+\,,
\end{aligned} \tag{C.17}$$

and

$$\begin{aligned}
\epsilon_a\,|u|^2 + \epsilon_b\,|v|^2 - \bar\epsilon(uv^*+u^*v) &= \frac{1}{2}\left(\left|\frac{\epsilon_+}{\epsilon}\right|+1\right)\epsilon_a + \frac{1}{2}\left(\left|\frac{\epsilon_+}{\epsilon}\right|-1\right)\epsilon_b - 2(-1)^n\left|\frac{\bar\epsilon}{2\epsilon}\right|\bar\epsilon \\
&= \frac{1}{2\,|\epsilon|}\Big[\big(\,|\epsilon_+|+|\epsilon|\,\big)\epsilon_a + \big(\,|\epsilon_+|-|\epsilon|\,\big)\epsilon_b - 2\,\mathrm{sgn}[\epsilon_+]\,|\bar\epsilon|^2\Big] \\
&= \frac{1}{2\,|\epsilon|}\Big[\,|\epsilon_+|\,(\epsilon_a+\epsilon_b) + |\epsilon|\,(\epsilon_a-\epsilon_b) - 2\,\mathrm{sgn}[\epsilon_+]\,\bar\epsilon^2\Big] \\
&= \frac{1}{2\,|\epsilon|}\Big[2\,\mathrm{sgn}[\epsilon_+]\,(\epsilon_+^2-\bar\epsilon^2) + 2\,|\epsilon|\,\epsilon_-\Big] \\
&= \mathrm{sgn}[\epsilon_+]\;|\epsilon| + \epsilon_-\,,
\end{aligned} \tag{C.18}$$

and

$$\begin{aligned}
\epsilon_a\,|v|^2 + \epsilon_b\,|u|^2 - \bar\epsilon(uv^*+u^*v) &= \frac{1}{2}\left(\left|\frac{\epsilon_+}{\epsilon}\right|-1\right)\epsilon_a + \frac{1}{2}\left(\left|\frac{\epsilon_+}{\epsilon}\right|+1\right)\epsilon_b - 2(-1)^n\left|\frac{\bar\epsilon}{2\epsilon}\right|\bar\epsilon \\
&= \frac{1}{2\,|\epsilon|}\Big[\big(\,|\epsilon_+|-|\epsilon|\,\big)\epsilon_a + \big(\,|\epsilon_+|+|\epsilon|\,\big)\epsilon_b - 2\,\mathrm{sgn}[\epsilon_+]\,|\bar\epsilon|^2\Big] \\
&= \frac{1}{2\,|\epsilon|}\Big[\,|\epsilon_+|\,(\epsilon_a+\epsilon_b) - |\epsilon|\,(\epsilon_a-\epsilon_b) - 2\,\mathrm{sgn}[\epsilon_+]\,\bar\epsilon^2\Big] \\
&= \frac{1}{2\,|\epsilon|}\Big[2\,\mathrm{sgn}[\epsilon_+]\,(\epsilon_+^2-\bar\epsilon^2) - 2\,|\epsilon|\,\epsilon_-\Big] \\
&= \mathrm{sgn}[\epsilon_+]\;|\epsilon| - \epsilon_-\,.
\end{aligned} \tag{C.19}$$

Hence, the Hamiltonian in Eq. (C.5) becomes

$$\mathcal{H} = \big[\mathrm{sgn}[\epsilon_+]\ |\epsilon| - \epsilon_+\big] + \big[\mathrm{sgn}[\epsilon_+]\ |\epsilon| + \epsilon_-\big]\alpha^\dagger\alpha + \big[\mathrm{sgn}[\epsilon_+]\ |\epsilon| - \epsilon_-\big]\beta^\dagger\beta \tag{C.20}$$

which is diagonal in terms of α and β.

Note that the first term, the ground state energy, can also be written as $\mathrm{sgn}[\epsilon_+]\left(|\epsilon| - |\epsilon_+|\right)$. Since $|\epsilon| < |\epsilon_+|$ by definition, the ground state energy is negative if $\epsilon_+ > 0$ and positive if $\epsilon_+ < 0$. Moreover, this state has single-particle occupation numbers given by

$$\left\langle a^\dagger a\right\rangle_{\mathrm{G}} = \langle \mathrm{G}|\left(u\,\alpha^\dagger - v^*\beta\right)\left(u^*\alpha - v\,\beta^\dagger\right)|\mathrm{G}\rangle = |v|^2\,\langle \mathrm{G}|\,\beta\beta^\dagger\,|\mathrm{G}\rangle = |v|^2\,, \tag{C.21}$$

$$\left\langle b^\dagger b\right\rangle_{\mathrm{G}} = \langle \mathrm{G}|\left(u\,\beta^\dagger - v^*\alpha\right)\left(u^*\beta - v\,\alpha^\dagger\right)|\mathrm{G}\rangle = |v|^2\,\langle \mathrm{G}|\,\alpha\alpha^\dagger\,|\mathrm{G}\rangle = |v|^2\,. \tag{C.22}$$

Appendix D

Symmetric polynomials and Jastrow factors

In this Appendix, we define the elementary and monomial symmetric polynomials and find the expansion of the latter polynomials in terms of certain symmetric polynomials with Jastrow factors, hereafter named symmetric Jastrow polynomials.

We consider a set of N variables, denoted by

$$\mathbf{z} = \{z_1, z_2, \ldots, z_N\}, \tag{D.1}$$

and a set of N exponents, denoted by

$$\boldsymbol{\alpha} = \{\alpha_1, \alpha_2, \ldots, \alpha_N\}. \tag{D.2}$$

The elementary symmetric polynomials defined on $\mathbf{z}$ are

$$\mathcal{S}_0(\mathbf{z}) = 1, \tag{D.3}$$

$$\mathcal{S}_1(\mathbf{z}) = \sum_{i_1} z_{i_1}, \tag{D.4}$$

$$\mathcal{S}_2(\mathbf{z}) = \sum_{i_1<i_2} z_{i_1} z_{i_2}, \tag{D.5}$$

$$\mathcal{S}_3(\mathbf{z}) = \sum_{i_1<i_2<i_3} z_{i_1} z_{i_2} z_{i_3}, \tag{D.6}$$

$$\vdots \tag{D.7}$$

$$\mathcal{S}_N(\mathbf{z}) = \sum_{i_1<i_2<\cdots<i_N} z_{i_1} z_{i_2} \cdots z_{i_N} = \prod_k z_k. \tag{D.8}$$

The monomial symmetric polynomials, denoted by $\mathcal{M}_{\boldsymbol{\alpha}}(\mathbf{z})$, are defined as the sum over all $z_1^{\alpha_{i_1}} z_2^{\alpha_{i_2}} \cdots z_N^{\alpha_{i_N}}$ where the exponents $\alpha_{i_1}, \alpha_{i_2}, \ldots, \alpha_{i_N}$ range over all *distinct* permutations one can get from the members of $\boldsymbol{\alpha}$ [97]. For example, for $N = 3$, we have

$$\mathcal{M}_{\{2,0,0\}}(z_1, z_2, z_3) = z_1^2 z_2^0 z_3^0 + z_1^0 z_2^2 z_3^0 + z_1^0 z_2^0 z_3^2 = z_1^2 + z_2^2 + z_3^2\,. \tag{D.9}$$

The identity $z_1^2+z_2^2 = (z_1-z_2)^2+2z_1z_2$ for $N=2$ can be rewritten in terms of the symmetric polynomials defined above as

$$\mathcal{M}_{\{2,0\}}(z_1,z_2) = (z_1-z_2)^2 + 2\,\mathcal{S}_2(z_1,z_2). \tag{D.10}$$

There exists a similar identity for $N=4$, namely

$$\begin{aligned} z_1^2z_2^2 + z_1^2z_3^2 + z_1^2z_4^2 + z_2^2z_3^2 + z_2^2z_4^2 + z_3^2z_4^2 =& \frac{1}{2}\big[(z_1-z_2)^2(z_3-z_4)^2 + (z_1-z_3)^2(z_2-z_4)^2 \\ &+ (z_1-z_4)^2(z_2-z_3)^2\big] \\ &+ \big[(z_1-z_2)^2z_3z_4 + (z_1-z_3)^2z_2z_4 + (z_1-z_4)^2z_2z_3 \\ &+ (z_2-z_3)^2z_1z_4 + (z_2-z_4)^2z_1z_3 + (z_3-z_4)^2z_1z_2\big] \\ &+ 6\,z_1z_2z_3z_4, \end{aligned} \tag{D.11}$$

which, in the language of symmetric polynomials, becomes

$$\begin{aligned} \mathcal{M}_{\{2,2,0,0\}}(z_1,z_2,z_3,z_4) =& \frac{1}{2}\Big[(z_1-z_2)^2(z_3-z_4)^2 + (z_1-z_3)^2(z_2-z_4)^2 + (z_1-z_4)^2(z_2-z_3)^2\Big] \\ &+ \Big[(z_1-z_2)^2z_3z_4 + (z_1-z_3)^2z_2z_4 + (z_1-z_4)^2z_2z_3 \\ &+ (z_2-z_3)^2z_1z_4 + (z_2-z_4)^2z_1z_3 + (z_3-z_4)^2z_1z_2\Big] \\ &+ 6\,\mathcal{S}_4(z_1,z_2,z_3,z_4). \end{aligned} \tag{D.12}$$

We now find a similar identity for general N, assuming, without loss of generality, that $N=2n$. Defining

$$\mathcal{M}_{\{\underbrace{2\ldots2}_{n},\underbrace{0\ldots0}_{n}\}}(\mathbf{z}) = \mathcal{P}\big[z_1^2z_2^2\cdots z_{n-1}^2z_n^2z_{n+1}^0z_{n+2}^0\cdots z_{2n-1}^0z_{2n}^0\big] \tag{D.13}$$

and

$$J_i(\mathbf{z}) = \mathcal{P}\big[\overbrace{(z_1-z_2)^2(z_3-z_4)^2\cdots(z_{2i-1}-z_{2i})^2}^{i\text{ Jastrow pairs}}\,z_{2i+1}z_{2i+2}\cdots z_{2n-1}z_{2n}\big], \tag{D.14}$$

we can write

$$\mathcal{M}_{\{\underbrace{2\ldots2}_{n},\underbrace{0\ldots0}_{n}\}}(\mathbf{z}) = \sum_{i=0}^{n} c_i\,J_i(\mathbf{z}). \tag{D.15}$$

Note that $J_0(\mathbf{z}) = \mathcal{S}_{2n}(\mathbf{z})$.

To find the coefficients, we proceed as follows. First, we set $z_j=1$ for all j. Therefore, in the expansion (D.15), only the c_0-term is non-zero. Since the number of terms in the monomial is $(2n)!/[n!n!]$ and all of

them are equal to 1 in this case, we find

$$\frac{(2n)!}{n!n!} \times 1 = c_0 \times 1 \quad \rightarrow \quad c_0 = \frac{(2n)!}{n!n!}\,. \tag{D.16}$$

Next, we set $z_1 = 0$ and $z_{j\neq 1} = 1$. We find that on the right side of Eq. (D.15), only the c_1-term could survive only if z_1 is one of the two variables in the Jastrow pair, while on the left side, z_1 should appear with a power of 0. On the right side, there are $\binom{2n-1}{1}$ ways to make a Jastrow pair with z_1 and one other variable while the remaining variables can be arranged in only one way. On the left side, once z_1 gets a power of 0, there are $(2n-1)!/[n!(n-1)!]$ ways to get a non-zero value (which is 1). Therefore, we have

$$\frac{(2n-1)!}{n!(n-1)!} \times 1 = c_1 \times \binom{2n-1}{1} \times 1 \quad \rightarrow \quad c_1 = \frac{(2n-2)!}{n!(n-1)!}\,. \tag{D.17}$$

Next, we set $z_1 = z_2 = 0$ and $z_{j\neq 1,2} = 1$. Likewise, from the right side, only the c_2-term could survive only if z_1 and z_2 belong to two distinct Jastrow pairs, while from the left side, both z_1 and z_2 should get powers of 0. Hence, the right side has $\binom{2n-2}{2} \times 2!$ distinct configurations (with value 1), and the left side has $(2n-2)!/[n!(n-2)!]$ non-zero configurations (with value 1) where both z_1 and z_2 have powers of 0. Thus,

$$\frac{(2n-2)!}{n!(n-2)!} \times 1 = c_2 \times \binom{2n-2}{2} 2! \times 1 \quad \rightarrow \quad c_2 = \frac{(2n-4)!}{n!(n-2)!}. \tag{D.18}$$

Generalizing this approach to find c_k (with $k \leq n$), we can set $z_1 = z_2 = \cdots = z_k = 0$ and the rest of z_i's equal to 1 and proceed just like before. It is straightforward to find

$$c_k = \frac{(2n-2k)!}{n!(n-k)!} \tag{D.19}$$

which, finally, yields

$$\mathcal{M}_{\{\underbrace{2\ldots2}_{N/2},\underbrace{0\ldots0}_{N/2}\}}(\mathbf{z}) = \sum_{i=0}^{N/2} \frac{(N-2i)!}{(N/2)!(N/2-i)!}\, J_i(\mathbf{z}). \tag{D.20}$$

This is a very general algebraic identity which relates certain kinds of N-variable monomial symmetric polynomials (as defined above) to symmetric Jastrow polynomials.

Let us now count the number of terms in each $J_j(\mathbf{z})$. We write the act of the permutation operator $\mathcal{P}$ as

$$J_j(\mathbf{z}) = \sum{}'(z_{i_1} - z_{i_2})^2 (z_{i_3} - z_{i_4})^2 \cdots (z_{i_{2j-1}} - z_{i_{2j}})^2 \prod_{k\neq i_1 \ldots i_{2j}} z_k \tag{D.21}$$

where the prime on the sum indicates the following conditions

$$\begin{gathered} i_1 < i_2, \quad i_3 < i_4, \quad \ldots, \quad i_{2j-1} < i_{2j}, \\ i_1 < i_3 < i_5 < \cdots < i_{2j-1}, \\ i_{2l} \neq i_{2l+1}, i_{2l+2}, \ldots, i_{2j} \text{ for } 1 \leq l < j. \end{gathered} \tag{D.22}$$

In order to construct the Jastrow factors, we choose the z's in them as follows. We pick two z's for the first Jastrow factor in $\binom{N}{2}$ distinct ways, then the two different z's for the second factor in $\binom{N-2}{2}$ distinct ways, and so on until the last one for which there are $\binom{N-2j+2}{2}$ distinct ways. Therefore, we have $N!/[(N-2j)!\,2^j]$ distinct ways to pick the z's for the Jastrow factors. (Or we could do it by first picking $2j$ different z's in $\binom{N}{2j}$ ways, then dividing them among the j factors in $\binom{2j}{2}\binom{2j-2}{2}\cdots\binom{2}{2}$ ways.) Moreover, the Jastrow factors can be permuted in $j!$ distinct ways among themselves while keeping $J_j(\mathbf{z})$ invariant; however, only one of these permutations satisfies the constraints above. The remaining z's can be arranged in only one way. Thus, each $J_j(\mathbf{z})$ has

$$\frac{N!}{(N-2j)!\,j!\,2^j} \tag{D.23}$$

distinct terms.

Using the above findings, we now proceed to relate another kind of N-variable monomial symmetric polynomial, namely

$$\mathcal{M}_{\{\underbrace{0\ldots0}_{m},\underbrace{2\ldots2}_{m},\underbrace{1\ldots1}_{N-2m}\}}(\mathbf{z}) = \mathcal{P}\big[z_1^0 z_2^0 \cdots z_{m-1}^0 z_m^0\, z_{m+1}^2 z_{m+2}^2 \cdots z_{2m-1}^2 z_{2m}^2\, z_{2m+1} z_{2m+2} \cdots z_{N-1} z_N\big], \tag{D.24}$$

which will be used in the expansion of the Bogoliubov ground state (3.6), to symmetric Jastrow polynomials. We rewrite this monomial as

$$\begin{aligned} \mathcal{M}_{\{0\ldots0,2\ldots2,1\ldots1\}}(\mathbf{z}) &= \sum_{i_1\neq\cdots\neq i_{2m}} \frac{1}{m!} z_{i_1}^0 \cdots z_{i_m}^0 \frac{1}{m!} z_{i_{m+1}}^2 \cdots z_{i_{2m}}^2 \prod_{k\neq i_1\ldots i_{2m}} z_k \\ &= \sum_{i_1\neq\cdots\neq i_{2m}} \frac{1}{(m!)^2} \frac{1}{(2m)!/(m!)^2}\, \mathcal{M}_{\{2\ldots2,0\ldots0\}}(z_{i_1}\ldots z_{i_{2m}}) \prod_{k\neq i_1\ldots i_{2m}} z_k \\ &= \frac{1}{(2m)!} \sum_{j=0}^{m} \frac{(2m-2j)!}{m!\,(m-j)!} \left[\sum_{i_1\neq\cdots\neq i_{2m}} J_j(z_{i_1}\ldots z_{i_{2m}}) \prod_{k\neq i_1\ldots i_{2m}} z_k \right] \end{aligned} \tag{D.25}$$

where (i) due to $i_1, \ldots, i_{2m}$ being dummy variables, we have used a method similar to (E.5) to get the second equality from the first line and to represent all the terms in the sum by a new monomial acting on a limited set of z's, i.e., $\{z_{i_1}, \ldots, z_{i_{2m}}\}$; and (ii) we use Eq. (D.20) to rewrite the monomial in the second line in terms

of symmetric Jastrow polynomials in the last equality.

To proceed further, we need to recast the square bracket above (which includes Jastrow polynomials defined on the subset $\{z_{i_1}, \ldots, z_{i_{2m}}\} \subset \mathbf{z}$) in terms of Jastrow polynomials acting on the set $\mathbf{z}$. The answer is

$$\sum_{i_1 \neq \cdots \neq i_{2m}} J_j(z_{i_1} \ldots z_{i_{2m}}) \prod_{k \neq i_1 \ldots i_{2m}} z_k = \left[(2m)! \binom{N}{2m} \delta_{j0} + \frac{(2m)!\, 2^{j-1}}{j!} (1 - \delta_{j0}) \right] J_j(\mathbf{z}) \tag{D.26}$$

where the details of this derivation are as follows. Clearly, the sum over $i_1, \ldots, i_{2m}$ leads to an overcounting which we need to determine separately for each j. Since $i_1, \ldots, i_{2m}$ are dummy variables, each term in $J_j(z_{i_1} \ldots z_{i_{2m}})$ produces the same polynomial after being summed over; this brings in an overcounting factor given by (D.23). On the other hand, since $\sum_{i_1 \neq i_2} \cdots = 2 \sum_{i_1 < i_2} \ldots$, due to the conditions (D.22), we are overcounting by a factor of 2 for each Jastrow factor (of which there are j) and by a factor of 2 for each two adjacent Jastrow factors (of which there are $j-1$), *in toto*, an overcounting factor of 2^{2j-1}. Permutations of the remaining z's outside the Jastrow factors in $J_j(z_{i_1} \ldots z_{i_{2m}})$ leave it invariant, and this leads to an overcounting factor of $(2m-2j)!$. Therefore, when we transform $J_j(z_{i_1} \ldots z_{i_{2m}})$ to $J_j(z_1 \ldots z_N)$, we overcount by a factor of

$$\frac{(2m)! 2^{j-1}}{j!} \tag{D.27}$$

for each $j \neq 0$. For the special case of $j = 0$, since there are no Jastrow factors present in $J_0(z_{i_1} \ldots z_{i_{2m}})$, we instantly end up with $J_0(z_1 \ldots z_N)$ but overcounted by a factor of

$$(2m)! \binom{N}{2m}. \tag{D.28}$$

Hence, we write the above-mentioned monomial symmetric polynomial in terms of symmetric Jastrow polynomials as

$$\mathcal{M}_{\{\underbrace{0 \ldots 0}_{m}, \underbrace{2 \ldots 2}_{m}, \underbrace{1 \ldots 1}_{N-2m}\}}(\mathbf{z}) = \frac{1}{m!} \sum_{j=0}^{m} \frac{(2m-2j)!}{(m-j)!} \left[\binom{N}{2m} \delta_{j0} + \frac{2^{j-1}}{j!} (1 - \delta_{j0}) \right] J_j(\mathbf{z}) \tag{D.29}$$

which is another general algebraic identity relating two different kinds of N-variable symmetric polynomials.

Appendix E

Expansion terms in the single-vortex Bogoliubov ground state

In this Appendix, we discuss the method we use to simplify the expansion terms in the Bogoliubov ground state, Eq. (3.6), and to bring out the Jastrow factors that represent interparticle correlations.

The $m = 1$ term in Eq. (3.6) is proportional to $\mathcal{P}\big[z_1^0 z_2 \cdots z_{N-1} z_N^2\big]$ where the permutations yield $\binom{N}{N-2}\binom{2}{1}$ distinct terms, i.e.,

$$\langle \mathbf{z} \,|1, N-2, 1\rangle = \frac{1}{\sqrt{\binom{N}{N-2}\binom{2}{1}}}\, \mathcal{P}\big[z_1^0 z_2 \cdots z_{N-1}\big(z_N^2/\sqrt{2}\big)\big]. \tag{E.1}$$

To proceed, we note that the indices of summation (and multiplication) are, in fact, dummy variables and find

$$\sum_{i\neq j} z_i^0 z_j^2 \prod_{k\neq i,j} z_k = \sum_{i\neq j} \tfrac{1}{2}\big(z_i^0 z_j^2 + z_i^2 z_j^0\big) \prod_{k\neq i,j} z_k = \sum_{i<j} \big[(z_i - z_j)^2 + 2 z_i z_j\big] \prod_{k\neq i,j} z_k. \tag{E.2}$$

We thus write

$$\mathcal{P}\big[z_1^0 z_2 \cdots z_{N-1} z_N^2\big] = \sum_{i<j} (z_i - z_j)^2 \prod_{k\neq i,j} z_k + 2\binom{N}{2} \prod_k z_k \tag{E.3}$$

which leads to the expansion of $\langle \mathbf{z} \,|1, N-2, 1\rangle$ in terms of symmetric Jastrow polynomials J_0 and J_1 defined previously in Appendix D.

The $m = 2$ term in Eq. (3.6) is proportional to $\mathcal{P}\big[z_1^0 z_2^0 z_3 \cdots z_{N-2} z_{N-1}^2 z_N^2\big]$ where the permutations yield $\binom{N}{N-4}\binom{4}{2}$ distinct terms, i.e.,

$$\langle \mathbf{z} \,|2, N-4, 2\rangle = \frac{1}{\sqrt{\binom{N}{N-4}\binom{4}{2}}}\, \mathcal{P}\big[z_1^0 z_2^0 z_3 \cdots z_{N-2}\big(z_{N-1}^2/\sqrt{2}\big)\big(z_N^2/\sqrt{2}\big)\big]. \tag{E.4}$$

The permutation operator can be expanded as

$$\begin{aligned}\sum_{i_1\neq i_2\neq i_3\neq i_4} \frac{1}{2!} z_{i_1}^0 z_{i_2}^0 \frac{1}{2!} z_{i_3}^2 z_{i_4}^2 \prod_{k\neq i_1 \ldots i_4} z_k = \frac{1}{4} \sum_{i_1\neq i_2\neq i_3\neq i_4} \frac{1}{6}\big(&z_{i_1}^0 z_{i_2}^0 z_{i_3}^2 z_{i_4}^2 + z_{i_1}^0 z_{i_2}^2 z_{i_3}^0 z_{i_4}^2 + z_{i_1}^0 z_{i_2}^2 z_{i_3}^2 z_{i_4}^0 \\ &+ z_{i_1}^2 z_{i_2}^0 z_{i_3}^0 z_{i_4}^2 + z_{i_1}^2 z_{i_2}^0 z_{i_3}^2 z_{i_4}^0 + z_{i_1}^2 z_{i_2}^2 z_{i_3}^0 z_{i_4}^0\big) \prod_{k\neq i_1 \ldots i_4} z_k\end{aligned} \tag{E.5}$$

where the unrestricted sum on the left side overcounts each factor of $z_{i_1}^{\alpha} z_{i_2}^{\alpha}$ (with $\alpha = 0, 2$) by 2! (e.g., $z_1^0 z_2^0$ and $z_2^0 z_1^0$); as before, the equality originates from the permutations on the dummy variables i_1, i_2, i_3, i_4. The terms in parentheses above can be rewritten in a more suitable form with the identity

$$\begin{aligned} z_1^2 z_2^2 + z_1^2 z_3^2 + z_1^2 z_4^2 + z_2^2 z_3^2 + z_2^2 z_4^2 + z_3^2 z_4^2 =& \frac{1}{2}\big[(z_1 - z_2)^2 (z_3 - z_4)^2 + (z_1 - z_3)^2 (z_2 - z_4)^2 \\ &+ (z_1 - z_4)^2 (z_2 - z_3)^2\big] \\ &+ \big[(z_1 - z_2)^2 z_3 z_4 + (z_1 - z_3)^2 z_2 z_4 + (z_1 - z_4)^2 z_2 z_3 \\ &+ (z_2 - z_3)^2 z_1 z_4 + (z_2 - z_4)^2 z_1 z_3 + (z_3 - z_4)^2 z_1 z_2\big] \\ &+ 6\, z_1 z_2 z_3 z_4. \end{aligned} \tag{E.6}$$

Using this in Eq. (E.5) leads to (i) 3 equal contributions from the first term on the right side of Eq. (E.6), each of which leads to a factor of 2×2 for converting the unrestricted sum to $i_1 < i_2$ and $i_3 < i_4$ and another factor of 2 for imposing the condition $i_1 < i_3$; and (ii) 6 equal contributions from the second term on the right side of Eq. (E.6), each of which leads to one factor of 2 for converting the sum to $i_1 < i_2$ and another factor of 2! to count interchangeability of i_3 and i_4. Therefore,

$$\begin{aligned} \sum_{i_1 \neq i_2 \neq i_3 \neq i_4} z_{i_1}^0 z_{i_2}^0 z_{i_3}^2 z_{i_4}^2 \prod_{k \neq i_1 \ldots i_4} z_k =& \frac{1}{6} \times \frac{1}{2} \times 3 \times 8 \sum{}' \big(z_{i_1} - z_{i_2}\big)^2 \big(z_{i_3} - z_{i_4}\big)^2 \prod_{k \neq i_1 \ldots i_4} z_k \\ &+ \frac{1}{6} \times 6 \times 2 \times 2! \sum_{i_1 < i_2} (z_{i_1} - z_{i_2})^2 \prod_{k \neq i_1, i_2} z_k \\ &+ \tbinom{N}{4} 4! \prod_k z_k \end{aligned} \tag{E.7}$$

where the prime on the sum indicates the conditions (D.22). We now have

$$\mathcal{P}\big[z_1^0 z_2^0 z_3 \cdots z_{N-2} z_{N-1}^2 z_N^2\big] = \frac{1}{2} \sum{}' \big(z_{i_1} - z_{i_2}\big)^2 \big(z_{i_3} - z_{i_4}\big)^2 \prod_{k \neq i_1 \ldots i_4} z_k + \sum_{i_1 < i_2} (z_{i_1} - z_{i_2})^2 \prod_{k \neq i_1, i_2} z_k + \tbinom{N}{4} 3! \prod_k z_k \tag{E.8}$$

and, in turn, the expansion of $\langle \mathbf{z} \,|2, N-4, 2\rangle$ in terms of symmetric Jastrow polynomials J_0, J_1, and J_2 defined previously in Appendix D.

As shown in Eq. (3.12), the m^{th} term in (3.6) is proportional to the monomial $\mathcal{M}_{\{\underbrace{0 \ldots 0}_{m}, \underbrace{2 \ldots 2}_{m}, \underbrace{1 \ldots 1}_{N-2m}\}}(\mathbf{z})$ which can be recast in terms of symmetric Jastrow polynomials as shown by Eq. (D.29). This yields the expansion of $\langle \mathbf{z} \,|m, N-2m, m\rangle$ in terms of symmetric Jastrow polynomials, given by Eq. (3.13).

Appendix F

Coarse-grained quantities for the vortex lattice state

In this Appendix, we calculate, in detail, the properties of the trial correlated wave function (3.21) using the elementary symmetric polynomials introduced in Appendix D. It is important to note that for brevity of notation, *all* quantities in this Appendix are treated as unitless.

F.1 Mean-field state

To begin, we start by expressing the non-normalized mean-field vortex lattice wave function (3.18) in terms of the elementary symmetric polynomials (D.8) defined on the set of vortex positions $\{\xi_j | j = 0, \ldots, N_\mathrm{v} - 1\}$. For simplicity and symmetry considerations, we assume that the lattice is perfectly triangular and, hence, has a 6-fold rotational symmetry. This is a very good approximation in the bulk of the lattice [24] for large number of vortices, as the deviations from a perfect triangular lattice become noticeable only at the edge of the cloud [24, 30] where the particle density is vanishingly small. We assume that $\xi_0 = 0$ is the vortex at the center of the trap [29], and define

$$N_\mathrm{v}' \equiv N_\mathrm{v} - 1; \tag{F.1}$$

in other words, the vortex at the center is treated separately from the rest, and we define a new set $\boldsymbol{\xi}' = \{\xi_j | j = 1, \ldots, N_\mathrm{v} - 1\}$. The single-particle condensate wave function, then, is

$$\psi(z) = C \prod_{j=0}^{N_\mathrm{v}-1} (z - \xi_j) = C \sum_{j=0}^{N_\mathrm{v}'/6} \mathcal{S}_{N_\mathrm{v}'-6j}(\boldsymbol{\xi}')\, z^{6j+1} \tag{F.2}$$

where C is the normalization constant, to be determined later. Hence, the only powers of z that appear in the expansion of $\psi(z)$ are $1, 7, 13, 19, 25, \ldots$ due to the lattice being triangular. Also, from now on, noting that the elementary symmetric polynomials, $\mathcal{S}$, are all defined on the set $\boldsymbol{\xi}'$, we suppress their argument as well for brevity.

Since the polynomials $\mathcal{S}_6, \mathcal{S}_{12}, \ldots, \mathcal{S}_{N_\mathrm{v}'}$ depend explicitly on the position of vortices in the lattice, calculating properties of lattice wave functions is a highly non-trivial task. Thus, we need to find a way to remove this explicit dependence on $\boldsymbol{\xi}'$ and, instead, replace it with coarse-grained quantities like the radius

of the cloud. By definition, $\mathcal{S}_{N'_\mathrm{v}}$, the coefficient of z in Eq. (F.2), is given by the multiplication of all the vortex coordinates (except the one at the center) together. By symmetry, $\mathcal{S}_{N'_\mathrm{v}}$ is a real number provided that a vortex on the first ring (the closest set of vortices to the center) lies on the real axis; therefore, $\left|\mathcal{S}_{N'_\mathrm{v}}\right| = \prod_{j=1}^{N'_\mathrm{v}} |\xi_j|$. Taking the logarithm of both sides leads to

$$\ln\left|\mathcal{S}_{N'_\mathrm{v}}\right| = \sum_{j=1}^{N'_\mathrm{v}} \ln|\xi_j| = \int d^2\boldsymbol{\xi}\, n'_\mathrm{v}(\boldsymbol{\xi}) \ln|\boldsymbol{\xi}| \tag{F.3}$$

where $n'_\mathrm{v}(\boldsymbol{\xi}) = \sum_{j>0} \delta(\boldsymbol{\xi} - \boldsymbol{\xi}_j)$ is the reduced vortex density (we are now using a vector notation). Noting that (a) $\int d^2\boldsymbol{\xi}\, n'_\mathrm{v}(\boldsymbol{\xi}) = N_\mathrm{v} - 1$ and (b) $n'_\mathrm{v}(\mathbf{0}) = 0$, we approximate this (reduced) vortex density with

$$n'_\mathrm{v}(\boldsymbol{\xi}) = \max[\overline{n_\mathrm{v}}]\, \Theta(|\boldsymbol{\xi}| - 1) \tag{F.4}$$

where $\max[\overline{n_\mathrm{v}}] = 1/\pi$ is the (unitless) maximum value of the average vortex density of a large uniform lattice [23, 24, 30]. Thus, we have

$$\ln\left|\mathcal{S}_{N'_\mathrm{v}}\right| = \frac{1}{\pi}\int_{\theta=0}^{2\pi}\int_{\xi=1}^{R} d\theta d\xi\, \xi \ln\xi = \frac{1}{2} + R^2\left[\ln R - \frac{1}{2}\right] \tag{F.5}$$

which, finally, yields

$$\left|\mathcal{S}_{N'_\mathrm{v}}\right| = \sqrt{e}\left(\frac{R}{\sqrt{e}}\right)^{N_\mathrm{v}} \tag{F.6}$$

where we have used the fact that $R^2 \simeq N_\mathrm{v}$ in the limit of very fast rotation.

We now find the normalization constant C. Writing $|\psi(z)|^2 = |C|^2 \exp\left[-|z|^2 + \sum_{j=0}^{N_\mathrm{v}-1} \ln|z-\xi_j|^2\right]$ (where the LLL exponential factor is explicitly mentioned for clarity), we find by integrating over the vortex coordinates

$$\begin{aligned}\sum_{j=0}^{N_\mathrm{v}-1} \ln\left|\mathbf{r} - \boldsymbol{\xi}_j\right|^2 = \sum_{j=0}^{N_\mathrm{v}-1} \ln\left(r^2 + \xi_j^2 - 2r\xi_j\cos\theta_j\right) &= \overline{n_\mathrm{v}}\int_{\theta=0}^{2\pi}\int_{\xi=0}^{R} d\theta d\xi\, \xi \ln\left(r^2 + \xi^2 - 2r\xi\cos\theta\right) \\ &= \pi\,\overline{n_\mathrm{v}}\left\{r^2 + R^2\left[\ln R^2 - 1\right]\right\}. \end{aligned} \tag{F.7}$$

Therefore, defining $\sigma^{-2} \equiv 1 - \pi\,\overline{n_\mathrm{v}}$ yields the coarse-grained particle probability density

$$|\psi(z)|^2 = |C|^2\left(\frac{R}{\sqrt{e}}\right)^{2N_\mathrm{v}} e^{-|z|^2/\sigma^2} \tag{F.8}$$

which has the Gaussian form first derived by Ho in Ref. [23]. We, then, find by normalizing $\psi(z)$ that

$$\int\limits_{0\leq|z|\leq R} |\psi(z)|^2 = |C|^2 \left(\frac{R}{\sqrt{e}}\right)^{2N_\mathrm{v}} \pi\sigma^2 \left[1 - e^{-R^2/\sigma^2}\right] = 1. \tag{F.9}$$

Note that $R^2/\sigma^2 = R^2 - N_\mathrm{v} \to 0$ in the fast rotation regime; hence, we expand the exponential and use Eq. (F.6) to finally find

$$\left|C\mathcal{S}_{N_\mathrm{v}'}\right|^2 = \frac{e}{\pi R^2}\,. \tag{F.10}$$

F.2 Trial correlated state

To proceed, we introduce the following notation

$$\mathrm{I} \equiv z_i \tag{F.11}$$

$$f_{ij} \equiv (z_i - z_j)^2 \tag{F.12}$$

$$\psi_i \equiv \psi(z_i) \tag{F.13}$$

$$\psi_{(i_1,i_2,\dots)} \equiv \prod_{k\neq i_1,i_2,\dots} \psi(z_k) \tag{F.14}$$

in order to simplify the presentation. Therefore, the trial correlated wave function defined in Eq. (3.21) can be written as $\psi_\mathrm{tr} = \sum_{i<j} f_{ij}\,\psi_{(ij)}$.

Let us start by determining the norm of the trial correlated wave function. We have

$$\langle\psi_\mathrm{tr}|\,\psi_\mathrm{tr}\rangle = \sum_{\substack{i<j\\ i'<j'}} \int f^*_{i'j'} f_{ij}\,\psi^*_{(i'j')}\psi_{(ij)} \tag{F.15}$$

where the integrations are over the two-dimensional surface elements $d\mathrm{I} \equiv d^2\mathbf{r}_i$. Since $f_{ij} = \mathrm{I}^2 + \mathrm{J}^2 - 2\mathrm{IJ}$ and the powers of z in the expansion (F.2) are only of the form $6j+1$, the only *non-zero* contributions in Eq. (F.15) are as follows:

- Cases where $i' = i$ and $j' = j$ of which there are $\binom{N}{2}$ terms

$$\begin{aligned}\int (\mathrm{I}^* - \mathrm{J}^*)^2(\mathrm{I} - \mathrm{J})^2\ \left|\psi_{(ij)}\right|^2 &= \int \left(\left|\mathrm{I}^2\right|^2 \left|\mathrm{J}^0\right|^2 + \left|\mathrm{I}^0\right|^2 \left|\mathrm{J}^2\right|^2 + 4\left|\mathrm{I}\right|^2 \left|\mathrm{J}\right|^2\right)\\ &= \pi 2! \times \pi 0! + \pi 0! \times \pi 2! + 4\pi 1! \times \pi 1!\\ &= 8\pi^2\end{aligned} \tag{F.16}$$

- Cases where $i' = i$ and $j' \neq i, j$ of which there are $\binom{N}{1}\binom{N-1}{2}2!$ terms

$$\begin{aligned}\int \left(\mathrm{I}^* - \mathrm{J}'^*\right)^2 (\mathrm{I} - \mathrm{J})^2 \, \psi_j^* \psi_{j'} \left|\psi_{(ijj')}\right|^2 &= \int 4 \left|\mathrm{I}\right|^2 \left(\mathrm{J}'^* \, \psi_{j'}\right) \left(\mathrm{J} \, \psi_j^*\right) \\ &= 4 \times \pi 1! \times \left(C\mathcal{S}_{N'_{\mathrm{v}}} \times \pi 1!\right) \times \left(C^* \mathcal{S}^*_{N'_{\mathrm{v}}} \times \pi 1!\right) \\ &= 4\pi^3 \left|C\mathcal{S}_{N'_{\mathrm{v}}}\right|^2 \end{aligned} \tag{F.17}$$

- Cases where $i' \neq i, j$ and $j' \neq i, j$ of which there are $\binom{N}{2}\binom{N-2}{2}$ terms

$$\begin{aligned}\int \left(\mathrm{I}'^* - \mathrm{J}'^*\right)^2 (\mathrm{I} - \mathrm{J})^2 \, \psi_i^* \psi_j^* \psi_{i'} \psi_{j'} \left|\psi_{(iji'j')}\right|^2 &= \int 4 \left(\mathrm{I}'^* \, \psi_{i'}\right) \left(\mathrm{J}'^* \, \psi_{j'}\right) \left(\mathrm{I} \, \psi_i^*\right) \left(\mathrm{J} \, \psi_j^*\right) \\ &= 4 \times \left(C\mathcal{S}_{N'_{\mathrm{v}}} \times \pi 1!\right)^2 \times \left(C^* \mathcal{S}^*_{N'_{\mathrm{v}}} \times \pi 1!\right)^2 \\ &= 4\pi^4 \left|C\mathcal{S}_{N'_{\mathrm{v}}}\right|^4 \end{aligned} \tag{F.18}$$

where we have used the identity

$$\int \left|z^m\right|^2 \, e^{-|z|^2} = \pi m! \, . \tag{F.19}$$

Hence, the norm is

$$\langle \psi_{\mathrm{tr}} | \, \psi_{\mathrm{tr}} \rangle = \pi^2 N(N-1) \left[4 + 4(N-2)\pi \left|C\mathcal{S}_{N'_{\mathrm{v}}}\right|^2 + (N-2)(N-3)\pi^2 \left|C\mathcal{S}_{N'_{\mathrm{v}}}\right|^4\right] . \tag{F.20}$$

Next, we find the expectation value of the total angular momentum operator $\mathcal{L}$ taken with respect to the state $|\psi_{\mathrm{tr}}\rangle$. Note that the total angular momentum of the N-body mean-field state (3.18) is given by Eq. (3.20) which, from now on, we denote by $L_{\mathrm{mf}}(N)$. Since $\mathcal{L} = \sum_{k=1}^{N} \ell_k$, we find

$$\langle \mathbf{z}| \, \mathcal{L} \, |\psi_{\mathrm{tr}}\rangle = \sum_{i<j} \left(\ell_i + \ell_j + \sum_{k \neq i,j} \ell_k\right) \left[f_{ij} \, \psi_{(ij)}\right] = \sum_{i<j} \left\{\psi_{(ij)} \left[(\ell_i + \ell_j) f_{ij}\right] + f_{ij} \mathcal{L}_{(ij)} \psi_{(ij)}\right\} \tag{F.21}$$

where $\mathcal{L}_{(ij)} = \sum_{k \neq i,j} \ell_k$. Trivially,

$$(\ell_i + \ell_j) f_{ij} = 2(\mathrm{I} - \mathrm{J})^2 = 2 f_{ij}. \tag{F.22}$$

Therefore, we can write

$$\langle \psi_{\mathrm{tr}}| \, \mathcal{L} \, |\psi_{\mathrm{tr}}\rangle = 2 \int \left|\psi_{\mathrm{tr}}\right|^2 + \sum_{\substack{i<j \\ i'<j'}} \int f^*_{i'j'} f_{ij} \left[\psi^*_{(i'j')} \mathcal{L}_{(ij)} \psi_{(ij)}\right]. \tag{F.23}$$

The only *non-zero* contributions in the second term of Eq. (F.23) are as follows:

- Cases where $i' = i$ and $j' = j$ of which there are $\binom{N}{2}$ terms

$$\int (\mathrm{I}^* - \mathrm{J}^*)^2 (\mathrm{I} - \mathrm{J})^2 \left[\psi^*_{(ij)} \mathcal{L}_{(ij)} \psi_{(ij)}\right] = \int \left|(\mathrm{I} - \mathrm{J})^2\right|^2 \times \int \psi^*_{(ij)} \mathcal{L}_{(ij)} \psi_{(ij)}$$
$$= 8\pi^2 \times L_{\mathrm{mf}}(N-2) \tag{F.24}$$

- Cases where $i' = i$ and $j' \neq i, j$ of which there are $\binom{N}{1}\binom{N-1}{2}2!$ terms

$$\int \left(\mathrm{I}^* - \mathrm{J}'^*\right)^2 (\mathrm{I} - \mathrm{J})^2 \left[\psi^*_{(ij')} \mathcal{L}_{(ij)} \psi_{(ij)}\right] = \int \left(\mathrm{I}^* - \mathrm{J}'^*\right)^2 (\mathrm{I} - \mathrm{J})^2 \left\{ \left[\psi^*_j \psi^*_{(ijj')}\right] \left[\ell_{j'} + \mathcal{L}_{(ijj')}\right] \left[\psi_{j'} \psi_{(ijj')}\right] \right\}$$
$$= \int \left(\mathrm{I}^* - \mathrm{J}'^*\right)^2 (\mathrm{I} - \mathrm{J})^2 \left\{ \left|\psi_{(ijj')}\right|^2 \psi^*_j \ell_{j'} \psi_{j'} + \psi^*_j \psi_{j'} \left[\psi^*_{(ijj')} \mathcal{L}_{(ijj')} \psi_{(ijj')}\right] \right\}$$
$$= \int 4 \left|\mathrm{I}\right|^2 \left(\mathrm{J}'^* \ell_{j'} \psi_{j'}\right) \left(\mathrm{J}\, \psi^*_j\right) + \int 4 \left|\mathrm{I}\right|^2 \left(\mathrm{J}'^*\, \psi_{j'}\right) \left(\mathrm{J}\, \psi^*_j\right) \times \int \psi^*_{(ijj')} \mathcal{L}_{(ijj')} \psi_{(ijj')}$$
$$= 4\pi^3 \left|C \mathcal{S}_{N'_{\mathrm{v}}}\right|^2 \left[1 + L_{\mathrm{mf}}(N-3)\right] \tag{F.25}$$

- Cases where $i' \neq i, j$ and $j' \neq i, j$ of which there are $\binom{N}{2}\binom{N-2}{2}$ terms

$$\int \left(\mathrm{I}^* - \mathrm{J}'^*\right)^2 (\mathrm{I} - \mathrm{J})^2 \left[\psi^*_{(i'j')} \mathcal{L}_{(ij)} \psi_{(ij)}\right]$$
$$= \int \left(\mathrm{I}^* - \mathrm{J}'^*\right)^2 (\mathrm{I} - \mathrm{J})^2 \left\{ \left[\psi^*_i \psi^*_j \psi^*_{(iji'j')}\right] \left[\ell_{i'} + \ell_{j'} + \mathcal{L}_{(iji'j')}\right] \left[\psi_{i'} \psi_{j'} \psi_{(iji'j')}\right] \right\}$$
$$= \int \left(\mathrm{I}^* - \mathrm{J}'^*\right)^2 (\mathrm{I} - \mathrm{J})^2 \left\{ \left|\psi_{(iji'j')}\right|^2 \left[\psi^*_i \psi^*_j \psi_{j'} \ell_{i'} \psi_{i'} + \psi^*_i \psi^*_j \psi_{i'} \ell_{j'} \psi_{j'}\right] \right.$$
$$\left. + \psi^*_i \psi^*_j \psi_{i'} \psi_{j'} \left[\psi^*_{(iji'j')} \mathcal{L}_{(iji'j')} \psi_{(iji'j')}\right] \right\}$$
$$= \int 4 \left(\mathrm{I}'^* \ell_{i'} \psi_{i'}\right) \left(\mathrm{J}'^*\, \psi_{j'}\right) \left(\mathrm{I}\, \psi^*_i\right) \left(\mathrm{J}\, \psi^*_j\right) + \int 4 \left(\mathrm{I}'^*\, \psi_{i'}\right) \left(\mathrm{J}'^* \ell_{j'} \psi_{j'}\right) \left(\mathrm{I}\, \psi^*_i\right) \left(\mathrm{J}\, \psi^*_j\right)$$
$$+ \int 4 \left(\mathrm{I}'^*\, \psi_{i'}\right) \left(\mathrm{J}'^*\, \psi_{j'}\right) \left(\mathrm{I}\, \psi^*_i\right) \left(\mathrm{J}\, \psi^*_j\right) \times \int \psi^*_{(iji'j')} \mathcal{L}_{(iji'j')} \psi_{(iji'j')}$$
$$= 4\pi^4 \left|C \mathcal{S}_{N'_{\mathrm{v}}}\right|^4 \left[2 + L_{\mathrm{mf}}(N-4)\right] \tag{F.26}$$

Thus, the expectation value of the angular momentum becomes

$$\langle \psi_{\mathrm{tr}} | \mathcal{L} | \psi_{\mathrm{tr}} \rangle = \pi^2 N(N-1) \Big\{ 4\big[2 + L_{\mathrm{mf}}(N-2)\big] + 4(N-2)\pi \left|C \mathcal{S}_{N'_{\mathrm{v}}}\right|^2 \left[3 + L_{\mathrm{mf}}(N-3)\right]$$
$$+ (N-2)(N-3)\pi^2 \left|C \mathcal{S}_{N'_{\mathrm{v}}}\right|^4 \left[4 + L_{\mathrm{mf}}(N-4)\right] \Big\}. \tag{F.27}$$

Finally, we calculate the interaction energy of this state. The interaction energy operator is $\mathcal{V} = \sum_{i<j} v_{ij}$ where v_{ij}, the two-body interaction, is given in position representation by Eq. (B.2b). Due to the symmetry

of the operator and the many-body wave function, we have $\langle \mathcal{V} \rangle = \frac{1}{2} N(N-1) \langle v_{12} \rangle$. To proceed, we write

$$\psi_{\rm tr} = \sum_{1<j} f_{1j}\, \psi_{(1j)}\, e^{-\frac{1}{2}(|1|^2+|2|^2)} + \sum_{2<j} f_{2j}\, \psi_{(2j)}\, e^{-\frac{1}{2}(|1|^2+|2|^2)} + \sum_{3\le i<j} f_{ij}\, \psi_{(ij)}\, e^{-\frac{1}{2}(|1|^2+|2|^2)} \tag{F.28}$$

where, for clarity, we have explicitly shown the LLL exponential factors corresponding to z_1 and z_2, whereas the remaining exponential factors are still suppressed, as before, for brevity. Note that '|1|' and '|2|' in the exponents are not numbers but refer to $|z_1|$ and $|z_2|$ respectively, as defined above. Acting on the state (F.28) by the Dirac delta function $\delta(\mathbf{r}_1 - \mathbf{r}_2)$ means substituting every z_2 by z_1 and leads to

$$\underbrace{2 \sum_{2<j} f_{1j}\, \psi_1\, \psi_{(12j)}\, e^{-|1|^2}}_{A} + \underbrace{\sum_{3\le i<j} f_{ij}\, \psi_1^2\, \psi_{(12ij)}\, e^{-|1|^2}}_{B}. \tag{F.29}$$

Therefore, we have

$$\langle \delta(\mathbf{r}_1 - \mathbf{r}_2) \rangle_{\rm tr} = \int \big\{ 4\, A^* A + B^* B + 4\, {\rm Re}[A^* B] \big\}. \tag{F.30}$$

We now have to find the *non-zero* contributions from each term above. The first term has two contributions as follows:

- Cases where $j' = j$ of which there are $\binom{N-2}{1}$ terms

$$\begin{aligned} \int \big(1^* - {\rm J}^*\big)^2 (1-{\rm J})^2 \left|\psi_{(12j)}\right|^2 |\psi_1|^2\, e^{-2|1|^2} &= \int \Big(\left|1^2\right|^2 \left|{\rm J}^0\right|^2 + \left|1^0\right|^2 \left|{\rm J}^2\right|^2 + 4 \left|1^1\right|^2 \left|{\rm J}^1\right|^2 \Big) |\psi_1|^2\, e^{-2|1|^2} \\ &= \int \Big\{ \pi 0! \Big[\left|1^2\right|^2 |\psi_1|^2\, e^{-2|1|^2} \Big] + \pi 2! \Big[\left|1^0\right|^2 |\psi_1|^2\, e^{-2|1|^2} \Big] + 4\pi 1! \Big[\left|1^1\right|^2 |\psi_1|^2\, e^{-2|1|^2} \Big] \Big\} \\ &= \pi \big(X_2 + 4X_1 + 2X_0 \big) \end{aligned} \tag{F.31}$$

- Cases where $j' \neq j$ of which there are $\binom{N-2}{2} 2!$ terms

$$\begin{aligned} \int \big(1^* - {\rm J'}^*\big)^2 (1-{\rm J})^2\, \psi_j^*\, \psi_{j'} \left|\psi_{(12jj')}\right|^2 |\psi_1|^2\, e^{-2|1|^2} &= \int 4 \Big(|1|^2 |\psi_1|^2 e^{-2|1|^2} \Big) \big({\rm J'}^*\, \psi_{j'}\big) \big({\rm J}\, \psi_j^*\big) \\ &= 4\pi^2 \left| C \mathcal{S}_{N'_{\rm v}} \right|^2 X_1 \end{aligned} \tag{F.32}$$

where $X_k = \int \left|{\rm I}^k\right|^2 |\psi_i|^2\, e^{-2|{\rm I}|^2}$, to be determined later. For the second term in Eq. (F.30), we find

- $\int \left|\psi_1^2\right|^2 e^{-2|1|^2} \times \int \left| \sum_{3\le i<j} f_{ij}\, \psi_{(12ij)} \right|^2 = Y \times \langle \psi_{\rm tr} |\, \psi_{\rm tr} \rangle \big|_{N \to N-2}$

where the last factor is just the norm of a $(N-2)$-particle trial state, given via substituting N by $N-2$ in Eq. (F.20) and $Y = \int \left|\psi_i^2\right|^2 e^{-2|{\rm I}|^2}$ will be determined later. And finally, the last term in Eq. (F.30) (the

cross term) leads to the following two contributions:

- Cases where $j' = i$ or j of which there are $\binom{N-2}{2}\binom{2}{1}$ terms

$$\int \left(1^* - \mathrm{J}^*\right)^2 (\mathrm{I} - \mathrm{J})^2 \, \psi_i^* \left|\psi_{(12ij)}\right|^2 \, \psi_1^* \psi_1^2 \, e^{-2|1|^2} = \int 4 \left(1^* \psi_1^* \psi_1^2 \, e^{-2|1|^2}\right) \left(\mathrm{I}\, \psi_i^*\right) |\mathrm{J}|^2$$
$$= 4\pi^2 \left(C\mathcal{S}_{N_\mathrm{v}'}\right)^* Z \tag{F.33}$$

- Cases where $j' \neq i, j$ of which there are $\binom{N-2}{3}\binom{3}{2}$ terms

$$\int \left(1^* - \mathrm{J}'^*\right)^2 (\mathrm{I} - \mathrm{J})^2 \, \psi_i^* \psi_j^* \psi_{j'} \left|\psi_{(12ijj')}\right|^2 \, \psi_1^* \psi_1^2 \, e^{-2|1|^2} = \int 4 \left(1^* \psi_1^* \psi_1^2 \, e^{-2|1|^2}\right) \left(\mathrm{I}\, \psi_i^*\right) \left(\mathrm{J}\, \psi_j^*\right) \left(\mathrm{J}'^* \psi_{j'}\right)$$
$$= 4\pi^3 \left|C\mathcal{S}_{N_\mathrm{v}'}\right|^2 \left(C\mathcal{S}_{N_\mathrm{v}'}\right)^* Z \tag{F.34}$$

where $Z = \int \mathrm{I}^* \, \psi_i^* \psi_i^2 \, e^{-2|\mathrm{I}|^2}$, to be determined. Hence, the interaction energy of this state is

$$\begin{aligned}
\langle \psi_{\mathrm{tr}} | \, \mathcal{V} \, | \psi_{\mathrm{tr}} \rangle = g_{2\mathrm{D}} \frac{N(N-1)}{2} \, \pi(N-2) \\
\times \Big\{ 4 \Big[\left(X_2 + 4X_1 + 2X_0\right) + \pi(N-3) Y \Big] \\
+ 4\pi(N-3) \Big[4 \left|C\mathcal{S}_{N_\mathrm{v}'}\right|^2 X_1 + \pi(N-4) \left|C\mathcal{S}_{N_\mathrm{v}'}\right|^2 Y + 4 \, \mathrm{Re}\big[\left(C\mathcal{S}_{N_\mathrm{v}'}\right)^* Z\big] \Big] \\
+ \pi^2 (N-3)(N-4) \Big[\pi(N-5) \left|C\mathcal{S}_{N_\mathrm{v}'}\right|^4 Y + 8 \left|C\mathcal{S}_{N_\mathrm{v}'}\right|^2 \mathrm{Re}\big[\left(C\mathcal{S}_{N_\mathrm{v}'}\right)^* Z\big] \Big] \Big\} .
\end{aligned} \tag{F.35}$$

We now proceed to evaluate X_k, Y, and Z defined previously. Starting with X_k, we note that the integrand includes the factor $|\psi_i|^2 \, e^{-|\mathrm{I}|^2}$ (particle probability density). Since we are dealing with very large lattices, we substitute that factor with its coarse-grained value, $\overline{n_i}$. Hence, we find for large R that

$$X_k = \int \left|\mathrm{I}^k\right|^2 |\psi_i|^2 \, e^{-2|\mathrm{I}|^2} \simeq \int \left|\mathrm{I}^k\right|^2 \overline{n_i} \, e^{-|\mathrm{I}|^2} \simeq \frac{2\,k!}{R^2} \tag{F.36}$$

where we have used the coarse-grained (single-particle) density in Eq. (1.27). For Y, however, we substitute $\left|\psi_i^2\right|^2 e^{-2|\mathrm{I}|^2}$ with $\overline{n_i}^2$ instead of $\overline{n_i^2}$. To take into account this approximation, we multiply the integrand by the Abrikosov lattice parameter [25] $b \simeq 1.158$ (we note that Y is exactly the integral one encounters when calculating the interaction energy of the mean-field vortex lattice state). Thus, we get

$$Y = \int \left|\psi_i^2\right|^2 e^{-2|\mathrm{I}|^2} \simeq b \int \overline{n_i}^2 = \frac{4b}{3\pi R^2} \, . \tag{F.37}$$

Finding Z, however, is more involved given that the integrand is complex. A naïve application of the same

procedure as before leads to

$$Z = \int \mathrm{I}^* \, \psi_i^* \psi_i^2 \, e^{-2|\mathrm{I}|^2} \stackrel{?}{\simeq} \int \mathrm{I}^* \, \psi_i \, \overline{n_i} \, e^{-|\mathrm{I}|^2} = C \mathcal{S}_{N_\mathrm{v}'} \, X_1 \tag{F.38}$$

which hinges upon the fact that after substituting the coarse-grained density in the integrand, the only non-zero contribution comes from the term proportional to I in ψ_i (which has a coefficient $C\mathcal{S}_{N_\mathrm{v}'}$). Careful consideration of the original integral reveals that there are many more terms that contribute to this integral. All is not lost, however, as this result correctly predicts the behavior of Z as a function of the radius of the cloud, $Z \sim R^{-3}$. This can be seen easily by writing the integrand in terms of its magnitude and phase and using Eq. (F.8) which brings out the R-dependence seen above. What is left to determine, then, is just the coefficient of proportionality. To determine Z, we proceed as follows. With the help of the elementary symmetric polynomials, we write $\psi(z) = C \sum_{j=0}^{N_\mathrm{v}} \mathcal{S}_{N_\mathrm{v}-j} \, z^j$ and find

$$\begin{aligned} Z &= C^3 \sum_{j,j',j''=0}^{N_\mathrm{v}} \mathcal{S}_{N_\mathrm{v}-j} \, \mathcal{S}_{N_\mathrm{v}-j'} \, \mathcal{S}^*_{N_\mathrm{v}-j''} \int z^{j+j'} \, z^{*(j''+1)} \, e^{-2|z|^2} \\ &= C^3 \sum_{j,j',j''=0}^{N_\mathrm{v}} \mathcal{S}_{N_\mathrm{v}-j} \, \mathcal{S}_{N_\mathrm{v}-j'} \, \mathcal{S}^*_{N_\mathrm{v}-j''} \, \pi \, \frac{(j+j')!}{2^{j+j'+1}} \, \delta_{j+j',j''+1} \\ &= C^3 \, \pi \sum_{j,j'=0}^{N_\mathrm{v}}{}' \frac{(j+j')!}{2^{j+j'+1}} \, \mathcal{S}_{N_\mathrm{v}-j} \, \mathcal{S}_{N_\mathrm{v}-j'} \, \mathcal{S}^*_{N_\mathrm{v}-(j+j'-1)} \end{aligned} \tag{F.39}$$

where the prime on the sum indicates the condition $0 \leq j + j' - 1 \leq N_\mathrm{v}$. Comparing this exact result with the one obtained previously, we can find the coefficient of proportionality. To do so, we construct with `MATHEMATICA` a triangular lattice with N_v vortices. Knowing the positions of vortices, we then find the condensate wave function, a polynomial in z of degree N_v, which, by construction, yields the exact values for the elementary symmetric polynomials above, $\{\mathcal{S}_j\}$, and the normalization constant, C. With all this information at hand, we find, for a certain N_v, the ratio of the exact value of Z to the incorrect value. We then change N_v and repeat this procedure. As expected (and explained above), the resulting coefficient is just a number with almost no dependence on the value of N_v. A least-square fit to the data leads to the coefficient which is $\simeq 0.5$ to a very good approximation. Therefore, we finally write

$$Z \simeq \frac{1}{2} \, C \mathcal{S}_{N_\mathrm{v}'} \, X_1 . \tag{F.40}$$

Using Eqs. (F.27), (F.20), and (F.10), we find the angular momentum of the state (3.21) for large N

$$L_{\rm tr} = \frac{\langle\psi_{\rm tr}|\,\mathcal{L}\,|\psi_{\rm tr}\rangle}{\langle\psi_{\rm tr}|\,\psi_{\rm tr}\rangle} \simeq (N-2)\left(\frac{R_{\rm tr}^2}{3}-1\right)+2-f_1(\nu)\left(\frac{R_{\rm tr}^2}{3}-2\right) \tag{F.41}$$

where $\nu = N/N_{\rm v}$ is the filling factor and

$$f_1(\nu) = \frac{2e\nu}{2+e\nu}\,. \tag{F.42}$$

In the regime where the Gross-Pitaevskii equation is valid and the vortex lattice is stable, ν is a very large number; therefore, we substitute $f_1(\nu)$ with its value in the limit of very large ν; that is, $f_1(\nu)\to 2$. Hence, the angular momentum becomes

$$L_{\rm tr} = (N-2)\left(\frac{R_{\rm tr}^2}{3}-1\right)+2-2\left(\frac{R_{\rm tr}^2}{3}-2\right). \tag{F.43}$$

Likewise, using Eqs. (F.35), (F.20), (F.10), (F.36), (F.37), and (F.40), we have for large N

$$V_{\rm tr} = \frac{\langle\psi_{\rm tr}|\,\mathcal{V}\,|\psi_{\rm tr}\rangle}{\langle\psi_{\rm tr}|\,\psi_{\rm tr}\rangle} \simeq V_0(N-2)\,\frac{1}{R_{\rm tr}^2}\left\{\frac{4b}{3}N\left[1-\frac{f_1(\nu)}{N}\right]+f_2(\nu)\right\} \tag{F.44}$$

where

$$f_2(\nu) = \frac{16(4-b)+16\big(3-\frac{4b}{3}\big)e\nu+4\big(2-\frac{5b}{3}\big)(e\nu)^2}{4+4e\nu+(e\nu)^2}\,. \tag{F.45}$$

Using Eq. (3.22) and defining $h(\nu) = (3/4b)f_2(\nu) - f_1(\nu)$, we find

$$V_{\rm tr} = V_0(N-2)\,\frac{4bN/3}{N_{\rm v}(1+4/N)}\left[1+\frac{h(\nu)}{N}\right]. \tag{F.46}$$

Note that $h(\nu)$ is a monotonically decreasing function of ν; it changes sign from positive to negative at $\nu\simeq 3$ and has a limiting value of $h(\nu)\to -1.82$ for $\nu\gg 1$. Therefore, in the range of validity of the Gross-Pitaevskii equation, we arrive at

$$V_{\rm tr} \simeq V_0\left(\frac{4b}{3}\right)\nu\,\frac{(N-2)\Big[1+\frac{h(\infty)}{N}\Big]}{1+\frac{4}{N}} \simeq V_0\left(\frac{4b}{3}\right)\nu\,(N-8). \tag{F.47}$$

We now determine the particle number density for the correlated state. It is not surprising that the trial wave function shows the same vortex lattice as the mean-field condensate wave function, given that the majority of particles (except two) are still uncorrelated and are in the mean-field condensed state. However, due to the correlations, we expect the vortex cores to acquire a rather small non-zero density. Since the

many-body density operator is $\sum_{i=1}^{N} \delta(\mathbf{r}-\mathbf{r}_i)$, the particle density associated with $|\psi_{\rm tr}\rangle$ is

$$n_{\rm tr}(\mathbf{r}) = \frac{1}{\langle\psi_{\rm tr}\,|\psi_{\rm tr}\rangle}\left[N\int d^2\mathbf{r}_1\cdots d^2\mathbf{r}_N\ |\psi_{\rm tr}(\mathbf{r}_1\mathbf{r}_2\ldots\mathbf{r}_N)|^2\,\delta(\mathbf{r}-\mathbf{r}_1)\right]. \tag{F.48}$$

The Dirac delta function replaces all $\mathbf{r}_1$'s with $\mathbf{r}$ in the integrand, so after integrating over $\mathbf{r}_1$, the probability density becomes

$$\begin{aligned}|\psi_{\rm tr}(\mathbf{r}\mathbf{r}_2\cdots\mathbf{r}_N)|^2 = \Bigg\{ &|\psi(z)|^2 \sum_{\substack{1<i<j\\1<i'<j'}} f^*_{i'j'} f_{ij}\,\psi^*_{(1i'j')}\psi_{(1ij)} + 2\,\mathrm{Re}\Bigg[\psi(z)\sum_{\substack{1<i<j\\1<j'}} f^*_{zj'} f_{ij}\,\psi^*_{(1j')}\psi_{(1ij)}\Bigg]\\ &+ \sum_{\substack{1<j\\1<j'}} f^*_{zj'} f_{zj}\,\psi^*_{(1j')}\psi_{(1j)}\Bigg\} e^{-|z|^2}\end{aligned} \tag{F.49}$$

where the LLL exponential factor associated with z is explicitly shown for clarity. Even without evaluating the other integrals, it is obvious that the first two terms in Eq. (F.49) would vanish if we set z equal to the position of any vortex in the lattice since $\psi(z=\xi_j)=0$ for $0\le j\le N'_{\rm v}$. In that case, the only non-zero contribution comes from the last term, and the particle density at a vortex core, after some algebra similar to those used to derive the norm, becomes

$$n_{\rm tr}(\xi_j) \simeq \left[\frac{\left(|\xi_j|^4+4|\xi_j|^2+2\right)+4e\nu\,|\xi_j|^2}{4+4e\nu+(e\nu)^2}\right]\frac{e^{-|\xi_j|^2}}{\pi}. \tag{F.50}$$

References

[1] F. Dalfovo, S. Giorgini, L. P. Pitaevskii, and S. Stringari, "Theory of Bose-Einstein condensation in trapped gases," *Reviews of Modern Physics* **71**, 463–512 (1999).

[2] R. J. Donnelly, *Quantized Vortices in Helium II.* Cambridge University Press, Cambridge, UK, 1991.

[3] M. H. Anderson, J. R. Ensher, M. R. Matthews, C. E. Wieman, and E. A. Cornell, "Observation of Bose-Einstein Condensation in a Dilute Atomic Vapor," *Science* **269**, 198–201 (1995).

[4] K. B. Davis, M.-O. Mewes, M. R. Andrews, N. J. van Druten, D. S. Durfee, D. M. Kurn, and W. Ketterle, "Bose-Einstein Condensation in a Gas of Sodium Atoms," *Physical Review Letters* **75**, 3969–3973 (1995).

[5] L. Onsager, "Statistical hydrodynamics," *Il Nuovo Cimento Series 9* **6**, 279–287 (1949).

[6] R. P. Feynman, "Application of quantum mechanics to liquid helium," *Progress in Low Temperature Physics* **1**, 17–53 (1955).

[7] E. J. Yarmchuk, M. J. V. Gordon, and R. E. Packard, "Observation of Stationary Vortex Arrays in Rotating Superfluid Helium," *Physical Review Letters* **43**, 214–217 (1979).

[8] M. R. Matthews, B. P. Anderson, P. C. Haljan, D. S. Hall, C. E. Wieman, and E. A. Cornell, "Vortices in a Bose-Einstein Condensate," *Physical Review Letters* **83**, 2498–2501 (1999).

[9] C. J. Pethick and H. Smith, *Bose-Einstein Condensation in Dilute Gases.* Cambridge University Press, Cambridge, UK, 2002.

[10] K. Huang, *Statistical Mechanics.* John Wiley & Sons, New York, 1987.

[11] K. W. Madison, F. Chevy, W. Wohlleben, and J. Dalibard, "Vortex Formation in a Stirred Bose-Einstein Condensate," *Physical Review Letters* **84**, 806–809 (2000).

[12] K. W. Madison, F. Chevy, W. Wohlleben, and J. Dalibard, "Vortices in a stirred Bose-Einstein condensate," *Journal of Modern Optics* **47**, 2715–2723 (2000).

[13] J. R. Abo-Shaeer, C. Raman, J. M. Vogels, and W. Ketterle, "Observation of Vortex Lattices in Bose-Einstein Condensates," *Science* **292**, 476–479 (2001).

[14] F. Dalfovo and S. Stringari, "Shape deformations and angular-momentum transfer in trapped Bose-Einstein condensates," *Physical Review A* **63**, 011601(R) (2000).

[15] N. R. Cooper, "Rapidly Rotating Atomic Gases," *Advances in Physics* **57**, 539–616 (2008).

[16] A. J. Leggett, *Quantum Liquids.* Oxford University Press, New York, 2007.

[17] P. Nozières and D. Pines, *The Theory of Quantum Liquids.* Perseus Books, Cambridge, MA, 1999.

[18] L. D. Landau and E. M. Lifshitz, *Statistical Physics, Part 1.* Elsevier, Oxford, UK, 1980.

[19] S. Viefers, "Quantum Hall physics in rotating Bose-Einstein condensates," *Journal of Physics: Condensed Matter* **20**, 123202 (2008).

[20] V. Schweikhard, I. Coddington, P. Engels, V. P. Mogendorff, and E. A. Cornell, "Rapidly Rotating Bose-Einstein Condensates in and near the Lowest Landau Level," *Physical Review Letters* **92**, 040404 (2004).

[21] N. K. Wilkin, J. M. F. Gunn, and R. A. Smith, "Do Attractive Bosons Condense?," *Physical Review Letters* **80**, 2265–2268 (1998).

[22] A. L. Fetter, "Rotating trapped Bose-Einstein condensates," *Reviews of Modern Physics* **81**, 647691 (2009).

[23] T.-L. Ho, "Bose-Einstein Condensates with Large Number of Vortices," *Physical Review Letters* **87**, 060403 (2001).

[24] G. Watanabe, G. Baym, and C. J. Pethick, "Landau Levels and the Thomas-Fermi Structure of Rapidly Rotating Bose-Einstein Condensates," *Physical Review Letters* **93**, 190401 (2004).

[25] G. Baym and C. J. Pethick, "Vortex core structure and global properties of rapidly rotating Bose-Einstein condensates," *Physical Review A* **69**, 043619 (2004).

[26] A. A. Abrikosov *J. Exp. Theor. Phys. (USSR)* **5**, 1174 (1957).

[27] W. H. Kleiner, L. M. Roth, and S. H. Autler, "Bulk Solution of Ginzburg-Landau Equations for Type-II Superconductors: Upper Critical Field Region," *Physical Review* **133**, A1226–A1227 (1964).

[28] D. A. Butts and D. S. Rokhsar, "Predicted signatures of rotating BoseEinstein condensates," *Nature* **397**, 327–329 (1999).

[29] N. R. Cooper, S. Komineas, and N. Read, "Vortex lattices in the lowest Landau level for confined Bose-Einstein condensates," *Physical Review A* **70**, 033604 (2004).

[30] A. Aftalion, X. Blanc, and J. Dalibard, "Vortex patterns in a fast rotating Bose-Einstein condensate," *Physical Review A* **71**, 023611 (2005).

[31] S. Baharian and G. Baym, "Fluctuations and correlations in rotating Bose-Einstein condensates," *Physical Review A* **82**, 063606 (2010).

[32] S. Baharian and G. Baym, "Correlations in lowest-Landau-level vortex states," *Physical Review A* **87**, 033619 (2013).

[33] G. M. Kavoulakis, B. Mottelson, and C. J. Pethick, "Weakly interacting Bose-Einstein condensates under rotation," *Physical Review A* **62**, 063605 (2000).

[34] A. D. Jackson and G. M. Kavoulakis, "Analytical Results for the Interaction Energy of a Trapped, Weakly Interacting Bose-Einstein Condensate," *Physical Review Letters* **85**, 2854–2856 (2000).

[35] G. F. Bertsch and T. Papenbrock, "Yrast Line for Weakly Interacting Trapped Bosons," *Physical Review Letters* **83**, 54125414 (1999).

[36] R. A. Smith and N. K. Wilkin, "Exact eigenstates for repulsive bosons in two dimensions," *Physical Review A* **62**, 061602(R) (2000).

[37] T. Papenbrock and G. F. Bertsch, "Rotational spectra of weakly interacting Bose-Einstein condensates," *Physical Review A* **63**, 023616 (2001).

[38] T. Papenbrock and G. F. Bertsch, "Exact solutions for interacting boson systems under rotation," *Journal of Physics A: Mathematical and General* **34**, 603 (2001).

[39] J. K. Jain, "Composite-fermion approach for the fractional quantum Hall effect," *Physical Review Letters* **63**, 199–202 (1989).

[40] N. R. Cooper and N. K. Wilkin, "Composite fermion description of rotating Bose-Einstein condensates," *Physical Review B* **60**, R16279–R16282 (1999).

[41] N. K. Wilkin and J. M. F. Gunn, "Condensation of Composite Bosons in a Rotating BEC," *Physical Review Letters* **84**, 6–9 (2000).

[42] G. Moore and N. Read, "Nonabelions in the fractional quantum hall effect," *Nuclear Physics B* **360**, 362–396 (1991).

[43] N. Read and E. Rezayi, "Beyond paired quantum Hall states: Parafermions and incompressible states in the first excited Landau level," *Physical Review B* **59**, 8084–8092 (1999).

[44] R. E. Prange and S. M. Girvin, *The Quantum Hall Effect (Second Edition)*. Springer-Verlag, New York, 1990.

[45] N. R. Cooper, N. K. Wilkin, and J. M. F. Gunn, "Quantum Phases of Vortices in Rotating Bose-Einstein Condensates," *Physical Review Letters* **87**, 120405 (2001).

[46] P. W. Anderson, *Basic Notions Of Condensed Matter Physics (Second Edition)*. Addison-Wesley, Reading, MA, 1984.

[47] C. Yannouleas and U. Landman, "Symmetry breaking and quantum correlations in finite systems: studies of quantum dots and ultracold Bose gases and related nuclear and chemical methods," *Reports on Progress in Physics* **70**, 2067 (2007).

[48] J. C. Cremon, G. M. Kavoulakis, B. R. Mottelson, and S. M. Reimann, "Vortices in Bose-Einstein condensates: Finite-size effects and the thermodynamic limit," *Physical Review A* **87**, 053615 (2013).

[49] V. K. Tkachenko, "Elasticity of vortex lattices," *Sov. Phys. JETP* **29**, 945–946 (1969).

[50] G. Baym and E. Chandler, "The hydrodynamics of rotating superfluids. I. Zero-temperature, nondissipative theory," *Journal of Low Temperature Physics* **50**, 57–87 (1983).

[51] G. Baym, "Tkachenko Modes of Vortex Lattices in Rapidly Rotating Bose-Einstein Condensates," *Physical Review Letters* **110402**, 91 (2003).

[52] I. Coddington, P. Engels, V. Schweikhard, and E. A. Cornell, "Observation of Tkachenko Oscillations in Rapidly Rotating Bose-Einstein Condensates," *Physical Review Letters* **91**, 100402 (2003).

[53] J. Sinova, C. B. Hanna, and A. H. MacDonald, "Quantum Melting and Absence of Bose-Einstein Condensation in Two-Dimensional Vortex Matter," *Physical Review Letters* **89**, 030403 (2002).

[54] G. Baym, "Vortex lattices in rapidly rotating Bose-Einstein condensates: Modes and correlation functions," *Physical Review A* **69**, 043618 (2004).

[55] A. Rozhkov and D. Stroud, "Quantum melting of a two-dimensional vortex lattice at zero temperature," *Physical Review B* **54**, R12697–R12700 (1996).

[56] S. Kivelson, C. Kallin, D. P. Arovas, and J. R. Schrieffer, "Cooperative ring exchange theory of the fractional quantized Hall effect," *Physical Review Letters* **56**, 873–876 (1986).

[57] T. K. Ghosh and G. Baskaran, "Cooperative ring exchange and quantum melting of vortex lattices in atomic Bose-Einstein condensates," *Physical Review A* **69**, 023603 (2004).

[58] A. Bourne, N. K. Wilkin, and J. M. F. Gunn, "Anomalous Hydrodynamics and Normal Fluids in Rapidly Rotating Bose-Einstein Condensates," *Physical Review Letters* **96**, 240401 (2006).

[59] H. E. Hall, "The Angular Acceleration of Liquid Helium. II," *Philosophical Transactions of the Royal Society, A* **250**, 359–385 (1957).

[60] A. J. Leggett, "Bose-Einstein condensation in the alkali gases: Some fundamental concepts," *Reviews of Modern Physics* **73**, 307–356 (2001).

[61] T. L. Gustavson, P. Bouyer, and M. A. Kasevich, "Precision Rotation Measurements with an Atom Interferometer Gyroscope," *Physical Review Letters* **78**, 2046–2049 (1997).

[62] A. Lenef, T. D. Hammond, E. T. Smith, M. S. Chapman, R. A. Rubenstein, and D. E. Pritchard, "Rotation Sensing with an Atom Interferometer," *Physical Review Letters* **78**, 760–763 (1997).

[63] B. T. Seaman, M. Krämer, D. Z. Anderson, and M. J. Holland, "Atomtronics: Ultracold-atom analogs of electronic devices," *Physical Review A* **75**, 023615 (2007).

[64] C. Ryu, M. F. Andersen, P. Cladé, V. Natarajan, K. Helmerson, and W. D. Phillips, "Observation of Persistent Flow of a Bose-Einstein Condensate in a Toroidal Trap," *Physical Review Letters* **99**, 260401 (2007).

[65] W. H. Heathcote, E. Nugent, B. T. Sheard, and C. J. Foot, "A ring trap for ultracold atoms in an RF-dressed state," *New Journal of Physics* **10**, 043012 (2008).

[66] B. E. Sherlock, M. Gildemeister, E. Owen, E. Nugent, and C. J. Foot, "Time-averaged adiabatic ring potential for ultracold atoms," *Physical Review A* **83**, 043408 (2011).

[67] A. Ramanathan, K. C. Wright, S. R. Muniz, M. Zelan, W. T. Hill, C. J. Lobb, K. Helmerson, W. D. Phillips, and G. K. Campbell, "Superflow in a Toroidal Bose-Einstein Condensate: An Atom Circuit with a Tunable Weak Link," *Physical Review Letters* **106**, 130401 (2011).

[68] S. Moulder, S. Beattie, R. P. Smith, N. Tammuz, and Z. Hadzibabic, "Quantized supercurrent decay in an annular Bose-Einstein condensate," *Physical Review A* **86**, 013629 (2012).

[69] J. F. Annett, *Superconductivity, Superfluids, and Condensates*. Oxford University Press, New York, 2004.

[70] L. D. Landau, "The theory of superfluidity of helium II," *J. Phys. USSR* **5**, 71 (1941).

[71] J. R. Anglin, "Local Vortex Generation and the Surface Mode Spectrum of Large Bose-Einstein Condensates," *Physical Review Letters* **87**, 240401 (2001).

[72] A. J. Leggett, "Superfluidity," *Reviews of Modern Physics* **71**, S318–S323 (1999).

[73] P. O. Fedichev and G. V. Shlyapnikov, "Critical velocity in cylindrical Bose-Einstein condensates," *Physical Review A* **63**, 045601 (2001).

[74] R. Dubessy, T. Liennard, P. Pedri, and H. Perrin, "Critical rotation of an annular superfluid Bose-Einstein condensate," *Physical Review A* **86**, 011602(R) (2012).

[75] P. Nozières, "Some Comments on Bose-Einstein Condensation," *Bose-Einstein Condensation* 15–30 (1995).

[76] E. J. Mueller, "Superfluidity and mean-field energy loops: Hysteretic behavior in Bose-Einstein condensates," *Physical Review A* **66**, 063603 (2002).

[77] M. V. Berry, "Catastrophe theory: a new mathematical tool for scientists," *Journal of Scientific and Industrial Research* **36**, 103–5 (1977).

[78] S. N. Rasband, *Chaotic Dynamics of Nonlinear Systems*. Wiley, New York, 1990.

[79] D. Diakonov, L. M. Jensen, C. J. Pethick, and H. Smith, "Loop structure of the lowest Bloch band for a Bose-Einstein condensate," *Physical Review A* **66**, 013604 (2002).

[80] B. Wu and Q. Niu, "Nonlinear Landau-Zener tunneling," *Physical Review A* **61**, 023402 (2000).

[81] S. Burger, F. S. Cataliotti, C. Fort, F. Minardi, M. Inguscio, M. L. Chiofalo, and M. P. Tosi, "Superfluid and Dissipative Dynamics of a Bose-Einstein Condensate in a Periodic Optical Potential," *Physical Review Letters* **86**, 4447–4450 (2001).

[82] J. Liu, B. Wu, and Q. Niu, "Nonlinear Evolution of Quantum States in the Adiabatic Regime," *Physical Review Letters* **90**, 170404 (2003).

[83] B. Wu and Q. Niu, "Superfluidity of Bose-Einstein condensate in an optical lattice: Landau-Zener tunnelling and dynamical instability," *New Journal of Physics* **5**, 104 (2003).

[84] B. P. Venkatesh, J. Larson, and D. H. J. O'Dell, "Band-structure loops and multistability in cavity QED," *Physical Review A* **83**, 063606 (2011).

[85] F. Mulansky, J. Mumford, and D. H. J. O'Dell, "Impurity in a Bose-Einstein condensate in a double well," *Physical Review A* **84**, 063602 (2011).

[86] S. Viefers, T. H. Hansson, and S. M. Reimann, "Bose condensates at high angular momenta," *Physical Review A* **62**, 053604 (2000).

[87] N. Regnault and T. Jolicoeur, "Quantum Hall fractions for spinless bosons," *Physical Review B* **69**, 235309 (2004).

[88] N. R. Cooper and E. H. Rezayi, "Competing compressible and incompressible phases in rotating atomic Bose gases at filling factor ν=2," *Physical Review A* **75**, 013627 (2007).

[89] Z. Wu, B. Feng, and D. Li, "Static structure factor and quantum melting of vortex lattices in two-dimensional Bose-Einstein condensates," *Physical Review A* **75**, 033620 (2007).

[90] S. A. Gifford and G. Baym, "Dislocation-mediated melting in superfluid vortex lattices," *Physical Review A* **78**, 043607 (2008).

[91] M. Linn and A. L. Fetter, "Stability of a vortex in a small trapped Bose-Einstein condensate," *Physical Review A* **60**, 4910–4917 (1999).

[92] H. M. Nilsen, G. Baym, and C. J. Pethick, "Velocity of vortices in inhomogeneous BoseEinstein condensates," *Proceedings of the National Academy of Sciences of the United States of America* **103**, 7978–7981 (2006).

[93] R. J. Dodd, K. Burnett, M. Edwards, and C. W. Clark, "Excitation spectroscopy of vortex states in dilute Bose-Einstein condensed gases," *Physical Review A* **56**, 587–590 (1997).

[94] D. S. Rokhsar, "Vortex Stability and Persistent Currents in Trapped Bose Gases," *Physical Review Letters* **79**, 2164–2167 (1997).

[95] A. L. Fetter and A. A. Svidzinsky, "Vortices in a trapped dilute Bose-Einstein condensate," *Journal of Physics: Condensed Matter* **13**, R135–R194 (2001).

[96] A. L. Fetter, "Nonuniform states of an imperfect Bose gas," *Annals of Physics* **70**, 67–101 (1972).

[97] I. G. MacDonald, *Symmetric Functions and Orthogonal Polynomials.* American Mathematical Society, Providence, 1998.

[98] E. H. Lieb and R. Seiringer, "Derivation of the Gross-Pitaevskii Equation for Rotating Bose Gases," *Communications in Mathematical Physics* **264**, 505–537 (2006).

[99] C. N. Yang, "Concept of Off-Diagonal Long-Range Order and the Quantum Phases of Liquid He and of Superconductors," *Reviews of Modern Physics* **34**, 694704 (1962).

[100] E. J. Mueller, P. M. Goldbart, and Y. Lyanda-Geller, "Multiply connected Bose-Einstein-condensed alkali-metal gases: Current-carrying states and their decay," *Physical Review A* **57**, R1505R1508 (1998).

[101] M. Ögren and G. M. Kavoulakis, "Stability of Persistent Currents in a Bose-Einstein Condensate Confined in a Toroidal Trap," *Journal of Low Temperature Physics* **154**, 30–40 (2009).

[102] A. J. Leggett, "Topics in superfluidity and superconductivity," *Low Temperature Physics* **394**, 1–92 (1991).

[103] O. Morizot, Y. Colombe, V. Lorent, H. Perrin, and B. M. Garraway, "Ring trap for ultracold atoms," *Physical Review A* **74**, 023617 (2006).

[104] A. Smerzi, S. Fantoni, S. Giovanazzi, and S. R. Shenoy, "Quantum Coherent Atomic Tunneling between Two Trapped Bose-Einstein Condensates," *Physical Review Letters* **79**, 4950–4953 (1997).

[105] S. Raghavan, A. Smerzi, S. Fantoni, and S. R. Shenoy, "Coherent oscillations between two weakly coupled Bose-Einstein condensates: Josephson effects, π oscillations, and macroscopic quantum self-trapping," *Physical Review A* **59**, 620–633 (1999).

[106] G. J. Milburn, J. Corney, E. M. Wright, and D. F. Walls, "Quantum dynamics of an atomic Bose-Einstein condensate in a double-well potential," *Physical Review A* **55**, 4318–4324 (1997).

[107] S. Zöllner, G. M. Bruun, C. J. Pethick, and S. M. Reimann, "Bosonic and Fermionic Dipoles on a Ring," *Physical Review Letters* **107**, 035301 (2011).

[108] S. K. Adhikari, "Dipolar Bose-Einstein condensate in a ring or in a shell," *Physical Review A* **85**, 053631 (2012).

[109] M. Abad, M. Guilleumas, R. Mayol, M. Pi, and D. M. Jezek, "Dipolar condensates confined in a toroidal trap: Ground state and vortices," *Physical Review A* **81**, 043619 (2010).

[110] M. Abad, M. Guilleumas, R. Mayol, M. Pi, and D. M. Jezek, "A dipolar self-induced bosonic Josephson junction," *Europhysics Letters* **94**, 10004 (2011).

[111] M. Abad, M. Guilleumas, R. Mayol, M. Pi, and D. M. Jezek, "Phase slippage and self-trapping in a self-induced bosonic Josephson junction," *Physical Review A* **84**, 035601 (2011).

[112] L. C. Qian, M. L. Wall, S. Zhang, Z. Zhou, and H. Pu, "Bose-Einstein condensates on a ring with periodic scattering length: Spontaneous symmetry breaking and entanglement," *Physical Review A* **77**, 013611 (2008).

[113] Z.-W. Zhou, S.-L. Zhang, X.-F. Zhou, G.-C. Guo, X. Zhou, and H. Pu, "Quantum phase transition of Bose-Einstein condensates on a nonlinear ring lattice," *Physical Review A* **83**, 043626 (2011).

[114] X.-F. Zhou, S.-L. Zhang, Z.-W. Zhou, B. A. Malomed, and H. Pu, "Bose-Einstein condensates in a ring-shaped trap with a nonlinear double-well potential," *Physical Review A* **85**, 023603 (2012).

[115] Y. Li, W. Pang, and B. A. Malomed, "Nonlinear modes and symmetry breaking in rotating double-well potentials," *Physical Review A* **86**, 023832 (2012).

[116] M. Ueda and A. J. Leggett, "Ground-State Properties of a Rotating Bose-Einstein Condensate with Attractive Interaction," *Physical Review Letters* **83**, 1489–1493 (1999).

[117] S. Giorgini, L. P. Pitaevskii, and S. Stringari, "Thermodynamics of a trapped Bose-condensed gas," *Journal of Low Temperature Physics* **109**, 309 (1997).

[118] A. L. Fetter *(private communication)* .

[119] L. J. Garay, J. R. Anglin, J. I. Cirac, and P. Zoller, "Sonic black holes in dilute Bose-Einstein condensates," *Physical Review A* **63**, 023611 (2001).

[120] G. Baym and C. J. Pethick, "Landau critical velocity in weakly interacting Bose gases," *Physical Review A* **86**, 023602 (2012).

[121] D. S. Rokhsar, "Phase coherence and "fragmented" Bose condensates," *arXiv:cond-mat/9812260* (1998).

[122] E. J. Mueller, T.-L. Ho, M. Ueda, and G. Baym, "Fragmentation of Bose-Einstein condensates," *Physical Review A* **74**, 033612 (2006).

[123] Y.-A. Chen, S. D. Huber, S. Trotzky, I. Bloch, and E. Altman, "Many-body Landau-Zener dynamics in coupled one-dimensional Bose liquids," *Nature Physics* **7**, 61–67 (2011).

[124] P. Bocchieri and A. Loinger, "Quantum Recurrence Theorem," *Physical Review* **107**, 337–338 (1957).

[125] I. C. Percival, "Almost Periodicity and the Quantal H Theorem," *Journal of Mathematical Physics* **2**, 235 (1961).

[126] I. Romanovsky, C. Yannouleas, L. O. Baksmaty, and U. Landman, "Bosonic Molecules in Rotating Traps," *Physical Review Letters* **97**, 090401 (2006).

[127] L. O. Baksmaty, C. Yannouleas, and U. Landman, "Rapidly rotating boson molecules with long- or short-range repulsion: An exact diagonalization study," *Physical Review A* **75**, 023620 (2007).

[128] I. Romanovsky, C. Yannouleas, and U. Landman, "Symmetry-conserving vortex clusters in small rotating clouds of ultracold bosons," *Physical Review A* **78**, 011606(R) (2008).

[129] J. E. Williams, E. Zaremba, B. Jackson, T. Nikuni, and A. Griffin, "Dynamical Instability of a Condensate Induced by a Rotating Thermal Gas," *Physical Review Letters* **88**, 070401 (2002).

[130] A. Griffin, T. Nikuni, and E. Zaremba, *Bose-Condensed Gases at Finite Temperatures.* Cambridge University Press, New York, 2009.

[131] N. P. Proukakis and B. Jackson, "Finite-temperature models of Bose-Einstein condensation," *Journal of Physics B: Atomic, Molecular and Optical Physics* **41**, 203002 (2008).

[132] L. P. Kadanoff and G. Baym, *Quantum Statistical Mechanics: Green's Function Methods in Equilibrium and Nonequilibrium Problems.* W. A. Benjamin, Inc., New York, 1962.

[133] A. Griffin, "Conserving and gapless approximations for an inhomogeneous Bose gas at finite temperatures," *Physical Review B* **53**, 9341–9347 (1996).

[134] S. Giorgini, L. P. Pitaevskii, and S. Stringari, "Thermodynamics of a Trapped Bose-Condensed Gas," *Journal of Low Temperature Physics* **109**, 309–355 (1997).

[135] E. Zaremba, T. Nikuni, and A. Griffin, "Dynamics of Trapped Bose Gases at Finite Temperatures," *Journal of Low Temperature Physics* **116**, 277–345 (1999).

[136] T. R. Kirkpatrick and J. R. Dorfman, "Transport in a dilute but condensed nonideal Bose gas: Kinetic equations," *Journal of Low Temperature Physics* **58**, 301–331 (1985).

[137] S. Konabe and T. Nikuni, "Instability of a superfluid Bose gas induced by a locked thermal gas in an optical lattice," *Journal of Physics B: Atomic, Molecular and Optical Physics* **39**, S101 (2006).

[138] G. B. Arfken and H. J. Weber, *Mathematical Methods for Physicists.* Academic Press, London, 2001.